

**SOFT NANOPARTICLE FLOTATION
COLLECTORS**

SOFT NANOPARTICLE FLOTATION COLLECTORS

By

XIAOFEI DONG, M.Sc.

A Thesis

Submitted to the School of Graduate Studies
in Partial Fulfillment of the Requirements
for the Degree
Doctor of Philosophy

McMaster University

© Copyright by Xiaofei Dong, October, 2016

DOCTOR OF PHILOSOPHY (2016)

McMaster University

(Chemical Engineering)

Hamilton, Ontario

TITLE: Soft Nanoparticle Flotation Collectors

AUTHOR: Xiaofei Dong

M.Sc. (Tianjin University)

SUPERVISOR: Professor Robert H. Pelton

NUMBER OF PAGES: x, 112

Abstract

Flotation is arguably the most important mineral separation technique. It has been demonstrated that hydrophobic nanoparticles adsorbed onto hydrophilic mineral surfaces can facilitate mineral particles attachment to air bubbles in flotation process. This thesis explores the effects of nanoparticle adhesiveness, size and shape on the performance of nanoparticle flotation collectors. For this, a series of rigid polystyrene, soft shelled polystyrene-poly (n-butyl methacrylate) (PS-PB) and soft lobed polystyrene/poly (n-butyl methacrylate) (PS/PB) Janus nanoparticles were prepared and characterized. Flotation experiments with glass beads, a model for mineral particles, revealed that soft-shelled particles were more effective collectors than were hard polystyrene particles. The small (92 nm) Janus particles were particularly good flotation collectors for glass beads.

The pull-off forces required to remove nanoparticles from glass were measured by AFM and the results were compared to the abilities of the nanoparticles to induce the flotation of hydrophilic glass beads. Soft PS-PB particles were strongly adhering and were very effective nanoparticle flotation collectors. By contrast, hard PS particles were weakly adhering and were poor flotation collectors. These observations led to the hypothesis that weakly adhering nanoparticles were dislodged from the glass bead surfaces during flotation. Experimental support for this hypothesis included: (1) the coverage of nanoparticle on glass bead surfaces decreased with increased conditioning time; (2) large nanoparticle aggregates were detected in flotation pulp as well as on bead surfaces; and, (3) dislodged soft-shelled PS-PB particles left polymeric patches, we call footprints, on the glass bead surfaces. Indeed, the presence of the footprints, suggests that a nano-scale stamping process can be used to cover surfaces with hydrophobic polymer footprints.

Arguments are made that hydrodynamic forces alone were insufficient to detach the small nanoparticles from the glass bead surfaces in our experiments. Instead, it is proposed that bead-bead collisions during conditioning and flotation caused weakly adhering particles to detach; a process is termed as “nano-scale ball milling”. Furthermore, geometric arguments show that during a bead-bead encounter, larger nanoparticles are more susceptible to removal than small particles which is consistent with the experimental data.

Although all experiments were performed with model glass beads and rather simple nanoparticles, this work has for the first time explained why larger polystyrene nanoparticles are ineffective flotation collectors. The work highlights the need to consider nanoparticle/mineral adhesion when designing collectors for real mineral systems.

Acknowledgements

Firstly, I would like to express my deepest gratitude to my supervisor, Prof. Robert H. Pelton, for his tremendous encouragements and continuous supports through my study and research work at McMaster. His enthusiasm, thoughts and great motivation to research inspired me to not only try out new ideas but also explore the fundamental scientific questions behind every subject I have worked on. I also benefited a lot from the great skills he taught me in paper writing, oral and poster presentation, and mathematical modeling. His advices on both research as well as my career is invaluable. Additionally, I appreciate the freedom he gave me to work on what I was mostly interested in with respect to the project, as well as the opportunities he gave me to work closely with industry partner and attend conferences.

I would also like to thank my advisory committee, Prof. Harald D.H. Stöver and Prof. David Latulippe for their insightful thoughts, suggestions, discussions and encouragements. Especially, I would like to acknowledge Prof. Harald D.H. Stöver for his great advices on nanoparticle synthesis, and to Prof. David Latulippe for his generous supports on fluid mechanics.

I would like to thank Natural Sciences and Engineering Research Council of Canada (NSERC) and VALE Base Metals Technology Development (VBMTD) for funding my research. I acknowledge VBMTD for organizing meetings on nanoparticle flotation collector project. Especially, I would like to acknowledge Dr. Zongfu Dai and Dr. Manqiu Xu for their general helps and useful discussions.

I would like to thank Prof. Emily Cranston for enhancing my knowledge of AFM and QCM-D. Prof. Carlos Filipe and Dr. Erlita Mastan are acknowledged for their mathematical helps. Dr. Glynis de Silveira is thanked for the training on SEM and EDS, and Ms. Marcia Reid is thanked for the training on TEM. Mr. Heera Marway, Dr. Emil Gustafsson and Dr. Danielle Covelli are thanked for the AFM and XPS supports. Prof. Todd Hoare, Prof. Raja Ghosh, and Prof. Michael Thompson are acknowledged for allowing me to access the NanoSight, Optical Microscopy and FTIR instruments. Prof. Shiping Zhu and Prof. Kim Jones are also acknowledged for their supports and encouragements on my research.

I would like to acknowledge our Lab Manager, Mr. Doug Keller, for his fast and friendly assistants with apparatus and chemicals purchase and safety training. I also would like to thank Ms. Sally Watson for handling all the administrative work and paperwork required by my project. Thanks to the Mechanical Technician, Mr. Paul Gatt, for the fabrication of customized apparatus required for my research. I would also like to thank Mr. Michael Clarke, Ms. Justyna Derkach, Mr. Dan Wright, Ms. Michelle Whalen, Ms. Kristina Trollip, Ms. Lynn Falkiner and Ms. Cathie Roberts from the Chemical Engineering Department for their technical supports and administrative assistants.

In addition, I would also like to acknowledge all my current and previous colleagues from

McMaster Interfacial Technologies Group for their helps and encouragements. I appreciate all instrument trainings and fruitful discussions from Dr. Songtao Yang, Dr. Zuohe Wang, Dr. Zhen Hu, Dr. Emil Gustafsson, Ms. Carla Abarca, Dr. Xudong Deng, Mr. Qiang Fu, Prof. Shuxian Shi, Dr. Roozbeh Mafi, Dr. Jingyun Wang, Mr. Lunquan Yu, Ms. Yuanhua Li, Mr. Dong Yang, Dr. Sana Jahanshahi Anbuhi, and Dr. Zhuyuan Zhang. I am also thankful for my excellent undergraduate students, Ms. Marie Price, Ms. Sarah Ballinger and Mr. Shishir Dhakal for their hard work and contributions. Special thanks are due to all my friends in Hamilton, Ms. Jennifer Faubert, Ms. Xiaodan Ni, Ms. Jingyan Chen, Mr. Dongyang Li, Ms. Fengyan Wang, Mr. Lu Zhu, Ms. Xue Bai, Mr. Shuiliang Wu, Mr. Xuan Yang, Dr. He Zhu, Ms. Fei Xu, et al. Thank you for sharing the past four years with me.

Last but not least, I would like to express my love and gratitude to my parents, my sister, Mr. Yuan Yao, my lovely nephew and my family members for their endless love, care and supports.

Table of Contents

Abstract.....	iv
Acknowledgements.....	v
Table of Contents.....	vii
Abbreviations.....	ix
Chapter 1 Introduction.....	1
1.1 Froth Flotation.....	1
1.1.1 Basic Steps of the Flotation Process.....	2
1.1.2 Flotation Regents.....	3
Collector.....	3
Frother and Modifier.....	5
1.1.3 Challenges in Nickel Ore Separation.....	5
1.2 Nanoparticle Flotation Collector.....	7
1.2.1 Development of Nanoparticle Flotation Collector.....	7
1.2.2 Working Mechanism of Nanoparticle Flotation Collector.....	9
1.2.3 Selection Criteria for Nanoparticle Flotation Collectors.....	10
Hydrophobicity.....	10
Colloidal Stability.....	11
Selectivity.....	11
1.2.4 Role of Nanoparticle Size and Softness in Flotation.....	13
1.2.5 Controversies and Unsolved Issues.....	14
1.3 Nanoparticles.....	15
1.3.1 Spherical Nanoparticles.....	15
1.3.2 Anisotropic Nanoparticles.....	16
Janus Nanoparticles.....	16
Core-shell Nanoparticles.....	17
1.4 Objectives.....	17
1.5 Thesis Outline.....	18
1.6 References.....	20

Chapter 2 Relating Nanoparticle Shape and Adhesiveness to Performance as Flotation Collectors	30
Chapter 3 Mineral-Mineral Particle Collision During Flotation Remove Adsorbed Nanoparticle Flotation Collectors	46
Abstract	47
Introduction	49
Experimental Section	50
Results	52
Discussion	61
Conclusions	62
References	64
Appendix: Supporting Information for Chapter 3	66
Chapter 4 Effects of Nano-scale Ball Milling on Soft Nanoparticle Collectors	80
Introduction	81
Experimental Section	82
Results	86
Discussion	94
Conclusions	98
References	99
Appendix: Supporting Information for Chapter 4	101
Chapter 5 Concluding Remarks	111

Abbreviations

AFM	atomic force microscopy
CA	contact angle
CTAB	cetyltrimethylammonium bromide
CCC	critical coagulation concentration
DLS	dynamic light scattering
EM	electrophoretic mobility
EDS	energy dispersive spectroscopy
FPS	frames per second
FTIR	Fourier transform infrared spectroscopy
HIC	high intensive conditioning
HTS	high-throughput screening
PAX	potassium amyl xanthate
PB	poly (<i>n</i> -butyl methacrylate)
PDI	polydispersity index
Pn	pentlandite
PS	polystyrene
PS-PB	polystyrene-core-poly (<i>n</i> -butyl methacrylate)-shell nanoparticle
PS/PB	polystyrene/poly (<i>n</i> -butyl methacrylate) Janus nanoparticle
QCM-D	quartz crystal microbalance with dissipation
RPM	revolutions per second
SE	standard deviation error

SEM	scanning electron microscopy
TEM	transmission electron microscopy
T _g	glass transition temperature
TPCL	three-phase contact line
V-50	2,2'-azobis(2-methylpropanimidamide) dihydrochloride
UNIFROTH 250C	a mixture of monomethyl polypropylene glycol, 250kDa and dipropylene glycol monomethyl ether
XPS	X-ray photoelectron spectroscopy

Chapter 1 Introduction

Polymeric nanoparticles adsorbed on mineral particle surfaces can promote flotation and nanoparticle collectors therefore have potential applications in commercial flotation practices. Flotation of nickel ultramafic ores using conventional molecular collectors has proven to be particularly challenging due to the severe depression of the collector efficiency by nanoscale contaminations on the mineral surface. Due to their particle nature and size, polymeric nanoparticles have the potential of reducing the effect of the nanoscale contaminations and thereby increase the flotation efficiency of nickel ultramafic ores. This thesis explores the role of the size, shape and adhesive properties of nanoparticles for their performance as flotation collectors, with the aim to formulate design rules for nanoparticle collectors. In this first chapter, the literature on nanoparticle flotation collectors is reviewed, with a focus on soft nanoparticles. First, an overview of the fundamental aspects of froth flotation and the challenges in ultramafic ore separation is presented, followed by a review of the previous development of nanoparticle flotation collectors in which controversies and unsolved issues will be identified and discussed. Finally, techniques available to synthesis nanoparticles with specific size, shape and adhesive properties will be summarized.

1.1 Froth Flotation

Ores mined from any land-based deposit usually contain a highly heterogeneous mixture of extractable minerals and extraneous non-valuable material known as gangue. Froth floatation, or simplify flotation, is a separation technique used to separate the minerals from the gangue first introduced in the mining industry at the end of the nineteenth century. Flotation is arguably the greatest metallurgical innovation over the past century ¹ and the method has since been expanded to applications outside the mining industry, such as deinking of waste paper ², treatment of industrial effluents ^{3,4} and oil recovery from oil sands ⁵.

Flotation exploits the difference in the ability of various minerals particles to adhere to air bubbles in a three-phase (solid-water-air) system ⁶. Prior to flotation, crushing and grinding operations are used to reduce the particle size to a diameter of approximately 100 μm . Figure 1 illustrates the principle of flotation in a mechanical flotation cell. An air sparging system at the bottom of the cell generates a carrying phase of air bubbles through the pulp. An impeller provides turbulence in the pulp phase that promotes collisions of particles and bubbles, resulting in the attachment of particles to bubbles. The flotation separation is achieved by utilizing the difference in hydrophobicity of different solids, which causes hydrophobic particles to be carried to the surface with the rising air bubbles and overflow into a collector launder, whereas unwanted hydrophilic particles are left at the bottom of the cell to be discharged ⁷.

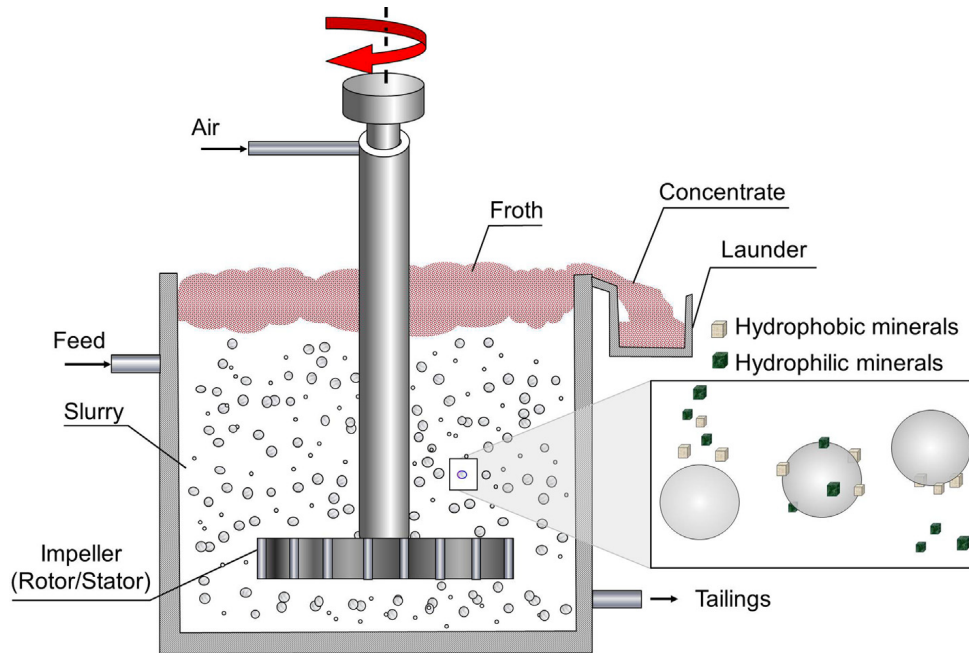


Figure 1 Illustration of the flotation process. (Figure adapted from reference ⁷. Copyright ©2015 Elsevier Ltd. Reprinted with permission.)

1.1.1 Basic Steps of the Flotation Process

Successful recovery of valuable minerals via flotation involves a number of steps, where the interaction between particle and air bubble usually is considered to be the decisive factor for effective flotation ⁸. The bubble-particle interaction is frequently divided into three sequential micro-processes: bubble-particle collision, attachment and detachment ⁹. The collision of mobile bubbles and particles, governed by the liquid flow ¹⁰, and the relative movement between the air bubbles and solid particles ¹¹, have been intensively studied in the flotation literature ¹²⁻¹⁶.

Unlike collisions that depend on the hydrodynamic environment in the flotation cell ^{10, 13, 16}, bubble-particle attachment and detachment are highly dependent on the surface chemistry and physical chemistry properties of mineral particles and air bubbles ⁶. By analysing the motions of individual particles on an air bubble surface, illustrated in Figure 2, Nguyen and his coworkers ⁹ identified three principle steps in the particle-bubble attachment process. The steps are (1) thinning of the liquid film between the particle and the air bubble; (2) rupture of the liquid film and formation of three-phase (water-air-solid) contact nuclei; (3) expansion of the three-phase contact line (TPCL) from the contact nucleus to form a firm and stable attachment ^{9, 17, 18}. By using a high-speed digital camera system, rupture of the water film as well as the subsequent formation of contact nuclei between hydrophobic particle and air bubble were directly observed ⁸. Note that for an effective attachment to take place, the particle-bubble attachment time required

to form a stable attachment should be shorter than the time the particle slides on the air bubble surface¹⁸. If the attachment time exceeds the sliding time particle detachment will occur, which is unfavorable in the flotation process.

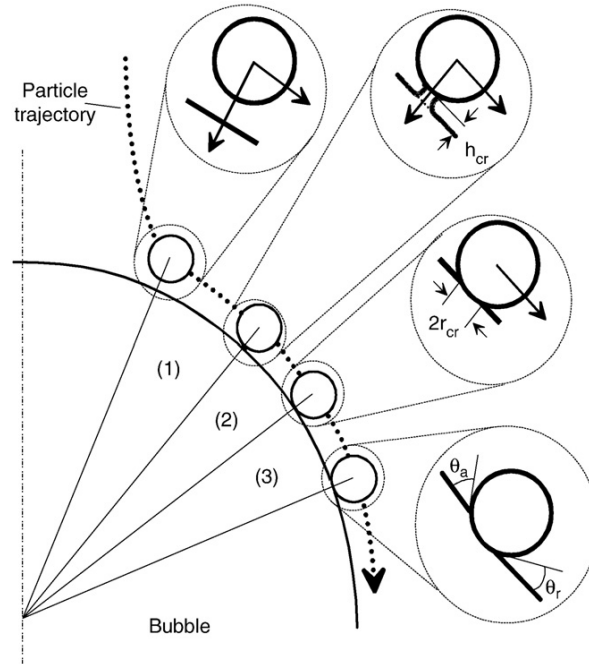


Figure 2 The bubble-particle attachment processes: (1) thinning of the wetting thin film to the critical thickness, h_{cr} , (2) rupture of the thin film when the bubble and particle are very close and the formation of the three-phase contact nucleus with radius of r_{cr} , and (3) the spreading of the TPCL from the critical radius to a stable wetting state with equilibrium contact angles (advancing angle, θ_a , and receding angle, θ_r). (Figure adapted from reference⁹. Copyright ©2010 Elsevier B.V. Reprinted with permission.)

1.1.2 Flotation Regents

In commercial operations, reagents are frequently added to facilitate the flotation process and the selection and controlled addition of these reagents are critical parts of the flotation strategy¹⁹. Flotation reagents are classified as collectors, frothers and modifiers, based on their function in the flotation process⁶.

Collector

Most mineral particle surfaces are naturally hydrophilic, whereas an air bubble can only pick up mineral particles that are sufficiently hydrophobic⁶. To increase the hydrophobicity of the

mineral particles in the pulp, hydrophobization agents known as collectors are used in a conditioning step prior to the flotation. The collector adsorbs selectively to the mineral particle of interest, forming a hydrophobic layer that promotes attachment to the hydrophobic air bubbles and subsequent recovery of the mineral in the developed froth phase. Conventional collectors are water soluble molecular surfactants consisting of a hydrophobic carbon tail and a reactive hydrophilic head⁶. The head group selectively reacts with the surface of a mineral particle, leaving the hydrophobic carbon chain oriented toward the water thus making the site hydrophobic⁷.

Xanthates are the most important collectors for the flotation of sulfide mineral ores^{20, 21} as well as oxides ores^{22, 23} (i. e. oxide zinc, lead and copper minerals). As illustrated in Figure 3a, the ionic form of xanthates has the general formula of $R-S^-$, with the length of the carbon chain ranging between C2 and C6 (i. e. ethyl, isopropyl, isobutyl and amyl)²⁴. The reaction of xanthates with mineral surfaces involves chemical bond formation through electron donor action between sulfur of the xanthate and the metal atom of the mineral surfaces^{25, 26}. Another important type of flotation collector for sulfide ore separation is chelating collectors²⁷⁻³⁰. These collectors bind to the mineral through formation of a five- or six-member ring by donation of the unshared pair of electrons from atoms such as O, N, S or P in organic compounds to metal atoms at the mineral surface. Successful attempts of using chelating collectors derived from imidazole have also been reported for the flotation of pentlandite³¹, chalcopyrite and pyrite³².

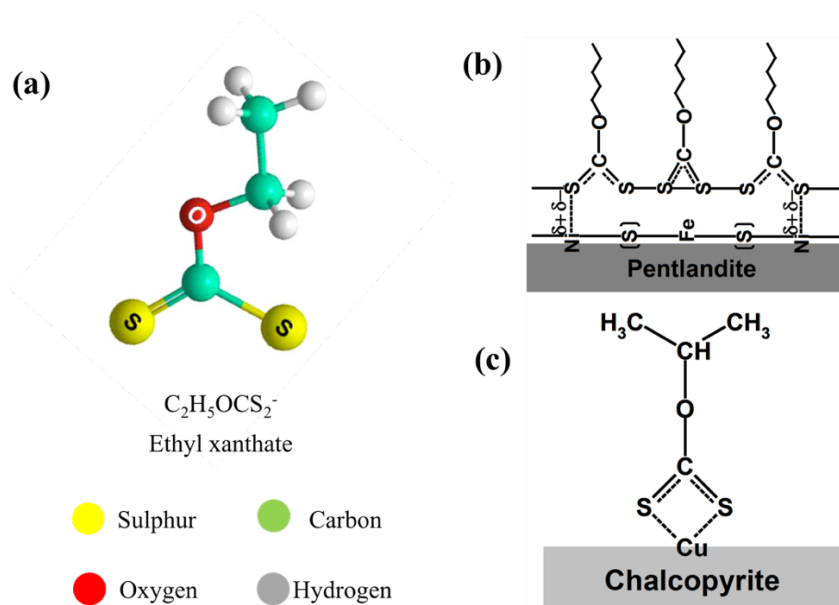


Figure 3 Schematic drawings showing the structure of (a) ethyl xanthate collector⁷, (b) Ni-dixanthogen (amyl xanthate collector for pentlandite)²⁵, and (c) Cu-diethyldixanthogen (isopropyl xanthate collector for chalcopyrite)²⁶. (Figure redrawn from references^{7, 25, 26}.)

Copyrights ©2015 Elsevier Ltd., ©1989 Taylor & Francis and ©2003 Elsevier B.V.
Reprinted with permissions.)

Frother and Modifier

Frothers are surface-active compounds that adsorb in the water-air interface³³ capable of preventing the air bubbles from collapsing and producing finer air bubbles with a narrow size distribution³⁴. Modifiers, commonly called regulators, are mainly used to control the interaction between collector and individual minerals in the pulp. For example, with the addition of copper sulfate, increased sodium isopropyl xanthate collector adsorption on sphalerite surface can be achieved³⁵. In contrast, sodium cyanide present in the pulp could dissolve copper from the sphalerite surface and depress the collector adsorption on sphalerite³⁶. In cases where the pH of the pulp is of large importance for the adsorption of collector on the mineral surface^{37,38} or the effectiveness of the frother^{19,39}, alkaline or acidic pH modifiers are added into the pulp to adjust the pH to the appropriate range.

1.1.3 Challenges in Nickel Ore Separation

With high corrosion resistance and non-toxic properties, nickel and nickel alloys have been widely used in the steel industry, coinage, food handling and pharmaceutical equipment⁷. The source of nickel and its associated mineral ores deposited in the earth crust are summarized in Table 1⁷. Sulphide ore and laterites are two major sources of nickel. Processing of laterite ore faces technical challenges as well as high costs caused by pre-treatment of the ore by pressure acid leaching⁴⁰. Therefore, extraction of nickel from sulphide ore is the dominating nickel processing practice in commercial operations.

The principal formula of nickel in sulphide ore, pentlandite (Pn, $\text{Ni}_{4.5}\text{Fe}_{4.5}\text{S}_8$), is usually associated with pyrrhotite (Fe_{1-x}S , $0 < x < 0.17$) and chalcopyrite (CuFeS_2) in the deposits at Sudbury and Voisey's Bay in Canada⁶. Separation of Pn from sulphide ore is achieved by flotation using xanthate collector (potassium amyl xanthate, PAX⁶), frother (a mixture of monomethyl polypropylene glycol, 250kDa and dipropylene glycol monomethyl ether UNIFROTH 250C), pH regulator (soda ash⁴¹), dispersant (carboxymethyl cellulose, CMC⁴²), and occasionally with the addition of depressant (diethylenetriamine, DETA⁴³) to reject pyrrhotite.

Table 1 Nickel sources and associate mineral ores ⁷.

Source	Formula	% Ni	Gravity	Occurrence/ Associations
Pentlandite	(Fe,Ni) ₉ S ₈	34.2	4.6-5.0	Empirical formula Fe ²⁺ _{4.5} Ni _{4.5} S ₈ . Occurs invariably with chalcopyrite, and often intergrown with pyrrhotite, millerite, cobalt, selenium, silver, and platinum metals.
Garnierite	Hydrated Ni-Mg silicate	Variable	2.4	Often occurs massive or earthy in decomposed serpentines (Mg ₃ Si ₂ O ₄ (OH) ₅), often with chromium ores. Deposits are known as “lateritic”.
Niccolite	NiAs	44.1	7.3-7.7	Occurs in igneous rock with chalcopyrite, pyrrhotite, and nickel sulfides. Also in veins with silver, silver-arsenic, and cobalt minerals.
Millerite	NiS	64.8	5.3-5.7	Occurs as needle-like radiating crystals in cavities and as replacement of other nickel minerals. Also in veins with other nickel minerals and sulfides.
Heazewoodite	Ni ₃ S ₂	73.3	5.8	Rare. Constituent of matte in Vale’s matte separation process.

Based on the nickel content, sulphide ores can be classified into massive sulphide (90% sulphide, up to 10% Ni), sulphide matrix (20% to 50% sulphide) and disseminated ultramafic ore (0.5% Ni)⁴⁴. As a result of decreasing high grade nickel ore reserves, increasing efforts are directed towards the processing of disseminated ultramafic deposits⁴⁴. Several hundred million tonnes of nickel resources are prospected in the ultramafic ore in the Thompson Nickel Belt in Manitoba, Canada⁴⁵. This is the deposit of interest in this thesis.

Extraction of nickel from ultramafic ore faces two main challenges: (1) high viscosity of flotation pulp containing large amount of fibrous serpentine ($\text{Mg}_3\text{Si}_2\text{O}_4(\text{OH})_5$)^{46,47} and (2) surface contamination of Pn with serpentine^{48,49}. Genc⁴⁶ and Patra⁴⁷ and their co-workers have showed that flotation pulp with high viscosity inhibits air bubble transportation through the pulp, which is unfavorable in flotation separation as the carrying phase cannot rise to the surface. The consequences of the serpentine fibers on the Pn surfaces have been investigated in a number of studies, and the key finding is that serpentine fibers on the surface^{50,51} act as a surface barrier that interferes with bubble attachment^{41,52}. Consider a Pn particle surface decorated with hydrophilic serpentine fibers with a height of 20 nm^{50,51}, whereas the size of the adsorbed hydrophobic PAX micelle is about 1 nm. When an air bubble collides with this surface, the geometry of the serpentine fibers will allow them to screen the hydrophobic PAX sites from coming in contact with the air bubble, which results in reduced Pn recovery. Laboratory studies⁵² have shown that the Pn recovery decreased from 90% to 25% when 30% serpentine was introduced into a previously serpentine free pulp. Deliberate removal of surface serpentine fibers by strong agitation is a practice used in high intensive conditioning (HIC)^{53,54}. Approaches involving disintegration of the fibers by acid leaching^{44,55} and by adding depressants⁵⁶ have also been attempted to improve nickel recovery. However, when the cost of energy and effluents treatment is taken into account, it is clear that these de-sliming operations have disadvantages.

Finally, the continued use of xanthate has raised ever increasing environmental concerns as carbon disulfide is readily emitted from xanthate decomposition and excess xanthate in discharge waters is an environmental threat to humans as well as the aquatic life⁵⁷. Engineers and scientists have therefore embarked on a journey looking for a replacement for xanthate collectors⁵⁸.

1.2 Nanoparticle Flotation Collector

1.2.1 Development of Nanoparticle Flotation Collector

In 2006, Dr. Pelton proposed the idea of using polymeric nanoparticles as flotation collector, where cationic hydrophobic nanoparticles can deposit on negatively charged Pn surface and facilitate the attachment to the air bubble in flotation (see Figure 4). A nanoparticle collector may offer advantages over molecular collectors for nickel ultramafic ore separation, since relatively large nanoparticles adsorbed on Pn surfaces are less affected by serpentine coating compared to

the 1 nm thick patches of traditional xanthate collector. The proposed working mechanism of a nanoparticle flotation collector for nickel ultramafic ore separation is included in Figure 5³¹.

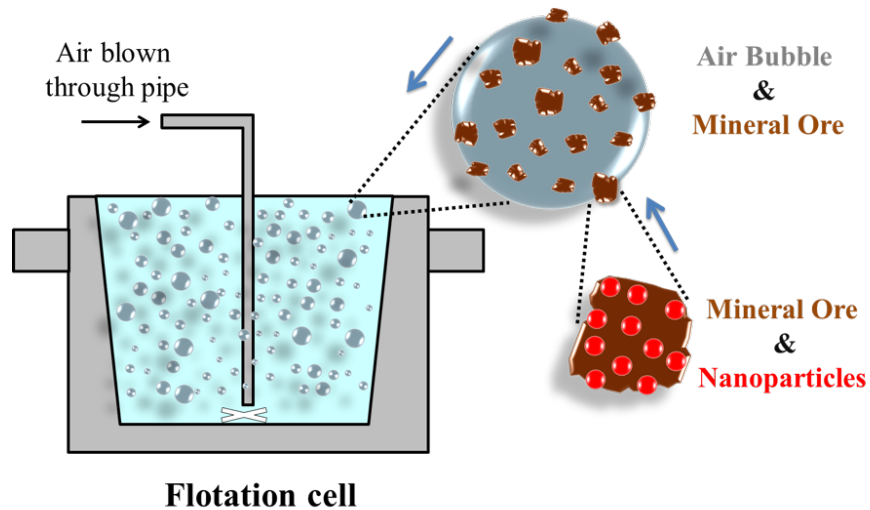


Figure 4 Proposed working mechanism of a nanoparticle flotation collector.

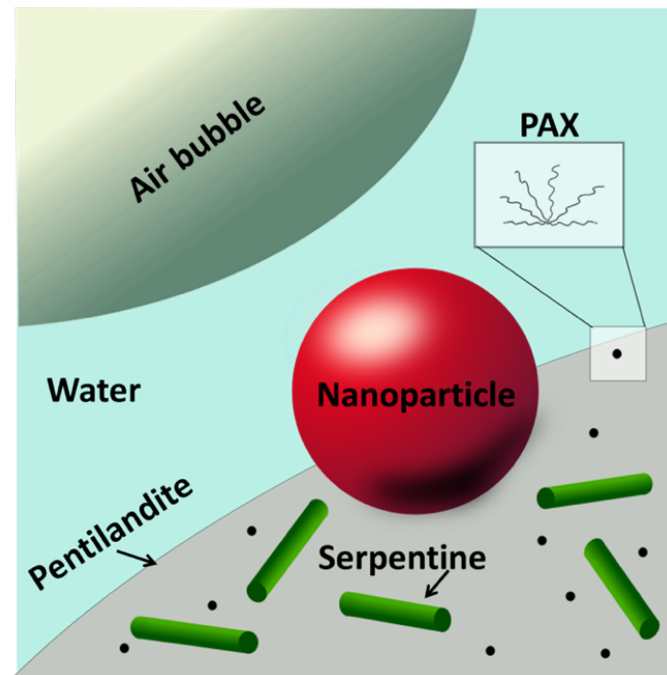


Figure 5 The proposed working mechanism of a nanoparticle collector for nickel ultramafic ore separation. (Figure redrawn from reference³¹. Copyright ©2013 Elsevier B.V. Reprinted with permission.)

Over the past ten years, Pelton's group have been developing flotation collectors based on polymeric nanoparticles. The efforts of developing new nanoparticle flotation collectors involve two steps: (1) Develop simple cationic polystyrene latexes and use a laboratory flotation experiment to assess the potential of the nanoparticles as flotation collectors, and (2) Develop more complex polystyrene-based nanoparticles with functional surface groups that can bind specifically to Pn^{31, 63}. The laboratory flotation experiment is a small-scale simplified system where negatively charged, hydrophilic glass beads are employed as the model for the mineral particle. The model glass bead experiments can answer specific mechanistic question, such as the extent of adsorption of the nanoparticles on the glass beads⁵⁹, as well as nanoparticle design questions relating to hydrophobicity⁶⁰, diameter⁶¹ and softness⁶². Pilot Pn flotation experiments have been conducted to assess the commercial feasibility of nanoparticle collectors with respect to recovery and grade. Additionally, automatic hydrophobicity and colloidal stability assays have also been developed for screening potential nanoparticle collectors in a high-throughput screening (HTS) workflow^{64, 65}.

1.2.2 Working Mechanism of Nanoparticle Flotation Collector

Yang et al. were the first to demonstrate that hydrophobic polystyrene nanoparticle adsorbed on the surface of much larger hydrophilic glass beads can promote flotation⁵⁹. Glass bead flotation experiments revealed that after addition of 46 nm PS nanoparticle, over 90% hydrophilic glass beads could be collected in the froth phase, compared to only 11% without nanoparticle collector (Figure 6). Water contact angle and air bubble contact angle measurements of polystyrene-coated glass slides suggested that adsorbed polystyrene nanoparticle work as a hydrophobilization agent. Micromechanical pull-off force measurements determined that the force required to pull a nanoparticle decorated glass bead off an air bubble was 1.9 nN, whereas the force required to remove an untreated glass bead was only 0.0086 nN. These results provided direct evidence that hydrophobic nanoparticles improve the adhesion between model glass beads and air bubbles and thus have the potential of preventing detachment of mineral particles from air bubbles during the flotation process. In addition, by analyzing the pull-off force data, a model for the wet patch contact between nanoparticle decorated solid surfaces and air bubble was proposed. Another important conclusion of this work was that when using an effective nanoparticle flotation collector, as little as 10% surface coverage of the glass bead was sufficient to achieve good flotation.

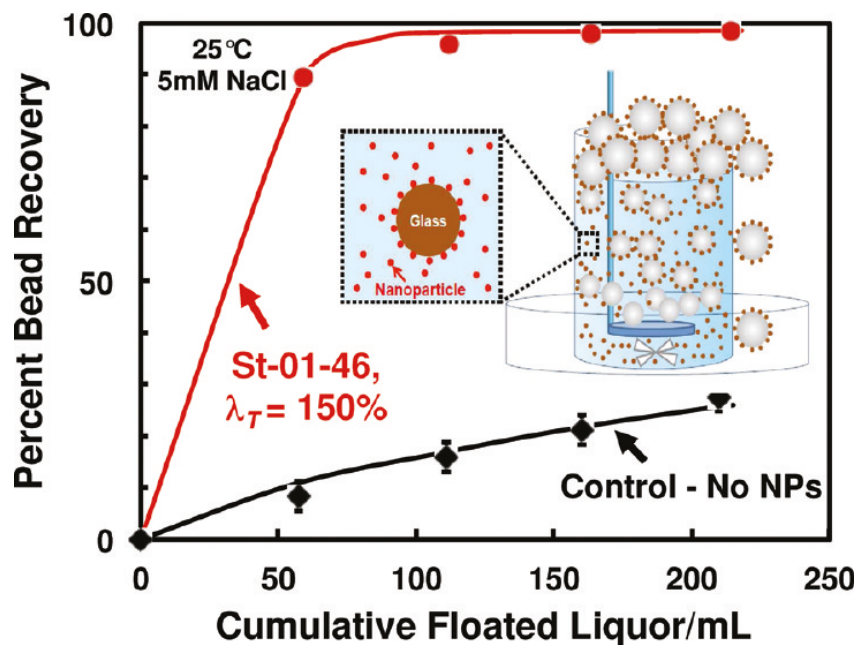


Figure 6 Glass beads flotation with and without the addition of 46 nm polystyrene nanoparticle collector. (Figure adapted from reference ⁵⁹. Copyright © 2011 American Chemical Society. Reprinted with permission.)

1.2.3 Selection Criteria for Nanoparticle Flotation Collectors

Hydrophobicity

Contact angle measurements have been employed to probe the wettability of hydrophilic surfaces decorated with a series of polystyrene based nanoparticles in order to correlate the contact angle with the flotation performance of glass beads decorated with the same set of nanoparticles ⁶⁰. As illustrated in Figure 7, glass beads modified with hydrophilic nanoparticles cannot attach to air bubbles, resulting in poor flotation recovery, whereas beads coated with hydrophobic nanoparticles firmly attaches to air bubbles and thus are carried out into the froth phase. Yang et al. ⁶⁰ concluded that in order to give high flotation recovery, a contact angle value of $51^\circ < \theta < 85^\circ$ is required for nanoparticle saturated glass surfaces.

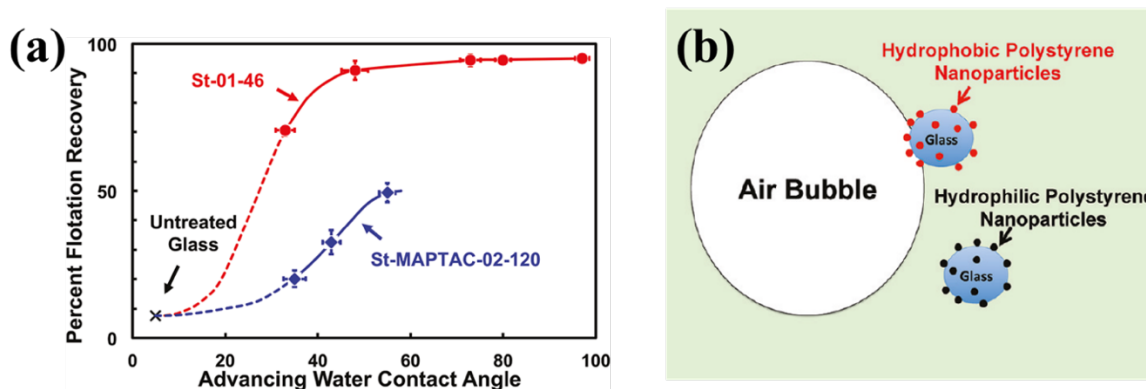


Figure 7 The role of nanoparticle hydrophobicity in flotation. Image (a) shows the influence of advancing water contact angle on flotation recovery, and image (b) illustrates the influence of nanoparticle hydrophobicity on the ability to facilitate air bubble attachment. (Figure redrawn from reference⁶⁰. Copyright © 2011 American Chemical Society. Reprinted with permission.)

Colloidal Stability

In a colloidal system, the term of “stability” means that there is no tendency of sedimentation of colloidal particles and no sign of phase separation over a long period of time⁶⁶. The key to evaluating the colloidal stability is to know the total potential energy of interaction or total forces between two particles⁶⁶. For a colloidal system consisting of charged particles, electrostatic surface potential is the main component of the pair potential, so characterization of electrostatic surface potential becomes a useful tool to predict the stability of the colloidal system. Electrophoretic light scattering is an easy way to quantify the magnitude of the electrostatic surface potential of colloidal particles dispersed in solution, and the calculated zeta-potential value is frequently used to judge the stability of a colloidal system^{67,68}. Particles with an absolute zeta-potential value larger than 20 mV is termed colloidal stable.

In practical flotation applications involving high ionic strength, the screening effect from the salt is significant⁶⁹. If the critical coagulation concentration (ccc) for the nanoparticle collector is lower than the salt concentration in the flotation pulp, large nanoparticle aggregates are formed during conditioning period, which will have a negative impact on the flotation. Thus, characterizing the ccc for newly developed nanoparticle collectors is essential. Abraca et al.⁶⁵ developed a fast and automatic colloidal stability assay to determine ccc values by analyzing the turbidity of latex samples in a HTS workflow. In their approach, both zeta-potential and ccc values were employed to characterize the colloidal stability of developed nanoparticle collectors.

Selectivity

For nanoparticles to function as effective flotation collectors for nickel ore separation, surface functional groups are required to promote specific deposition on nickel-rich particle surfaces. Imidazole groups, which can chelate with nickel atoms, have been introduced into polystyrene-based nanoparticles via an emulsion polymerization method. The performance for pentlandite flotation, both in terms of cumulative recovery and grade of nickel, was improved compared to plain polystyrene nanoparticles^{31 64}. An imidazole functionalized nanoparticle collector could at high dosage give flotation performance comparable to the conventional collector PAX³¹, indicating that nanoparticle collectors may be attractive for complicated systems, such as nickel ultramafic ores, where PAX struggle. Nanoparticles with triazole functional groups for nickel ore separation were also synthesized using a click reaction of surface azide and pentyne⁶³.

There is a delicate balance between nanoparticle surface properties to achieve colloidal stability and selectivity while still maintaining sufficient hydrophobicity to facilitate air bubble attachment in flotation. For example, by introducing 2000 Da poly(ethylene glycol) methyl ether methacrylate (PEG-M) at the polystyrene nanoparticle surface the ccc value is increased, but at the cost of reduced floatation performance since PEG-M modified nanoparticles are too hydrophilic to promote flotation⁶⁴. Hydrophobic nanoparticles with low ccc value are more likely to form large aggregates in the flotation pulp, which deteriorates flotation. The green area indicated in Figure 8 is the flotation domain of nanoparticle flotation collectors.

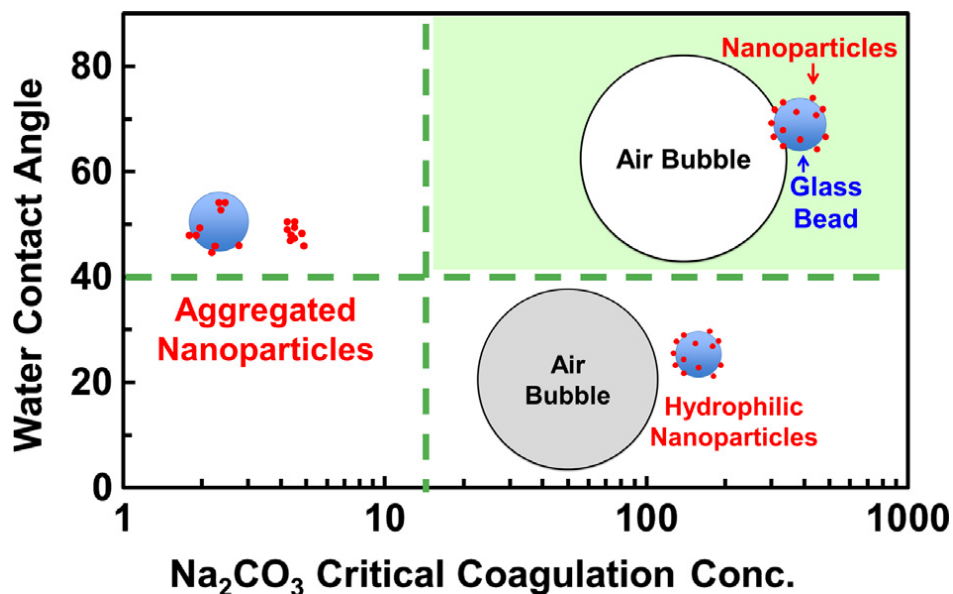


Figure 8 Selection criteria for nanoparticle flotation collectors. (Figure adapted from reference⁶⁴. Copyright ©2015 Elsevier Inc. Reprinted with permission.)

1.2.4 Role of Nanoparticle Size and Softness in Flotation

Yang et al.⁶¹ reported the flotation performance of nanoparticle collectors as a function of particle diameter. In their study, a series of polystyrene nanoparticles with diameters ranging from 46 nm to 2227 nm with constant contact angle values were tested. Flotation experiments revealed that smaller nanoparticles are more effective collectors than large particles. The large nanoparticles (> 100 nm) were poor collectors even at a high dosage that could give the same number concentration as the smaller nanoparticles. The authors speculated that large nanoparticles have lower attachment efficiency to air bubbles (Figure 9a), and proposed that the difference in the ability to attach to an air bubble depend on (1) the deposition kinetics, (2) the surface coverage, and (3) abilities to promote TPCL expansion. QCM-D experiments revealed that it took 10 minutes to achieve saturation when adsorbing 120 nm polystyrene nanoparticles onto a silica sensor, resulting in 28% to 37% surface coverage, while for 46 nm polystyrene nanoparticles the time was less than 5 minutes. For a given mass dosage, smaller nanoparticles cover more surface area, resulting in higher contact angle values due to lower exposure of the hydrophilic substrate. For a given coverage, the distance that the TPCL is required to jump is decreasing with the nanoparticle diameter. The authors also concluded that adsorbed nanoparticles were not removed during the flotation, since dried recovered beads could be refloated without adding additional collector.

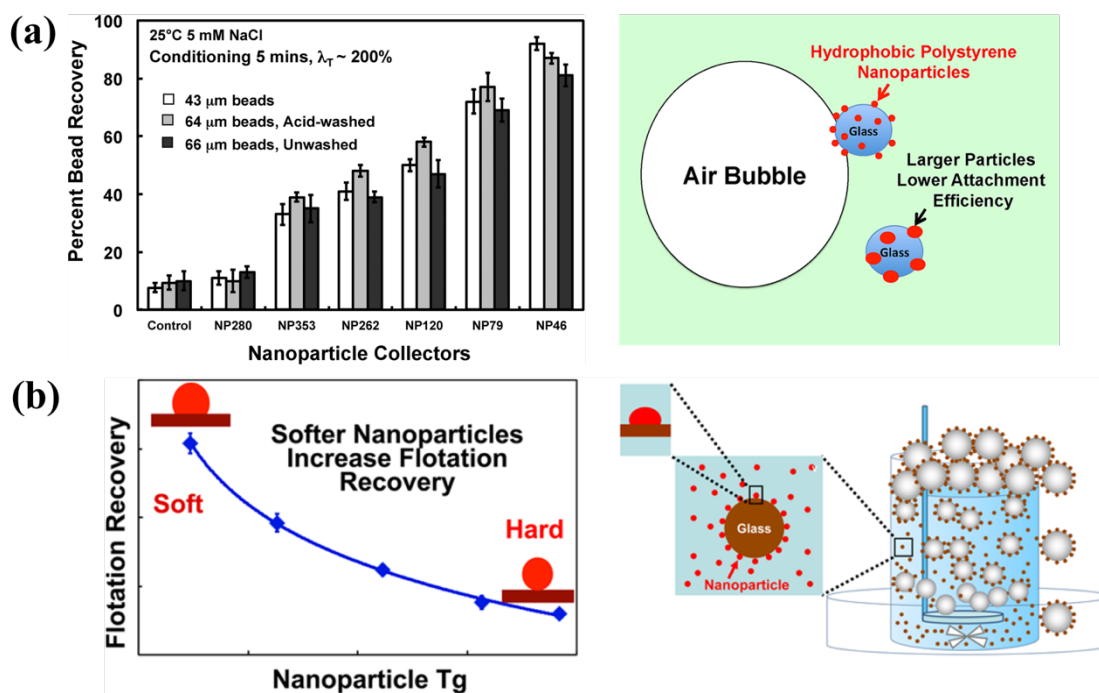


Figure 9 Influence of the (a) size and (b) softness of nanoparticle collectors on flotation performance. (Figure redrawn from references^{61,62}. Copyrights © 2011 and 2013 American Chemical Society. Reprinted with permissions.)

The influence of nanoparticle softness on flotation performance has also been assessed in the literature⁶². Figure 9b shows the flotation recovery of five poly (styrene-co-n-butyl acrylate) nanoparticles with approximately constant size, surface charge density and hydrophobicity, but variable glass transition temperature (T_g) ranging from 14 °C to 115 °C. The flotation performance of soft nanoparticle collectors was superior to the performance of rigid nanoparticles. The Young-Laplace equation was used to estimate the contact area of the liquid-like soft particles and they had 10 times larger contact area⁶² than what was estimated for rigid particles by JKR theory⁷⁰⁻⁷². Based on the influence of nanoparticle softness on the adhesion to surfaces⁷³⁻⁷⁵, the authors concluded that softer nanoparticles could be expected to have a larger contact area with glass beads/pentlandite particles, giving stronger adhesion resulting in higher flotation efficiency.

1.2.5 Controversies and Unsolved Issues

The efficiency of nanoparticle flotation collectors is a function of the particle hydrophobicity, size and softness. Studies of nanoparticle size have concluded that nanoparticles with a hydrodynamic diameter over 100 nm were a poor collector (recovering less than 50% glass beads)⁶¹, while over 90% recovery could be achieved for soft nanoparticle collectors with a diameter of about 250 nm⁶². It is possible that adsorbed large soft nanoparticles deform on the bead surface and then cover equivalent surface as a hard particle of small diameter. Therefore, an independent evaluation of the role of nanoparticle size and softness in flotation will be conducted in this thesis.

The previous nanoparticle softness study⁶² revealed that soft nanoparticles were superior since they gave strong nanoparticle/glass bead (model of mineral particles) adhesion that could induce high recovery. The poor flotation performance of rigid nanoparticles was conversely concluded to be a result of weak adhesion. The suggested mechanism was that adsorbed rigid nanoparticles with weak adhesion to glass could not withstand the mechanical and dynamic forces in the flotation cell and were therefore dislodged from bead surface. Dislodged nanoparticles leave behind hydrophilic sites that have relatively low attachment efficacy with air bubbles and therefore do not promote flotation. However, it was claimed that the flotation operation was unable to remove adsorbed nanoparticles⁶¹, since dried recovered beads could be refloated without adding additional collector⁶¹, which is conflict with the discussions addressed in the nanoparticle softness study⁶². Additionally, provided evidence is insufficient to draw a firm conclusion about the unlikely nanoparticle desorption in flotation, since the adhesion between surfaces is humidity dependent⁷⁶⁻⁷⁸ and the nanoparticle/glass adhesion in a never dried flotation system is weaker than that experienced a dry state. Further assessments of nanoparticle immobilization on bead surfaces and measurements of the nanoparticle/mineral adhesion will be included in this thesis.

Finally, since there was a lack of direct evidence included in the nanoparticle size study to support the conclusion that large nanoparticle present lower surface coverage on bead surface than small nanoparticles, more electron microscopy analysis of glass beads will be presented in this thesis.

1.3 Nanoparticles

Manipulation of particle morphology is an essential part of producing a nanoparticle flotation collector with specific hydrophobicity, size and adhesion. Multiple processes are available to create nanoparticles with homogenous spherical and anisotropic morphologies, and main strategies related to the work in this thesis are outlined below. A number of different techniques that can be used to characterize particle morphology and chemical composition. Scanning electron microscopy (SEM) and transmission electron microscopy (TEM) are the most common techniques for imaging of particles for morphology characterization purposes. If the equipment is fitted with energy dispersive X-ray spectroscopy (EDS), the elemental composition of selected parts of the sample can be obtained. In addition, atomic force microscopy (AFM) can be used to analyze the nanoparticle topography as well as, using a customized colloidal probe, the adhesive properties of the nanoparticle.

1.3.1 Spherical Nanoparticles

A versatile method to produce spherical polymeric nanoparticles in an aqueous system is emulsion polymerization⁷⁹. Ingredients in the recipes and process strategies are the two main aspects that determine the size of synthesized nanoparticles. In a classical emulsion polymerization recipe, water soluble surfactant and initiator; and monomer with low water solubility are fed into a reactor filled with water⁸⁰. The polymerization starts rapidly as the initiator decomposes into free radicals. Polymer particle nuclei form with monomers inside surfactant micelles and then grow from the micelle into the aqueous phase⁸¹. Surfactant from the micelles are eventually adsorbed on the nanoparticle surface.

Mono-disperse spherical nanoparticles can also be produced by surfactant free emulsion polymerization, which differs from classical emulsion polymerization through the lack of surfactant. Polymerization starts by the addition of a radical to a water solution containing a portion of the total monomer amount. As the carbon chain grows, the formed oligomers with a hydrophilic end group become immiscible with water and therefore act as “surfactants” and assemble into micelles⁸². After this initial step, the process is similar to classical emulsion polymerization with the subsequent polymerization occurring exclusively in the micelles formed in the initial step. Amino groups deriving from initiator are covalently linked to the nanoparticle surface, and thus synthesized polymeric nanoparticles remain fully dispersed in solution. As a result of the short nucleation time and long chain growth time, particles synthesized this way have a narrow size distribution⁸³.

Addition of a large quantity of surfactant allows for synthesis of ultrafine nanoparticles via micro-emulsion polymerization⁸⁴. However, the difficulty to remove the excess surfactant from the latex is a major drawback of micro-emulsion polymerization. An alternative method for synthesis of small nanoparticles is monomer-starved semi batch emulsion polymerization where monomers are added at a fixed rate⁸⁵.

1.3.2 Anisotropic Nanoparticles

Janus Nanoparticles

The concept of Janus particle was coined by de Gennes in 1992⁸⁶. He borrowed the name “Janus” from the Roman God, who has two faces looking in opposite directions, to describe a special class of nanoparticles with different properties on two sides. Figure 10 summarizes the different types of Janus nanoparticles⁸⁷. Distinct interfacial properties in terms of composition, polarity, electrical properties, functionality and chemistry promote Janus nanoparticles for applications as stabilizers⁸⁸⁻⁹¹; in switchable display devices⁹²; in chemical⁹³, optical⁹⁴ and biological⁹⁵ sensors; and as anisotropic building blocks for super structures⁹⁶⁻⁹⁹. Janus nanoparticles are frequently fabricated by surface functionalization of homogenous nanoparticles or through phase separation methods. Surface functionalization techniques involve immobilizing nanoparticles at an interface, such as wax/water¹⁰⁰, solid/liquid^{101, 102}, and Pickering emulsion¹⁰³⁻¹⁰⁵ interfaces, to perform selective chemical or physical modification of half of the particle. However, the step of stabilizing nanoparticles in a monolayer at an interface limits the quantities of Janus nanoparticles that can be produced^{106, 107} in one batch. Seeded emulsion polymerization strategies, which take advantage of phase separation, allow for bulk fabrication of Janus nanoparticles in solution¹⁰⁸⁻¹¹⁶.

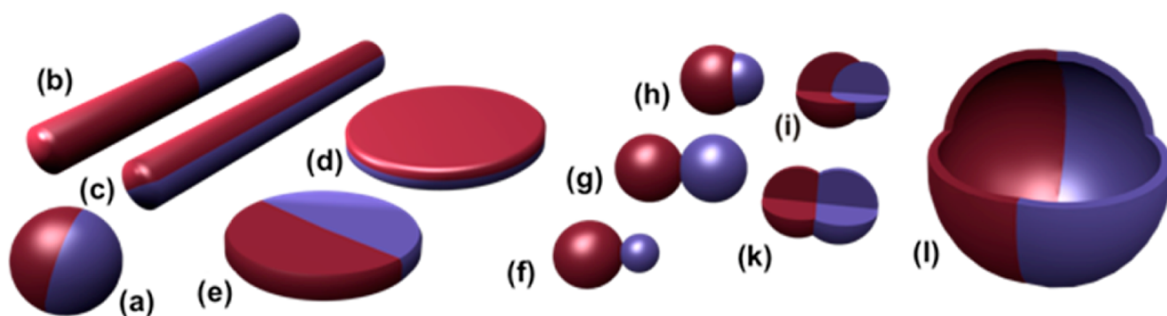


Figure 10 Illustration of Janus nanoparticle with different morphologies. (Figure adapted from reference⁸⁷. Copyright © 2013 American Chemical Society. Reprinted with permission.)

Core-shell Nanoparticles

Core-shell nanoparticle is another type of highly functional anisotropic nanoparticle. The properties arising from the shell and core materials can be distinctly different, and can be manipulated by changing either the constituting materials or the relative ratio of core and shell¹¹⁷. The purpose for adding a shell to the core particle vary and include surface modification to increase the functionality^{118, 119} and stability¹²⁰; controlling the release from the core¹²¹; and reduction in consumption of precious materials¹²². In general, core-shell nanoparticles are synthesized via a two-step process; the core particles are prepared in an initial step, followed by coating with the shell material¹²³.

Sundberg and his coworkers reported a simple route to fabricate anisotropic polystyrene/poly (n-butyl methacrylate) nanoparticles via seeded emulsion polymerization method¹⁰⁸. n-BMA monomer was added to PS seed nanoparticles, and allowed to swell seed particles at room temperature under stirring. Upon initiation, PB polymer chains starts to grow and the immiscibility between PS and PB causes a phase separation to occur. The consequent morphology depending on the experimental conditions, can be predicted using a commercial software package, UNHLATEX™_EQMORPH¹²⁴. Figure 11 illustrates the predicted morphologies from varying the sodium dodecyl sulfate (SDS) concentration¹⁰⁸. At low surfactant level, the interfacial tension between the two polymers and the water phase is relatively high, which tends to generate a core-shell structure. At a high SDS concentration, the polymer/water interfacial tension is reduced and the polymer/polymer interfacial tension becomes the dominating factor such that newly formed PB is more likely to form a lobe attached on a PS seed particle.

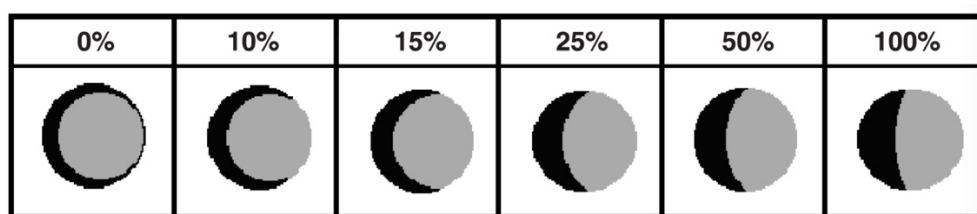


Figure 11 Predicted morphologies for PS/PB nanoparticle with various surface coverage of SDS (Figure adapted from reference¹⁰⁸. Copyright ©2003 Taylor & Francis. Reprinted with permission.)

1.4 Objectives

Because of decreasing high grade nickel ore reserves, and the technical and environmental challenges of using conventional molecular xanthate collector to separate low-grade nickel ultramafic ore, increasing efforts are directed towards finding a replacement for xanthate. Previous attempts have demonstrated that hydrophobic polymeric nanoparticles adsorbed onto hydrophilic solid surfaces can promote flotation, and these nanoparticle collectors may offer advantages over molecular collectors for ultramafic ore separation. The selection criteria for nanoparticle flotation collectors were defined as hydrophobic, colloiddally stable and selective. Experimental work revealed that hydrophobic, small and soft nanoparticle collectors were the most effective. However, there was a lack of evidence to understand the role of nanoparticle softness and size in flotation, and investigating the role of nanoparticle size and softness independently was a struggle. Two critical questions, why strong nanoparticle/mineral adhesion is required in flotation and why small nanoparticles work better than large nanoparticle collectors, will be addressed and answered in this thesis. Understanding of the mechanisms behind will be used formulate design rules for an optimal nanoparticle flotation collector. The overall objective of my work in this thesis was to evaluate the potential of soft nanoparticle collectors. The specific objectives are summarized below:

1. To expand the design rules for nanoparticle flotation collectors using a group of nanoparticle types covering a range of particle softness, shape and size.
2. To explore the relationships between, nanoparticle properties, nanoparticle/glass adhesion and the ability of the nanoparticles to promote glass bead (a model of mineral particles) flotation.
3. To understand the role why small nanoparticles are more effective than larger flotation collectors even when compared at constant surface coverage on glass bead mineral models.
4. To explain why conditioning negatively impacts nanoparticle flotation collector performance, an observation first made in this work.

1.5 Thesis Outline

Chapter 1: This chapter reviews the background of this project and contains the principle of flotation, challenges in nickel ore separation, progress and unsolved issues on the subject of nanoparticle flotation collectors, and a literature review on nanoparticle synthesis. The specific objectives of the soft nanoparticle flotation collector project and an outline of this thesis are also presented herein.

- Chapter 2: This chapter exploits the influence of nanoparticle shape and adhesive properties on the flotation. Spherical polystyrene (PS) nanoparticle, polystyrene-core-poly (butyl methacrylate)-shell (PS-PB) nanoparticle, and polystyrene/poly (butyl methacrylate) (PS/PB) Janus nanoparticle are synthesized using emulsion polymerization and their flotation performance is ranked. In addition, the critical soft shell thickness of PS-PB to achieve good flotation is determined by comparing the flotation performance of a series of PS-PB nanoparticle with different shell thickness. Adhesion of rigid PS and soft shelled PS-PB nanoparticles is characterized by colloidal probe atomic force microscopy (AFM). The critical shear force required to remove a single PS or PS-PB particle from a surface is estimated using JKR theory and adhesion values determined by AFM. This work has been published in *Industrial & Engineering Chemistry Research*, 2016, 55, 9633-9638¹²⁵.
- Chapter 3: This chapter describes the removal of adsorbed rigid nanoparticle flotation collectors by mineral particle-particle collision during flotation, named nano-scale ball milling. Removal of rigid nanoparticles by nano-scale ball milling is suggested based on observations from conditioning time studies and scanning electron microscopy observations. The fate of the dislodged nanoparticles is also explored. In addition, a mathematical model is developed to predict the surface coverage of nanoparticles by considering their deposit rate and removal rate. The corresponding flotation time for nanoparticles with different diameters and dosages are also simulated. This work was submitted to *International Journal of Mineral Processing* on July 30, 2016¹²⁶.
- Chapter 4: This chapter evaluates the effects of nano-scale ball milling on soft nanoparticle collectors. Conditioning time studies of soft shelled PS-PB and soft lobed PS/PB Janus nanoparticles with varied size are performed. Footprints, which present further evidence that nano-scale ball milling causes the removal of adsorbed nanoparticle collectors is reported in this work. A mechanism for the formation of footprints is proposed based on analysis of the morphology and composition of footprints left produced by soft-shelled core/shell nanoparticles and Janus nanoparticles with a soft lobe. In addition, the potential influence of footprints on flotation performance is assessed by a captive air bubble pickup test and an air bubble-particle attachment experiment. This chapter is in preparation for publication.
- Chapter 5: This chapter summarizes the main conclusions and major contribution of this thesis work.

1.6 References

- (1) Maurice C. Fuerstenau, G. J. a. R.-H. Y., *Froth Flotation: A Century of Innovation*. 2007, Colorado, USA.
- (2) Mousa, H. and Qasaimeh, M., Experimental Investigation of the De-inking of Recycled Newspaper Using Plastic Particles. *Separation Science and Technology* **1996**, *31*, 1093-1104.
- (3) Rubio, J.; Souza, M. L. and Smith, R. W., Overview of flotation as a wastewater treatment technique. *Minerals Engineering* **2002**, *15*, 139-155.
- (4) Ramaswamy, B.; Kar, D. D. and De, S., A study on recovery of oil from sludge containing oil using froth flotation. *Journal of Environmental Management* **2007**, *85*, 150-154.
- (5) Schramm, L. L. and Mikula, R. J., *Froth Flotation of Oil Sand Bitumen*, in *Foam Engineering*. 2012, John Wiley & Sons, Ltd. p. 251-281.
- (6) Rao, S. R., *Surface Chemistry of Froth Flotation*. Second ed. 2004, US: Springer
- (7) Wills B., F. J., *Wills' Mineral Processing Technology-An Introduction to the Practical Aspects of Ore Treatment and Mineral Recovery*. Eighth ed. 2016, USA: Elsevier.
- (8) Nguyen, A. V. and Evans, G. M., Attachment interaction between air bubbles and particles in froth flotation. *Experimental Thermal and Fluid Science* **2004**, *28*, 381-385.
- (9) Albijanic, B.; Ozdemir, O.; Nguyen, A. V. and Bradshaw, D., A review of induction and attachment times of wetting thin films between air bubbles and particles and its relevance in the separation of particles by flotation. *Advances in Colloid and Interface Science* **2010**, *159*, 1-21.
- (10) Nguyen, A. V., Hydrodynamics of liquid flows around air bubbles in flotation: a review. *International Journal of Mineral Processing* **1999**, *56*, 165-205.
- (11) Brabcová, Z.; Karapantsios, T.; Kostoglou, M.; Basařová, P. and Matis, K., Bubble–particle collision interaction in flotation systems. *Colloids and Surfaces A: Physicochemical and Engineering Aspects* **2015**, *473*, 95-103.
- (12) Firouzi, M.; Nguyen, A. V. and Hashemabadi, S. H., The effect of microhydrodynamics on bubble–particle collision interaction. *Minerals Engineering* **2011**, *24*, 973-986.
- (13) Dai, Z.; Dukhin, S.; Fornasiero, D. and Ralston, J., The Inertial Hydrodynamic Interaction of Particles and Rising Bubbles with Mobile Surfaces. *Journal of Colloid and Interface Science* **1998**, *197*, 275-292.
- (14) Hubička, M.; Basařová, P. and Vejražka, J., Collision of a small rising bubble with a large falling particle. *International Journal of Mineral Processing* **2013**, *121*, 21-30.

- (15) Nguyen, A. V.; Ralston, J. and Schulze, H. J., On modelling of bubble–particle attachment probability in flotation. *International Journal of Mineral Processing* **1998**, *53*, 225-249.
- (16) Schulze, H. J., Hydrodynamics of Bubble-Mineral Particle Collisions. *Mineral Processing and Extractive Metallurgy Review* **1989**, *5*, 43-76.
- (17) Nguyen, A. V.; Schulze, H. J. and Ralston, J., Elementary steps in particle—bubble attachment. *International Journal of Mineral Processing* **1997**, *51*, 183-195.
- (18) Nguyen-Van, A.; Kmet, S. and Schulze, H. J. *Collection events in flotation: The quantitative analysis of the particle-bubble collision and the attachment of particle onto bubble surface*. 1995. United States: Society for Mining, Metallurgy, and Exploration, Inc., Littleton, CO (United States).
- (19) Bulatovic, S. M., *Handbook of flotation reagents: chemistry, theory and practice: volume 1: flotation of sulfide ores*. 2007: Elsevier.
- (20) Bozkurt, V.; Xu, Z. and Finch, J. A., Pentlandite/pyrrhotite interaction and xanthate adsorption. *International Journal of Mineral Processing* **1998**, *52*, 203-214.
- (21) Agar, G. E., Flotation of chalcopyrite, pentlandite, pyrrhotite ores. *International Journal of Mineral Processing* **1991**, *33*, 1-19.
- (22) Lee, J. S.; Nagaraj, D. R. and Coe, J. E., Practical aspects of oxide copper recovery with alkyl hydroxamates. *Minerals Engineering* **1998**, *11*, 929-939.
- (23) Lee, K.; Archibald, D.; McLean, J. and Reuter, M. A., Flotation of mixed copper oxide and sulphide minerals with xanthate and hydroxamate collectors. *Minerals Engineering* **2009**, *22*, 395-401.
- (24) Adkins, S. J. and Pearse, M. J., The influences of collector chemistry on kinetics and selectivity in base-metal sulphide flotation. *Minerals Engineering* **1992**, *5*, 295-310.
- (25) Hodgson, M. and Agar, G. E., Eilectrochemical Investigations into the Flotation Chemistry of Pentlandite and Pyrrhotite: Process Water and Xanthate Interactions. *Canadian Metallurgical Quarterly* **1989**, *28*, 189-198.
- (26) Andreev, G. N. and Barzev, A., Raman spectroscopic study of some chalcopyrite–xanthate flotation products. *Journal of Molecular Structure* **2003**, *661–662*, 325-332.
- (27) Barbaro, M.; Herrera Urbina, R.; Cozza, C.; Fuerstenau, D. and Marabini, A., Flotation of oxidized minerals of copper using a new synthetic chelating reagent as collector. *International Journal of Mineral Processing* **1997**, *50*, 275-287.
- (28) Marabini, A. M.; Ciriachi, M.; Plescia, P. and Barbaro, M., Chelating reagents for flotation. *Minerals Engineering* **2007**, *20*, 1014-1025.

- (29) Ma, X.; Hu, Y.; Zhong, H.; Wang, S.; Liu, G. and Zhao, G., A novel surfactant S-benzoyl-N,N-diethyldithiocarbamate synthesis and its flotation performance to galena. *Applied Surface Science* **2016**, *365*, 342-351.
- (30) Jordens, A.; Marion, C.; Grammatikopoulos, T.; Hart, B. and Waters, K. E., Beneficiation of the Nechalacho rare earth deposit: Flotation response using benzohydroxamic acid. *Minerals Engineering*.
- (31) Yang, S.; Pelton, R.; Abarca, C.; Dai, Z.; Montgomery, M.; Xu, M. and Bos, J.-A., Towards nanoparticle flotation collectors for pentlandite separation. *International Journal of Mineral Processing* **2013**, *123*, 137-144.
- (32) Ackerman, P. K.; Harris, G. H.; Klimpel, R. R. and Aplan, F. F., Use of xanthogen formates as collectors in the flotation of copper sulfides and pyrite. *International Journal of Mineral Processing* **2000**, *58*, 1-13.
- (33) Aldrich, C. and Feng, D., The effect of mothers on bubble size distributions in flotation pulp phases and surface froths. *Minerals Engineering* **2000**, *13*, 1049-1057.
- (34) Finch, J. A.; Nasset, J. E. and Acuña, C., Role of frother on bubble production and behaviour in flotation. *Minerals Engineering* **2008**, *21*, 949-957.
- (35) Pérez-Garibay, R.; Ramírez-Aguilera, N.; Bouchard, J. and Rubio, J., Froth flotation of sphalerite: Collector concentration, gas dispersion and particle size effects. *Minerals Engineering* **2014**, *57*, 72-78.
- (36) Chandra, A. P. and Gerson, A. R., A review of the fundamental studies of the copper activation mechanisms for selective flotation of the sulfide minerals, sphalerite and pyrite. *Advances in Colloid and Interface Science* **2009**, *145*, 97-110.
- (37) Ansari, A. and Pawlik, M., Floatability of chalcopyrite and molybdenite in the presence of lignosulfonates. Part II. Hallimond tube flotation. *Minerals Engineering* **2007**, *20*, 609-616.
- (38) Finkelstein, N. P., The activation of sulphide minerals for flotation: a review. *International Journal of Mineral Processing* **1997**, *52*, 81-120.
- (39) Fuerstenau, D. W. and Pradip, Adsorption of frothers at coal/water interfaces. *Colloids and Surfaces* **1982**, *4*, 213-227.
- (40) Dalvi, A. D.; Bacon, W. G. and Osborne, R. C. *The past and the future of nickel laterites*. in *PDAC 2004 International Convention, Trade Show & Investors Exchange*. 2004. Toronto: The prospectors and Developers Association of Canada.
- (41) Pietrobon, M. C.; Grano, S. R.; Sobieraj, S. and Ralston, J., Recovery mechanisms for pentlandite and MgO-bearing gangue minerals in nickel ores from Western Australia. *Minerals Engineering* **1997**, *10*, 775-786.

- (42) Wellham, E. J.; Elber, L. and Yan, D. S., The role of carboxy methyl cellulose in the flotation of a nickel sulphide transition ore. *Minerals Engineering* **1992**, 5, 381-395.
- (43) Xu, Z.; Rao, S. and Finch, J., Role of diethylene triamine(DETA) in pentlandite-pyrrhotite separation. Pt. 1: complexation of metals with DETA. *Transactions of the Institution of Mining and Metallurgy. Section C. Mineral Processing and Extractive Metallurgy* **1997**, 106.
- (44) Uddin, S.; Rao, S. R.; Mirnezami, M. and Finch, J. A., Processing an ultramafic ore using fiber disintegration by acid attack. *International Journal of Mineral Processing* **2012**, 102–103, 38-44.
- (45) Dai, Z.; Bos, J.; Quinn, P.; Lee, A. and Xu, M. *Flowsheet development for Thompson ultramafic low-grade nickel ores*. in *Advances in Mineral Processing Science and Technology, 48th Annual Conference of Metallurgists of CIM*. 2009. Canadian Institute of Mining, Metallurgy and Petroleum Westmount, Quebec, Canada.
- (46) Merve Genc, A.; Kilickaplan, I. and Laskowski, J. S., Effect of pulp rheology on flotation of nickel sulphide ore with fibrous gangue particles. *Canadian Metallurgical Quarterly* **2012**, 51, 368-375.
- (47) Patra, P.; Bhambhani, T.; Vasudevan, M.; Nagaraj, D. R. and Somasundaran, P., Transport of fibrous gangue mineral networks to froth by bubbles in flotation separation. *International Journal of Mineral Processing* **2012**, 104–105, 45-48.
- (48) Bremmell, K. E.; Fornasiero, D. and Ralston, J., Pentlandite–lizardite interactions and implications for their separation by flotation. *Colloids and Surfaces A: Physicochemical and Engineering Aspects* **2005**, 252, 207-212.
- (49) Peng, Y. and Bradshaw, D., Mechanisms for the improved flotation of ultrafine pentlandite and its separation from lizardite in saline water. *Minerals Engineering* **2012**, 36–38, 284-290.
- (50) Xu, M.; Dai, Z.; DONG, J.; Ford, F. and Lee, A., Fibrous minerals in ultramafic nickel sulphide ores. *CIM Journal* **2012**, 3, 223-235.
- (51) Yada, K., Study of microstructure of chrysotile asbestos by high-resolution electron microscopy. *Acta Crystallographica Section A* **1971**, 27, 659-664.
- (52) Mani, H.; Xu, M.; Quinn, P. and Stratton-Crawley, R., The effect of ultramafic mineralogy on pentlandite flotation. *Processing of complex ores* **1997**, 1101, 63-76.
- (53) Chen, G.; Grano, S.; Sobieraj, S. and Ralston, J., The effect of high intensity conditioning on the flotation of a nickel ore. Part 1: Size-by-size analysis. *Minerals Engineering* **1999**, 12, 1185-1200.

- (54) Chen, G.; Grano, S.; Sobieraj, S. and Ralston, J., The effect of high intensity conditioning on the flotation of a nickel ore, part 2: Mechanisms. *Minerals Engineering* **1999**, *12*, 1359-1373.
- (55) Feng, B.; Feng, Q. and Lu, Y., The effect of lizardite surface characteristics on pyrite flotation. *Applied Surface Science* **2012**, *259*, 153-158.
- (56) Peng, Y. J. and Seaman, D., Effect of feed preparation on copper activation in flotation of Mt Keith pentlandite. *Mineral Processing and Extractive Metallurgy* **2012**, *121*, 131-139.
- (57) DONG, J. and Xu, M., Evaluation of environmentally friendly collectors for xanthate replacement. *Proceedings of the 43rd Annual Meeting of the Canadian Mineral Processors Conference, CIM, Ottawa, ON, Canada* **2011**, 289-302.
- (58) Nagaraj, D. R. and Farinato, R. S., Evolution of flotation chemistry and chemicals: A century of innovations and the lingering challenges. *Minerals Engineering* **2016**, *96–97*, 2-14.
- (59) Yang, S.; Pelton, R.; Raegen, A.; Montgomery, M. and Dalnoki-Veress, K., Nanoparticle Flotation Collectors: Mechanisms Behind a New Technology. *Langmuir* **2011**, *27*, 10438-10446.
- (60) Yang, S. and Pelton, R., Nanoparticle Flotation Collectors II: The Role of Nanoparticle Hydrophobicity. *Langmuir* **2011**, *27*, 11409-11415.
- (61) Yang, S.; Pelton, R.; Montgomery, M. and Cui, Y., Nanoparticle Flotation Collectors III: The Role of Nanoparticle Diameter. *ACS Applied Materials & Interfaces* **2012**, *4*, 4882-4890.
- (62) Yang, S.; Razavizadeh, B. B. M.; Pelton, R. and Bruin, G., Nanoparticle Flotation Collectors—The Influence of Particle Softness. *ACS Applied Materials & Interfaces* **2013**, *5*, 4836-4842.
- (63) Abarca, C.; Ali, M. M.; Bowie, D. and Pelton, R. H., A simple assay for azide surface groups on clickable polymeric nanoparticles. *Colloids and Surfaces A: Physicochemical and Engineering Aspects* **2016**, *508*, 192-196.
- (64) Abarca, C.; Yang, S. and Pelton, R. H., Towards high throughput screening of nanoparticle flotation collectors. *Journal of Colloid and Interface Science* **2015**, *460*, 97-104.
- (65) Abarca, C.; Ali, M. M.; Yang, S.; Dong, X. and Pelton, R. H., A Colloidal Stability Assay Suitable for High-Throughput Screening. *Analytical Chemistry* **2016**, *88*, 2929-2936.
- (66) Goodwin, J., *Colloids and Interfaces with Surfactants and Polymers* 2009, WILEY.
- (67) Williams, D. J. A. and Williams, K. P., Electrophoresis and zeta potential of kaolinite. *Journal of Colloid and Interface Science* **1978**, *65*, 79-87.

- (68) Doane, T. L.; Chuang, C.-H.; Hill, R. J. and Burda, C., Nanoparticle ζ -Potentials. *Accounts of Chemical Research* **2012**, *45*, 317-326.
- (69) Israelachvili, J. N., *Intermolecular and Surface Forces-Third Edition*. 2011, Elsevier. p. 263.
- (70) Kevin, K., *Molecular Adhesion and Its Application-The Sticky Universe*. 2001, New York, USA.
- (71) Berg, J. C., *An introduction to interfaces & colloids: the bridge to nanoscience*. 2010: World Scientific.
- (72) Assemi, S.; Nalaskowski, J. and Johnson, W. P., Direct force measurements between carboxylate-modified latex microspheres and glass using atomic force microscopy. *Colloids and Surfaces A: Physicochemical and Engineering Aspects* **2006**, *286*, 70-77.
- (73) Engqvist, C.; Forsberg, S.; Norgren, M.; Edlund, H.; Andreasson, B. and Karlsson, O., Interactions between single latex particles and silica surfaces studied with AFM. *Colloids and Surfaces A: Physicochemical and Engineering Aspects* **2007**, *302*, 197-203.
- (74) Tomas, J., Adhesion of ultrafine particles—A micromechanical approach. *Chemical Engineering Science* **2007**, *62*, 1997-2010.
- (75) Carrillo, J.-M. Y.; Raphael, E. and Dobrynin, A. V., Adhesion of Nanoparticles. *Langmuir* **2010**, *26*, 12973-12979.
- (76) Fuji, M.; Machida, K.; Takei, T.; Watanabe, T. and Chikazawa, M., Effect of Wettability on Adhesion Force between Silica Particles Evaluated by Atomic Force Microscopy Measurement as a Function of Relative Humidity. *Langmuir* **1999**, *15*, 4584-4589.
- (77) Jones, R.; Pollock, H. M.; Cleaver, J. A. S. and Hodges, C. S., Adhesion Forces between Glass and Silicon Surfaces in Air Studied by AFM: Effects of Relative Humidity, Particle Size, Roughness, and Surface Treatment. *Langmuir* **2002**, *18*, 8045-8055.
- (78) White, C.; Tan, K. T.; Hunston, D.; Steffens, K.; Stanley, D. L.; Satija, S. K.; Akgun, B. and Vogt, B. D., Mechanisms of criticality in environmental adhesion loss. *Soft matter* **2015**, *11*, 3994-4001.
- (79) van Herk, A. and Heuts, H., *Emulsion Polymerization*, in *Encyclopedia of Polymer Science and Technology*. 2002, John Wiley & Sons, Inc.
- (80) Warson, H., Emulsion polymerization, a mechanistic approach. R. G. Gilbert. Academic Press, London, 1995. pp. xviii + 362, price £55.00. ISBN 0-12-283060-1. *Polymer International* **1996**, *41*, 352-352.
- (81) Harkins, W. D., A General Theory of the Mechanism of Emulsion Polymerization I. *Journal of the American Chemical Society* **1947**, *69*, 1428-1444.

- (82) Goodall, A. R.; Wilkinson, M. C. and Hearn, J., Mechanism of emulsion polymerization of styrene in soap-free systems. *Journal of Polymer Science: Polymer Chemistry Edition* **1977**, *15*, 2193-2218.
- (83) Goodwin, J. W.; Ottewill, R. H. and Pelton, R., Studies on the preparation and characterization of monodisperse polystyrene latices V.: The preparation of cationic latices. *Colloid and Polymer Science* **1979**, *257*, 61-69.
- (84) Guo, J. S.; El-Aasser, M. S. and Vanderhoff, J. W., Microemulsion polymerization of styrene. *Journal of Polymer Science Part A: Polymer Chemistry* **1989**, *27*, 691-710.
- (85) Sajjadi, S., Nanoparticle Formation by Monomer-Starved Semibatch Emulsion Polymerization. *Langmuir* **2007**, *23*, 1018-1024.
- (86) de Gennes, P. G., Soft Matter. *Science* **1992**, *256*, 495.
- (87) Walther, A. and Müller, A. H. E., Janus Particles: Synthesis, Self-Assembly, Physical Properties, and Applications. *Chemical Reviews* **2013**, *113*, 5194-5261.
- (88) Glaser, N.; Adams, D. J.; Böker, A. and Krausch, G., Janus Particles at Liquid–Liquid Interfaces. *Langmuir* **2006**, *22*, 5227-5229.
- (89) Teo, B. M.; Suh, S. K.; Hatton, T. A.; Ashokkumar, M. and Grieser, F., Sonochemical Synthesis of Magnetic Janus Nanoparticles. *Langmuir* **2011**, *27*, 30-33.
- (90) Kim, S.-H.; Lee, S. Y. and Yang, S.-M., Janus Microspheres for a Highly Flexible and Impregnable Water-Repelling Interface. *Angewandte Chemie International Edition* **2010**, *49*, 2535-2538.
- (91) Ikem, V. O.; Menner, A. and Bismarck, A., High Internal Phase Emulsions Stabilized Solely by Functionalized Silica Particles. *Angewandte Chemie International Edition* **2008**, *47*, 8277-8279.
- (92) Nisisako, T.; Torii, T.; Takahashi, T. and Takizawa, Y., Synthesis of Monodisperse Bicolored Janus Particles with Electrical Anisotropy Using a Microfluidic Co-Flow System. *Advanced Materials* **2006**, *18*, 1152-1156.
- (93) Şologan, M.; Marson, D.; Polizzi, S.; Pengo, P.; Boccardo, S.; Pricl, S.; Posocco, P. and Pasquato, L., Patchy and Janus Nanoparticles by Self-Organization of Mixtures of Fluorinated and Hydrogenated Alkanethiolates on the Surface of a Gold Core. *ACS Nano* **2016**.
- (94) McConnell, M. D.; Kraeutler, M. J.; Yang, S. and Composto, R. J., Patchy and Multiregion Janus Particles with Tunable Optical Properties. *Nano Letters* **2010**, *10*, 603-609.

- (95) Sánchez, A.; Díez, P.; Martínez-Ruiz, P.; Villalonga, R. and Pingarrón, J. M., Janus Au-mesoporous silica nanoparticles as electrochemical biorecognition-signaling system. *Electrochemistry Communications* **2013**, *30*, 51-54.
- (96) Glotzer, S. C. and Solomon, M. J., Anisotropy of building blocks and their assembly into complex structures. *Nature materials* **2007**, *6*, 557-562.
- (97) Chen, T.; Yang, M.; Wang, X.; Tan, L. H. and Chen, H., Controlled assembly of eccentrically encapsulated gold nanoparticles. *Journal of the American Chemical Society* **2008**, *130*, 11858-11859.
- (98) Du, X.; Liu, X.; Chen, H. and He, J., Facile fabrication of raspberry-like composite nanoparticles and their application as building blocks for constructing superhydrophilic coatings. *The Journal of Physical Chemistry C* **2009**, *113*, 9063-9070.
- (99) Kim, J. W.; Kim, J. H. and Deaton, R., DNA-Linked Nanoparticle Building Blocks for Programmable Matter. *Angewandte Chemie International Edition* **2011**, *50*, 9185-9190.
- (100) Hong, L.; Jiang, S. and Granick, S., Simple Method to Produce Janus Colloidal Particles in Large Quantity. *Langmuir* **2006**, *22*, 9495-9499.
- (101) Wang, B.; Li, B.; Zhao, B. and Li, C. Y., Amphiphilic Janus Gold Nanoparticles via Combining “Solid-State Grafting-to” and “Grafting-from” Methods. *Journal of the American Chemical Society* **2008**, *130*, 11594-11595.
- (102) Anderson, K. D.; Luo, M.; Jakubiak, R.; Naik, R. R.; Bunning, T. J. and Tsukruk, V. V., Robust Plasma Polymerized-Titania/Silica Janus Microparticles. *Chemistry of Materials* **2010**, *22*, 3259-3264.
- (103) Liu, B.; Wei, W.; Qu, X. and Yang, Z., Janus Colloids Formed by Biphasic Grafting at a Pickering Emulsion Interface. *Angewandte Chemie* **2008**, *120*, 4037-4039.
- (104) Suzuki, D.; Tsuji, S. and Kawaguchi, H., Janus Microgels Prepared by Surfactant-Free Pickering Emulsion-Based Modification and Their Self-Assembly. *Journal of the American Chemical Society* **2007**, *129*, 8088-8089.
- (105) Pardhy, N. P. and Budhlall, B. M., Pickering Emulsion as a Template to Synthesize Janus Colloids with Anisotropy in the Surface Potential. *Langmuir* **2010**, *26*, 13130-13141.
- (106) Du, J. and O'Reilly, R. K., Anisotropic particles with patchy, multicompartments and Janus architectures: preparation and application. *Chemical Society Reviews* **2011**, *40*, 2402-2416.
- (107) Bradley, L. C.; Stebe, K. J. and Lee, D., Clickable Janus Particles. *Journal of the American Chemical Society* **2016**, *138*, 11437-11440.
- (108) Sundberg, D. C. and Durant, Y. G., Latex Particle Morphology, Fundamental Aspects: A Review. *Polymer Reaction Engineering* **2003**, *11*, 379-432.

- (109) Sheu, H. R.; El-Aasser, M. S. and Vanderhoff, J. W., Uniform nonspherical latex particles as model interpenetrating polymer networks. *Journal of Polymer Science Part A: Polymer Chemistry* **1990**, *28*, 653-667.
- (110) Sheu, H. R.; El-Aasser, M. S. and Vanderhoff, J. W., Phase separation in polystyrene latex interpenetrating polymer networks. *Journal of Polymer Science Part A: Polymer Chemistry* **1990**, *28*, 629-651.
- (111) Kim, J.-W.; Larsen, R. J. and Weitz, D. A., Synthesis of Nonspherical Colloidal Particles with Anisotropic Properties. *Journal of the American Chemical Society* **2006**, *128*, 14374-14377.
- (112) Mock, E. B. and Zukoski, C. F., Emulsion Polymerization Routes to Chemically Anisotropic Particles. *Langmuir* **2010**, *26*, 13747-13750.
- (113) Park, J.-G.; Forster, J. D. and Dufresne, E. R., High-Yield Synthesis of Monodisperse Dumbbell-Shaped Polymer Nanoparticles. *Journal of the American Chemical Society* **2010**, *132*, 5960-5961.
- (114) Pan, M.; Yang, L.; Guan, B.; Lu, M.; Zhong, G. and Zhu, L., Surface nucleation-induced fluoropolymer Janus nanoparticles via emulsifier-free batch-seeded emulsion polymerization. *Soft Matter* **2011**, *7*, 11187-11193.
- (115) van Ravensteijn, B. G. P.; Kamp, M.; van Blaaderen, A. and Kegel, W. K., General Route toward Chemically Anisotropic Colloids. *Chemistry of Materials* **2013**, *25*, 4348-4353.
- (116) Liu, B.; Liu, J.; Liang, F.; Wang, Q.; Zhang, C.; Qu, X.; Li, J.; Qiu, D. and Yang, Z., Robust Anisotropic Composite Particles with Tunable Janus Balance. *Macromolecules* **2012**, *45*, 5176-5184.
- (117) Oldenburg, S. J.; Averitt, R. D.; Westcott, S. L. and Halas, N. J., Nanoengineering of optical resonances. *Chemical Physics Letters* **1998**, *288*, 243-247.
- (118) Kim, J.; Kim, H. S.; Lee, N.; Kim, T.; Kim, H.; Yu, T.; Song, I. C.; Moon, W. K. and Hyeon, T., Multifunctional uniform nanoparticles composed of a magnetite nanocrystal core and a mesoporous silica shell for magnetic resonance and fluorescence imaging and for drug delivery. *Angewandte Chemie International Edition* **2008**, *47*, 8438-8441.
- (119) Giannakopoulos, G.; Masania, K. and Taylor, A. C., Toughening of epoxy using core-shell particles. *Journal of Materials Science* **2011**, *46*, 327-338.
- (120) Wang, D.; Xin, H. L.; Hovden, R.; Wang, H.; Yu, Y.; Muller, D. A.; DiSalvo, F. J. and Abruña, H. D., Structurally ordered intermetallic platinum-cobalt core-shell nanoparticles with enhanced activity and stability as oxygen reduction electrocatalysts. *Nature materials* **2013**, *12*, 81-87.

- (121) Haag, R., Supramolecular drug-delivery systems based on polymeric core-shell architectures. *Angewandte Chemie International Edition* **2004**, *43*, 278-282.
- (122) Mayrhofer, K. J. J.; Juhart, V.; Hartl, K.; Hanzlik, M. and Arenz, M., Adsorbate-Induced Surface Segregation for Core-Shell Nanocatalysts. *Angewandte Chemie International Edition* **2009**, *48*, 3529-3531.
- (123) Ghosh Chaudhuri, R. and Paria, S., Core/Shell Nanoparticles: Classes, Properties, Synthesis Mechanisms, Characterization, and Applications. *Chemical Reviews* **2012**, *112*, 2373-2433.
- (124) Durant, Y. G. and Sundberg, D. C., An advanced computer algorithm for determining morphology development in latex particles. *Journal of Applied Polymer Science* **1995**, *58*, 1607-1618.
- (125) Dong, X.; Marway, H. S.; Cranston, E. D. and Pelton, R. H., Relating Nanoparticle Shape and Adhesiveness to Performance as Flotation Collectors. *Industrial & Engineering Chemistry Research* **2016**, *55*, 9633-9638.
- (126) Dong, X.; Price, M.; Dai, Z.; Xu, M. and Pelton, R., Mineral-Mineral Particle Collisions During Flotation Remove Adsorbed Nanoparticle Flotation Collectors. *International Journal of Mineral Processing* **2016**, *Submitted*.

Chapter 2 Relating Nanoparticle Shape and Adhesiveness to Performance as Flotation Collectors

In chapter 2, all experiments, except AFM, were conducted by myself. I came up the AFM experimental plan, prepared the AFM samples. Heera Marway performed the AFM force measurements and trained me how to use the software to process the AFM data. Dr. Cranston and Heera Marway contributed useful discussions on the AFM data analysis. I plotted all experimental data. Dr. Pelton did the calculation of nanoparticle displacement shear rate. I wrote the manuscript, and Dr. Cranston edited the part related with AFM. Dr. Pelton edited the rest sections into this final version. This work has been published in *Industrial & Engineering Chemistry Research*, 2016, 55, 9633-9638¹²⁵. Copyright ©2016 American Chemical Society. Reprinted with permission.

This is an open access article published under an ACS AuthorChoice License, which permits copying and redistribution of the article or any adaptations for non-commercial purposes.



Article

pubs.acs.org/IECR



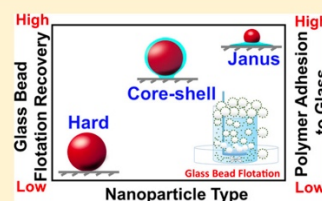
Relating Nanoparticle Shape and Adhesiveness to Performance as Flotation Collectors

Xiaofei Dong, Heera S. Marway, Emily D. Cranston, and Robert H. Pelton*

Department of Chemical Engineering, McMaster University, 1280 Main Street West, Hamilton, Ontario, Canada L8S 4L8

Supporting Information

ABSTRACT: Cationic polystyrene-core-poly(*n*-butyl methacrylate)-shell (PS–PB) nanoparticles perform as flotation collectors as they spontaneously adsorb onto 43 μm glass beads in water, promoting glass bead attachment to air bubbles. Under our flotation conditions at room temperature, polystyrene is a hard plastic, whereas, with glass transition near room temperature, poly(*n*-butyl methacrylate) is a soft polymer. Colloidal probe atomic force microscopy measurements revealed that the pull-off forces and the work of adhesion of PS–PB nanoparticles to glass were significantly higher than observed with harder PS particles. Glass bead recovery in laboratory flotation experiments increased significantly with thickness of the soft PB shells on the PB–PS core/shell nanoparticles. Ninety-two nm Janus particles consisting of one PS and one PB lobe were also very effective collectors. We propose that high nanoparticle/glass bead adhesion minimizes nanoparticle removal by bead/bead collisions (nanoscale ball milling) during mixing and flotation.



INTRODUCTION

Froth flotation is arguably the most important unit operation in mineral processing.¹ Flotation is often the most practical approach to the isolation of a small quantity of mineral rich material diluted with a large quantity of unwanted gangue. A critical step in flotation is the selective hydrophobization of mineral-rich particles (typically 100 μm diameter) with a hydrophobization agent called a collector. The treated particles adhere to air bubbles and rise to the froth phase, leaving behind the unwanted gangue. For nickel ore recovery, a typical collector is potassium amyl xanthate, a small molecule that chemisorbs onto nickel sulfide surfaces.

For the past few years we have been exploring the use of hydrophobic polymer nanoparticles as flotation collectors as they may offer advantages when the mineral particle surfaces are contaminated. We have reported both mechanistic studies^{2–4} and more practical mineral separation trials.^{5,6} Although we have done a substantial amount of mechanistic work, two important observations remain unexplained: first, smaller 50 nm diameter particles are consistently more effective than 100 nm and larger particles, even when compared at the same density of adsorbed particles on the mineral surface;⁴ and, second, soft polymer nanoparticles whose glass transition temperatures are near the flotation temperature are superior to hard polymer particles.⁷ In this work we give evidence to explain why softer and smaller nanoparticles are superior. This is important information for optimizing the design of nanoparticle flotation collectors.

We first explored the role of nanoparticle softness by preparing a series of polystyrene-co-poly(*n*-butyl methacrylate) uniform copolymer particles.⁷ The softer the particle, the higher the flotation recovery. We speculated that the softer particles gave stronger adhesion to mineral particle surfaces. There was

no proof for this hypothesis, and no estimate of the required strength of adhesion. Both of these issues are resolved in this work.

Most commercial flotation systems are very complex mixtures, both in terms of size, shape, and chemical composition. Effective nanoparticle collectors must have surface functionality that promotes specific adhesion to the mineral rich ore particles and not on the unwanted gangue. For example, amine and imidazole groups promote selective adhesion to pentlandite, the predominant nickel mineral.⁶ However, it is difficult to tease out fundamental mechanisms using complex ore suspensions. Instead, we have found that flotation measurements employing uniform glass bead suspensions treated with cationic polymer nanoparticles (latex) yield many important details. For example, with the most effective small nanoparticles, as little as 5% surface area coverage with adsorbed nanoparticles gave efficient flotation separation.³ This was an important observation because it suggested that nanoparticle flotation collectors could be economically viable. One limitation of the glass bead model is that it does not address the ability of collectors to specifically deposit onto mineral rich ore particles in complex ore mixtures. Ultimately potential new collectors must be evaluated in real ore suspensions. However, in this work we rely on glass bead models to explore the role of nanoparticle/mineral particle adhesion.

In this paper we compare results of these pristine glass bead flotation experiments for polystyrene (PS), polystyrene-core-

Received: June 29, 2016

Revised: August 8, 2016

Accepted: August 22, 2016

Published: August 22, 2016

poly(*n*-butyl methacrylate)-shell (PS–PB), and Janus nanoparticles (hard PS lobe and a soft PB lobe). In addition, colloidal probe atomic force microscopy (AFM) adhesion measurements are used to compare the adhesion characteristics of hard PS and soft-shelled PS–PB nanoparticles.

■ EXPERIMENTAL SECTION

Materials. Styrene (>99%), *n*-butyl methacrylate (>99%), and methyl methacrylate (>99%) were purchased from Sigma-Aldrich and passed through a prepacked inhibitor removing column before use. 2,2'-Azobis(2-methylpropionamide) dihydrochloride (V50, 97%), hexadecyltrimethylammonium bromide (CTAB, >98%), potassium bromide (>99%, FTIR grid), and Dowex MB mixed bed ion-exchange resin were purchased from Sigma-Aldrich and used as supplied. Sodium chloride (>95%), sulfuric acid (>98%), and hydrogen peroxide were purchased from Fisher Scientific and used as supplied. Glass beads with a mean diameter of 43 μm and a standard deviation of 11 μm , determined by a Malvern Mastersizer 2000, were purchased from Polysciences Inc. and used as supplied. The flotation frother, UNIFROTH 250C (>99%), a mixture of monomethyl polypropylene glycol, 250 kDa, and dipropylene glycol monomethyl ether, was donated by VALE Canada Limited (Mississauga, ON) and used as supplied. All water was processed with a Barnstead Nanopure Diamond System (Thermo Scientific) and had a resistance over 18 M Ω cm.

Core–Shell Nanoparticle Synthesis. A series of cationic polystyrene-core-poly(*n*-butyl methacrylate)-shell (PS–PB) were prepared. The recipes are summarized in Table 1, and

Table 1. Summary of the PS–PB Core-Shell Latex Polymerization Recipes

nanoparticle designation	PS317 seed latex (3.6 wt %), g	water, g	<i>n</i> -butyl methacrylate, g	V50, g
PS–PB1	20	20	0.09	0.005
PS–PB2	20	20	0.18	0.01
PS–PB3	20	20	0.36	0.018

the core–shell particle properties are summarized in Table 2. The preparation of PS–PB3 is now described. The cationic PS317 seed latex was prepared by surfactant-free emulsion polymerization.⁸ 100 g of water was charged into a 250 mL three-neck round-bottom flask fitted with a 2-bladed Teflon flat plate stirrer. The temperature was controlled at 70 °C with an oil bath heated by a hot plate (IKA, C-MAG HS 7) equipped with an electronic contact thermometer (IKA, ETS-D5). After a 30 min nitrogen purge, styrene (5 g) and V50 (0.1 g, dissolved in 5 mL of water) were added to the flask. The reaction mixture was stirred at a speed of 250 rpm (IKA, EUROSTAR 20 digital) for 5 h with a slight nitrogen overpressure. The PS seed

latex was purified by mixing with 50 g of mixed bed ion-exchange resin for 30 min, followed by filtration to remove the resin. The procedure was repeated several times until the conductivity was lower than 20 $\mu\text{S}/\text{cm}$.

For the shell polymerization, a mixture of purified PS317 seed latex (20 g, solids content: 3.6 wt %) and water (20 g) was sonicated in an ultrasonic bath for 30 min and followed by purging with nitrogen for 30 min. Then *n*-butyl methacrylate (0.36 g) was added and stirred (350 rpm) constantly for 1 h, after which V50 (18 mg, well dissolved in water) was charged into the flask. The polymerization was conducted at 70 °C for 5 h under nitrogen.

Janus Nanoparticle Synthesis. Polystyrene-poly(*n*-butyl methacrylate) Janus particles were prepared by a two-step procedure based on published recipes⁹ that were modified to give smaller particles. A polystyrene seed latex (PS63) was synthesized by monomer-starved batch emulsion polymerization. 100 g of water was added to a 250 mL three-neck round-bottom flask fitted with a 2-bladed Teflon propeller stirrer. After a 30 min nitrogen purge, 0.5 g of styrene, 0.1 g of CTAB (well dissolved in 5 mL water), and 0.1 g of V50 (well dissolved in 5 mL of water) were sequentially added. After 15 min polymerization, 4.5 g of styrene was added with a syringe pump (1 mL/h). The reaction was conducted under nitrogen purging at 70 °C with stirring (250 rpm) and was stopped after 20 h.

In the second step, a mixture of PS63 seed latex (20 g of 3.5 wt %) and water (20 g) was dispersed in an ultrasonic bath for 30 min and followed by purging with nitrogen for 30 min. Then *n*-butyl methacrylate (1.4 g) was added and stirred for 1 h, after which V50 (24 mg dissolved in mL of water) was added. The polymerization was conducted at 70 °C for 5 h in a nitrogen atmosphere.

Nanoparticle Characterization. Hydrodynamic diameters were determined using dynamic light scattering (Brookhaven Instruments Corporation) with a detector angle of 90°. Latex samples were diluted with 5 mM NaCl solution to give a scattering intensity between 100 and 150 kcps. Dispersions were equilibrated to 25 °C for 3 min before analyzing. The duration of each measurement was set at 3 min. Three sets of measurements were undertaken for each sample. The results were analyzed by BIC dynamic light scattering software (Windows 9KDLWS version 3.34) using the cumulants model, whereas the CONTIN model was used to generate the particle size distribution expressed as a polydispersity index (PDI).

Electrophoretic mobility (EM) measurements were performed on a Zeta PALS instrument (Brookhaven Instruments Corporation) at 25 °C in phase analysis light scattering mode. 1.5 mL dilute nanoparticle dispersion in 5 mM NaCl was

Table 2. Spherical Polystyrene (PS) and Polystyrene-Core-Poly(*n*-butyl methacrylate)-Shell (PS–PB) Properties^a

nanoparticle designation	diameter, nm (PDI)	shell thickness, nm	EM, $\times 10^{-8} \text{ m}^2 \text{ s}^{-1} \text{ V}^{-1}$ (SE)	water CA
PS317	317.2 (0.002)	0	4.53 (0.14)	56.7° \pm 1.5
PS–PB1	329.5 (0.032)	6.2	2.66 (0.14)	62.8° \pm 0.4
PS–PB2	344.6 (0.046)	13.7	3.73 (0.14)	64.7° \pm 0.5
PS–PB3	356.2 (0.016)	19.5	4.33 (0.10)	60.0° \pm 1.3

^aThe electrophoretic mobilities (EM) were measured in 5 mM NaCl solution at ambient pH. The thicknesses of the PB shells were determined by comparing the PS–PB diameters to the parent PS seed particle diameter; mass balance estimates give similar values. The standard errors (SE) for the reported EM values were estimated from the average of 10 runs with each consisting of 15 scans. The standard errors for the contact angle values were calculated from the average of 3 measurements, where the duration for each measurement is 30 s.

dispensed into a clear cuvette and thermally equilibrated to 25 °C before analyzing. The reported EM values were the average of 10 runs with each consisting of 15 scans.

Transmission electron microscopy (TEM) and scanning electron microscope (SEM) were used to acquire high resolution images of synthesized nanoparticles. TEM images were recorded using a JEOL 1200EX TEMSCAN microscope. A drop of diluted nanoparticle dispersion was dropped on a Formvar-coated TEM grid and air-dried prior to analysis. SEM images were recorded using a JEOL JSM 7000F microscope. Dried nanoparticles were placed on a conductive carbon tape and sputtering coated with 5 nm platinum prior to analysis. SEM images were taken at a working distance of 6.8 mm and beam energy of 2.8 kV.

Water Contact Angle (CA) Measurements. Water sessile drop contact angles on glass slides coated with nanoparticles were measured with a Krüss Drop Shape Analysis System DSA 10 running DSA software (version 1.80.0.2). In a typical water contact angle experiment, precut glass slides (1 cm squares, Gold Line Microscope Slides, VWR) were cleaned in ethanol with sonication for 30 min, followed by rinsing with water and treating with UV-Ozone (UV-Ozone ProCleaner, Bio Force Nanosciences, Ames, IA, USA) for 20 min. Cleaned glass slides were immersed in 0.5 wt % nanoparticle dispersion in 5 mM NaCl for 30 min and then dipped into 5 mM NaCl solution to rinse off unbound nanoparticles. The slides were air-dried at room temperature. Scanning electron microscopy (SEM) measurements revealed dense but single layer coverages of adsorbed particles. Example micrographs are given in the [Supporting Information](#) (Figure S1).

Colloidal Probe AFM Adhesion Measurements. The adhesion between silica sphere colloidal probes and latex coated wafers was measured by atomic force microscopy using a MFP-3D system (Asylum Research an Oxford Instruments Company, Santa Barbara, CA, USA). Precut silicon wafers (1 × 1 cm) were cleaned in 100 °C piranha solution (containing 85 mL of sulfuric acid and 35 mL of hydrogen peroxide) for 3 h. The silicon wafers were then carefully removed from cooled piranha solution, rinsed thoroughly with water, and dried with compressed air.

The cleaned wafers were immersed into 0.5 wt % nanoparticle dispersion in 5 mM NaCl for 30 min with the polished side facing upward. The treated silicon wafer was dipped into 5 mM NaCl solution to rinse off unbound nanoparticles and stored in a glass vial filled with 5 mM NaCl solution before performing force measurements.

Deflection versus distance measurements were carried out via colloidal probe AFM with an open fluid cell filled with 5 mM NaCl solution, and data were converted to force versus separation curves (based on the contact point determined as the intersection of the regions of zero deflection and constant compliance) to demonstrate pull-off forces and work of adhesion. Silica colloidal probes (2.5 μm) attached to cantilevers with nominal spring constants of 0.09 N/m were purchased from Novascan Technologies (Ames, IA, USA) and used as supplied. The spring constants of the cantilevers were calibrated by the Sader method as described elsewhere.¹⁰ All force profiles between the silica probe and never-dried nanoparticle treated silicon wafers were recorded at a constant approach and retraction velocity of 500 nm/s. Work of adhesion was calculated from the area under the retraction force curves. Igor Pro software with Asylum Research add-on (version 13) was used to collect and process all AFM data.

Flotation Testing. In our standard flotation testing, 125 mL of 5 mM NaCl solution, 0.57 mL of 3.5 wt % nanoparticle dispersion, and 2 g of 43 μm glass beads were added to a 125 mL plastic beaker. The suspension was mixed for 5 min condition time with a 25 × 25 mm cross shape magnetically stirring bar at 600 rpm, giving the cationic latex an opportunity to deposit onto the anionic glass beads. After conditioning, 0.125 mL of 1% UNIFROTH 250C frother was added and mixed for 30 s.

Flotation was performed by introducing nitrogen gas flow at a rate of 2.0 L/min through a gas dispersion tube, a 30 mm coarse glass frit attached by a 90 deg elbow (Corning, Inc. 3952530C, Fisher Scientific). During flotation, the stirring speed was increased to 900 rpm to avoid glass bead sedimentation. Foam accumulating on the beaker surface was manually scraped into a 17 cm plastic Petri dish underneath the flotation beaker. Flotation was stopped after 2 min. The masses of both the beads collected in the froth and remaining in the flotation beaker were measured, and the flotation recovery was calculated as the mass fraction of glass beads that was collected in the froth. An illustration of the flotation experiment is shown in the [Supporting Information](#) (Figure S2).

■ RESULTS

A series of core/shell particles with hard polystyrene cores and soft poly(*n*-butyl methacrylate) shells were prepared. The synthetic recipes are given in [Table 1](#), and the properties are summarized in [Table 2](#). The electron micrograph images and FTIR spectra of the nanoparticles are shown in the [Supporting Information](#) (Figures S3 and S4). The nanoparticles sizes (317 to 356 nm) are about seven times larger than the optimum size of homogeneous polystyrene nanoparticle collectors.⁴ All the particles are cationic with pristine, surfactant-free surfaces. The water contact angles were measured on a dried surface coated with a dense layer of nanoparticles. Previously we compared three types of contact angle measurements – sessile drops on a dense latex coating (the type used here), sessile drops on smooth polymer films of coalesced particles, and captive bubble (i.e., receding angles) on submerged latex coated surfaces.⁵ Each type of measurement gives a different answer; however, each method gives the same ranking when comparing a series of nanoparticles as flotation collectors.

Core/Shell Particles. Flotation experiments were performed with a very simple model system of water, 43 μm diameter glass beads, nanoparticle collector, and frother, a nonionic surfactant that promotes foam formation. The glass beads act as a model for the mineral particles in commercial flotation operations. All of our nanoparticles are cationic, giving spontaneous deposition onto the negatively charged glass surfaces. [Figure 1](#) shows the flotation recovery as a function of the shell thickness for the PS–PB series of core/shell nanoparticles. The particle diameters increased slightly with shell thickness, whereas the water contact angles on glass surfaces saturated with nanoparticles were similar – see [Table 2](#). Thus, the thickness of the soft polymer shell was the key variable in this series.

The shell thicknesses were determined by comparing the PS–PB diameters to the parent PS seed particle diameters. The parent PS seed particle (zero shell thickness) gave no improvement in flotation recovery compared to the no-collector control. Note that even though the untreated hydrophilic beads do not adhere to air bubbles, some beads are always carried to the froth phase by hydrolytic entrainment.

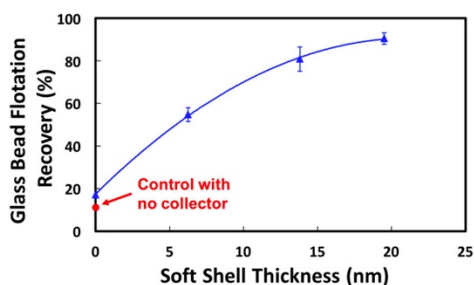


Figure 1. Influence of the soft, poly(*n*-butyl methacrylate) shell thickness on glass bead flotation recovery using nanoparticles PS317, PS–PB1, PS–PB2, and PS–PB3. The nanoparticle properties are summarized in Table 2. Measurements were made under our standard conditions using 20 mg of nanoparticles. Error bars reflect the standard deviation of three measurements.

Previously we have shown that PS particles as big as 300 nm are ineffective, which is consistent with the result here.⁴ By contrast, the soft shell particles gave substantially higher recoveries. Indeed, this was the first time we obtained high recoveries with such large particles.

Figure 1 clearly shows that flotation recovery increases with the thickness of the soft PB shell, approaching a limit at about 20 nm. Again the water contact angles on PS–PB surfaces were similar to PS, so this result is not a reflection of hydrophobicity differences. Note that previously we have shown that pure PB nanoparticles are poor collectors, possibly because the very soft particles flatten too much after deposition.⁷

The glass transition temperature of PB is 24–31 °C, approximately equal to the flotation temperature.¹¹ To further illustrate the role of particle softness, for PS–PB3 with a shell thickness of 20 nm, the glass bead recovery was 90% when the flotation temperature was 22 °C, whereas at 6 °C, the recovery decreased to 65%. We propose that softer particles give increased adhesion to glass – this hypothesis is now tested.

Colloidal probe AFM measurements were performed to measure the adhesion between silica spherical probes and Si wafer surfaces coated with polymer nanoparticles and submerged in 5 mM NaCl. Figure 2 compares two example pull-off curves, one for hard PS317 and the other for PS–PB3.

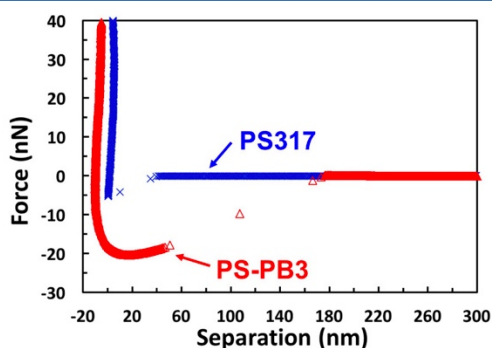


Figure 2. Examples of pull-off force curves for a 2.5 μm SiO_2 probe adhering to saturated layers of nanoparticles fixed to silicon wafer in 5 mM NaCl solution. Measurements were performed at room temperature where PS317 was a hard plastic, whereas the PS–PB3 particles had a soft, 20 nm thick shell.

Pull-off probability distribution plots and sequential adhesion maps are shown in Figures S5 and S6. Pull-off forces for the soft shell nanoparticle surfaces were about four times greater than for the hard PS particles.

White et al. report fracture energies, measured with blister tests, for the PB/silica interfaces as functions of relative humidity (RH).¹² The fracture energy was $\sim 20 \text{ J/m}^2$ at 100% RH, a value not very sensitive to RH. By contrast the work of adhesion, W_a , decreased from 82 mJ/m^2 in dry air to 5 mJ/m^2 in 100% RH. They also reported that cohesive failure within the PB layer was the dominant failure mechanism. We examined our probes by SEM (see Figure S7) and saw no evidence of significant contamination with PB.

Figure 3 compares the adhesion work probability plots for the two surfaces. The average work for the PS–PB3 surface was

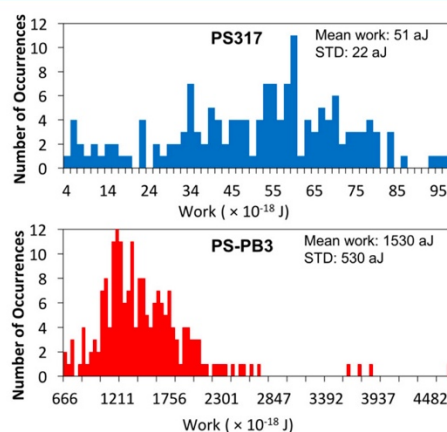


Figure 3. Distributions of the work of adhesion based on 155 measurements for PS317 and 196 measurements for PS–PB3. Work was expressed as attojoules, aJ = 10^{-18} J.

30 times higher than the value for PS. Soft-shelled particles give stronger adhesion to surfaces.

PS/PB Janus Nanoparticles. Nanoparticle flotation collector particles must perform two distinct functions: 1) they must specifically deposit onto the desired mineral surfaces, and 2) they must render the mineral sufficiently hydrophobic to adhere to air bubbles. One approach to these two different functions is to prepare nonspherical Janus particles, where one face is optimized for deposition/adhesion and the other for hydrophobization. Following Sundberg's work,⁹ we synthesized small PS/PB Janus particles; TEM images are shown in Figure 4. Clearly the Janus particles were not as uniform as the other nanoparticle types we prepared; however, the flotation performance was exceptional.

Table 3 compares the properties and flotation performance of all the types of particles we evaluated. Particularly when compared at low dosages, the Janus particles were the superior flotation collectors. The flotation ranking of the remaining particles was small PS > PS–PB \gg large PS. The contact angle measurements and electrophoretic mobilities suggest that the small PS and the Janus particles were slightly more hydrophobic. Additionally, the smaller particles covered more area when compared at a constant mass dosage. For example, 5 mg of PS63 particles potentially cover 98% of glass bead surface area, whereas the much larger PS–PB particles cover only 17%. The mass fraction of soft PB in the Janus particles was about

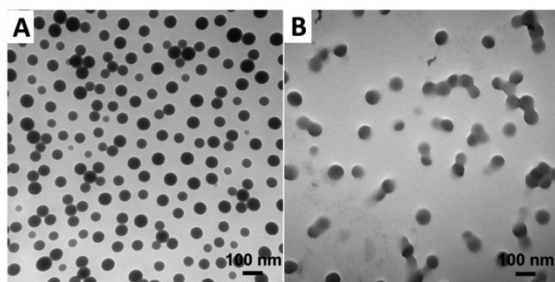


Figure 4. TEM image A is of the polystyrene seed particles, whereas image B shows the Janus particles formed in the second stage polymerization.

67% based on monomer feed, whereas the highest PB content in the core/shell particles was PS–PB3 which contained 33 wt % PB. However, because the Janus particles were much smaller (92 vs 356 nm) we cannot conclude that the nonspherical Janus morphology is superior to core/shell. It is possible that small core/shell particles would be equally effective. On the other hand, all evidence suggests that the presence of softer polymer improves flotation and gives stronger adhesion to the surface.

DISCUSSION

Somewhat hydrophobic (i.e., water contact angles $>50^\circ$) nanoparticles adsorbed on mineral surfaces promote the attachment of mineral particles to air bubbles, leading to successful separation in a flotation cell.³ To perform this function, the nanoparticles must deposit onto the mineral surfaces and remain there. In this work we tackled two questions: why are small nanoparticles more effective and why are soft particles more effective. We will now argue that the answers to these questions are linked to the polymer/glass (mineral) adhesion.

It is well-known that polymers near their T_g (glass transition temperature) exhibit greater adhesion compared to hard polymers ($T \ll T_g$). For example, Israelachvili et al. used the surface force apparatus to measure adhesion between PB coated mica surfaces.¹³ At temperatures below the T_g ($\sim 25^\circ\text{C}$ for PB), the adhesion results were close to the JKR model,¹⁴ whereas at the T_g , pull-off forces were far greater, reflecting the viscous dissipation. Therefore, our results comparing PS versus PS–PB or comparing PS–PB at 6°C versus 25°C are consistent with the explanation that softer polymers give better flotation because of increased nanoparticle adhesion. If adhesion is important, what processes are tending to dislodge nanoparticles

adhering to glass or mineral surfaces? Initially, we speculated that hydrodynamic forces in flotation cells detached adsorbed nanoparticles. However, we provide the following analysis that concludes that hydrodynamic forces are unlikely to be sufficiently intense to dislodge our small particles from glass bead surfaces.

To identify mechanisms by which nanoparticles are removed from surfaces, we need to estimate the nanoparticle/glass adhesion forces. For this we employed JKR theory to link pull-off (adhesion) force, F_{po} , to the work of adhesion, W_a , for a sphere of radius r on a flat surface – see eq 1.¹⁴ The JKR model does not account for viscous dissipation for adhesives near the T_g so our approach is approximate at best.^{13,15} We first employed eq 1 to estimate apparent work of adhesion from the pull-off force measurements in Figure 2. Based on the average experimental values of 4.2 nN for PS and 15.2 nN for PS–PB for pulling off the silica colloidal probe, the corresponding W_a values are 0.7 mN/m for PS and 2.6 mN/m for PS–PB surfaces. Our estimate of W_a of PS–PB completely submerged in NaCl solution was close to White's value of 5 mN/m for PB adhesion to silica at 100% relative humidity.¹²

$$F_{po} = -\frac{3}{2}\pi W_a r \quad (1)$$

The corresponding force to pull an individual nanoparticle off glass was estimated by reapplying eq 1 using the nanoparticle radii and the W_a values estimated above. The estimated pull-off force for our 317 nm PS particles was 0.5 nN, and the force for the 356 nm PS–PB particles was 2.2 nN. Are hydrodynamic forces sufficient to displace these particles?

Goldman et al. derived the following equation for the displacement force experienced by a sphere on a surface in laminar flow where F_d is the lateral displacement force, S is the shear rate, r is the nanoparticle radius, and η is the viscosity.¹⁶ For a given shear rate, the displacement force increases with the square of the particle radius, suggesting that there is always a particle size above which hydrodynamic displacement forces exceed adhesion forces.

$$F_d = 1.7(6\pi\eta r^2 S) \quad (2)$$

Eq 2 was used to estimate the corresponding minimum shear rate by equating the estimated (vertical) pull-off forces, F_{po} , to the (horizontal) displacement force, F_d . The estimated removal shear rates were $7.4 \times 10^5 \text{ s}^{-1}$ for PS particles and $2.4 \times 10^6 \text{ s}^{-1}$ for PS–PB particles. Considering that these are very high values for the shear rates and that JKR theory greatly underestimates adhesion for viscoelastic PB at room temperature,¹³ we conclude that hydrodynamic forces are unlikely able to dislodge

Table 3. Comparison of Uniform (PS), Core/Shell (PS–PB), and PS/PB Janus Nanoparticle Properties and Flotation Performance^a

nanoparticle designation	diameter (PDI), nm	water CA	EM $\times 10^{-8} \text{ m}^2 \text{ s}^{-1} \text{ V}^{-1}$ (SE)	nanoparticle dosage, mg	flotation recovery (STD)
PS63	62.9 (0.035)	76.0 \pm 1.1	1.90 (0.36)	2	60.0 (0.8)%
				5	82.9 (5.5)%
PS/PB Janus	92.0 (0.036)	84.1 \pm 1.7	1.95 (0.20)	2	84.6 (1.5)%
				5	98.8 (0.8)%
PS317	317.2 (0.002)	56.7 \pm 1.5	4.53 (0.14)	5	12.2 (0.2)%
				20	17.3 (0.7)%
PS–PB3 core–shell	356.2 (0.016)	60.0 \pm 1.3	4.33 (0.10)	5	62.2 (2.8)%
				20	90.6 (0.02)%

^aStandard deviation of flotation recovery values was determined from 3 repeated flotation experiments.

~300 nm PS or PS–PB particles from the glass bead surfaces in our experiments. There must be another mechanism requiring strong nanoparticle/glass adhesion, resulting in the poorer flotation performance of PS compared to PS–PB nanoparticles.

We propose that glass bead–bead collisions dislodge adsorbed nanoparticles in the bead–bead contact zone, a process we call “nano-scale ball milling”. A future report will give evidence supporting this mechanism and offering a model predicting the influence of nanoparticle size on removal kinetics.

CONCLUSIONS

Thin (15–20 nm) shells of soft poly(*n*-butyl methacrylate), PB, on 317 nm polystyrene, PS, particles transform the non-performing PS nanoparticles into very effective PS–PB nanoparticle flotation collectors, greatly expanding the upper limit of particle size for this application. The stronger adhesion of soft-shelled particles to glass accounts for the improved flotation performance. Small, nonspherical Janus nanoparticles with soft PB lobes are particularly effective flotation collectors. We argue that the requirement of high nanoparticle/glass adhesion is not because hydrodynamic forces are removing adsorbed nanoparticles. Instead, we propose that glass bead–bead collisions erode adsorbed nanoparticles – “nano-scale ball milling”. Future reports will provide direct evidence for the nanoscale ball milling mechanism.

ASSOCIATED CONTENT

Supporting Information

The Supporting Information is available free of charge on the ACS Publications website at DOI: 10.1021/acs.iecr.6b02488.

Nanoparticle details characterization with XPS, FTIR data, TEM and SEM images; an illustration of the froth flotation process; statistical distribution of colloidal probe AFM pull-off forces and sequential maps represent the distribution of pull-off force and adhesion work measurements; and a SEM image of a AFM colloidal probe after performing adhesion measurements (PDF)

AUTHOR INFORMATION

Corresponding Author

*E-mail: peltonrh@mcmaster.ca.

Notes

The authors declare no competing financial interest.

ACKNOWLEDGMENTS

The authors acknowledge useful discussions and technical assistance from Drs. Manqui Xu and Zongfu Dai from VALE and from Dr. Songtao Yang from AuTec Innovative Extractive Solutions Ltd. We thank the Natural Sciences and Engineering Research Council of Canada (NSERC) and VALE Base Metals for funding this project. Some measurements were performed in the McMaster Biointerfaces Institute funded by the Canadian Foundation for Innovation. R.P. holds the Canada Research Chair in Interfacial Technologies.

REFERENCES

- (1) Fuerstenau, M.; Jameson, G.; Yoon, R. *Froth Flotation: A Century of Innovation*; Society for Mining, Metallurgy, and Exploration: Littleton, CO, 2007.
- (2) Yang, S.; Pelton, R.; Raegen, A.; Montgomery, M.; Dalnoki-Veress, K. Nanoparticle Flotation Collectors – Mechanisms Behind a New Technology. *Langmuir* **2011**, *27*, 10438–10446.
- (3) Yang, S.; Pelton, R. Nanoparticle Flotation Collectors II: The Role of Nanoparticle Hydrophobicity. *Langmuir* **2011**, *27*, 11409–11415.
- (4) Yang, S.; Pelton, R.; Montgomery, M.; Cui, Y. Nanoparticle Flotation Collectors III – the Role of Nanoparticle Diameter. *ACS Appl. Mater. Interfaces* **2012**, *4*, 4882–4890.
- (5) Yang, S.; Pelton, R.; Xu, M.; Dai, Z. *Nanoparticle Flotation Collectors for Pentlandite*. In *Proceedings of the 44th Annual Canadian Mineral Processors Conference*, Canadian Institute of Mining Metallurgy and Petroleum: Ottawa, 2012; pp 225–236.
- (6) Yang, S.; Pelton, R.; Abarca, C.; Dai, Z.; Montgomery, M.; Xu, M.; Bos, J.-A. Towards Nanoparticle Flotation Collectors for Pentlandite Separation. *Int. J. Miner. Process.* **2013**, *123*, 137–144.
- (7) Yang, S.; Razavizadeh, B. M.; Pelton, R.; Bruin, G. Soft Nanoparticle Flotation Collectors. *ACS Appl. Mater. Interfaces* **2013**, *5*, 4836–4842.
- (8) Goodwin, J. W.; Ottewill, R. H.; Pelton, R. Studies on the Preparation and Characterization of Monodisperse Polystyrene Lattices 0.5. Preparation of Cationic Lattices. *Colloid Polym. Sci.* **1979**, *257*, 61–69.
- (9) Durant, Y. G.; Sundberg, D. C.; Guillot, J. Determination of Interfacial Tensions for Latex Particles. *J. Appl. Polym. Sci.* **1994**, *53*, 1469–1476.
- (10) Sader, J. E.; Larson, I.; Mulvaney, P.; White, L. R. Method for the Calibration of Atomic Force Microscope Cantilevers. *Rev. Sci. Instrum.* **1995**, *66*, 3789–3798.
- (11) Schröter, K.; Unger, R.; Reissig, S.; Garwe, F.; Kahle, S.; Beiner, M.; Donth, E. Dielectric Spectroscopy in the $\alpha\beta$ Splitting Region of Glass Transition in Poly(Ethyl Methacrylate) and Poly(N-Butyl Methacrylate): Different Evaluation Methods and Experimental Conditions. *Macromolecules* **1998**, *31*, 8966–8972.
- (12) White, C.; Tan, K. T.; Hunston, D.; Steffens, K.; Stanley, D. L.; Satija, S. K.; Akgun, B.; Vogt, B. D. Mechanisms of Criticality in Environmental Adhesion Loss. *Soft Matter* **2015**, *11*, 3994–4001.
- (13) Luengo, G.; Pan, J.; Heuberger, M.; Israelachvili, J. N. Temperature and Time Effects on the Adhesion Dynamics of Poly(Butyl Methacrylate) (Pbma) Surfaces. *Langmuir* **1998**, *14*, 3873–3881.
- (14) Johnson, K. L.; Kendall, K.; Roberts, A. D. Surface Energy and the Contact of Elastic Solids. *Proc. R. Soc. London, Ser. A* **1971**, *324*, 301–313.
- (15) Tirrell, M. Measurement of Interfacial Energy at Solid Polymer Surfaces. *Langmuir* **1996**, *12*, 4548–4551.
- (16) Goldman, A. J.; Cox, R. G.; Brenner, H. Slow Viscous Motion of a Sphere Parallel to a Plane Wall—II Couette Flow. *Chem. Eng. Sci.* **1967**, *22*, 653–660.

Supporting Information: Relating nanoparticle shape and adhesiveness to performance as flotation collectors

Xiaofei Dong, Heera S. Marway, Emily D. Cranston, Robert H. Pelton*

Department of Chemical Engineering, McMaster University, 1280 Main Street West, Hamilton, Ontario, Canada L8S 4L8

*Corresponding author: peltonrh@mcmaster.ca

Nanoparticle Characterization:

Infrared spectroscopy spectra of dried nanoparticles were collected with a Nexus 6700 Fourier-transform infrared (FTIR) spectrometer (Thermo Fisher Scientific Inc.). The nanoparticle tablets were prepared by mixing dried nanoparticles with KBr and pressing at 10,000 psi with a hydraulic press (Carver, Inc. USA) for 5 min at room temperature in a stainless steel mold.

X-ray photoelectron spectroscopy (XPS) measurements were performed on dried nanoparticles using a PHI Quantera II XPS scanning microprobe (Physical Electronics (Phi), Chanhassen, MN) equipped with a 1486.7 eV monochromatic Al-K-alpha X-ray source. All settings were controlled through supplied software (Multipak 9.4.0.7) and spectra were collected using a beam size of 200 μm and a pass energy of 280 eV.

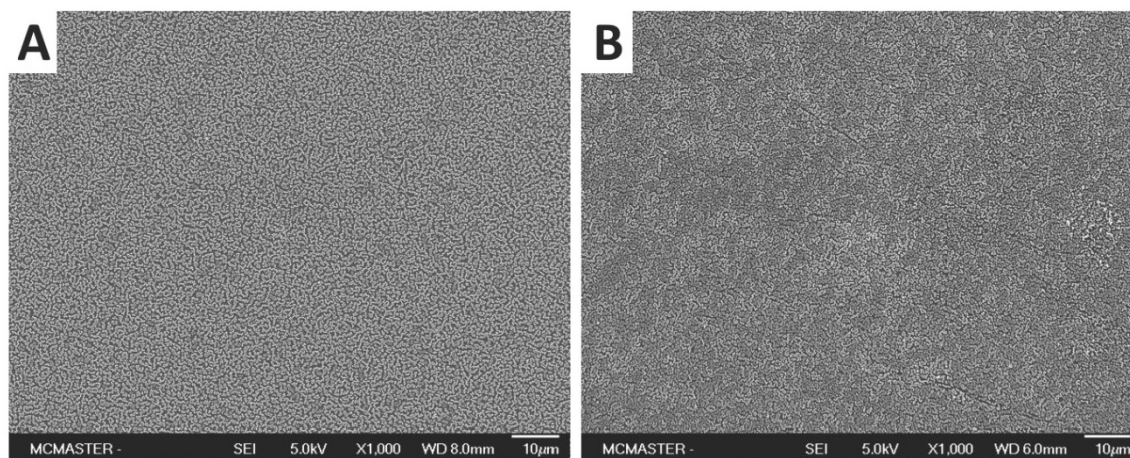


Figure S1. Image A is the SEM image of polystyrene nanoparticles (PS317) treated glass slide whereas image B shows the core-shell nanoparticles (PS-PB3) treated glass slide for contact angle measurements.

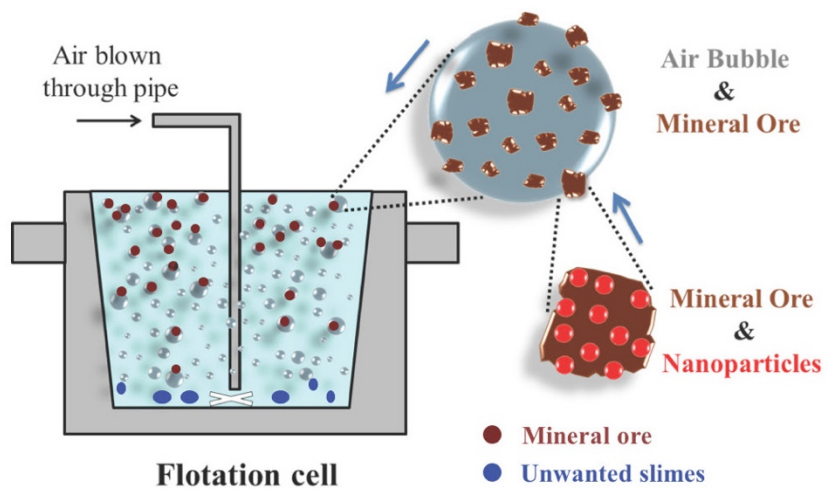


Figure S2. Illustration of the froth flotation process.

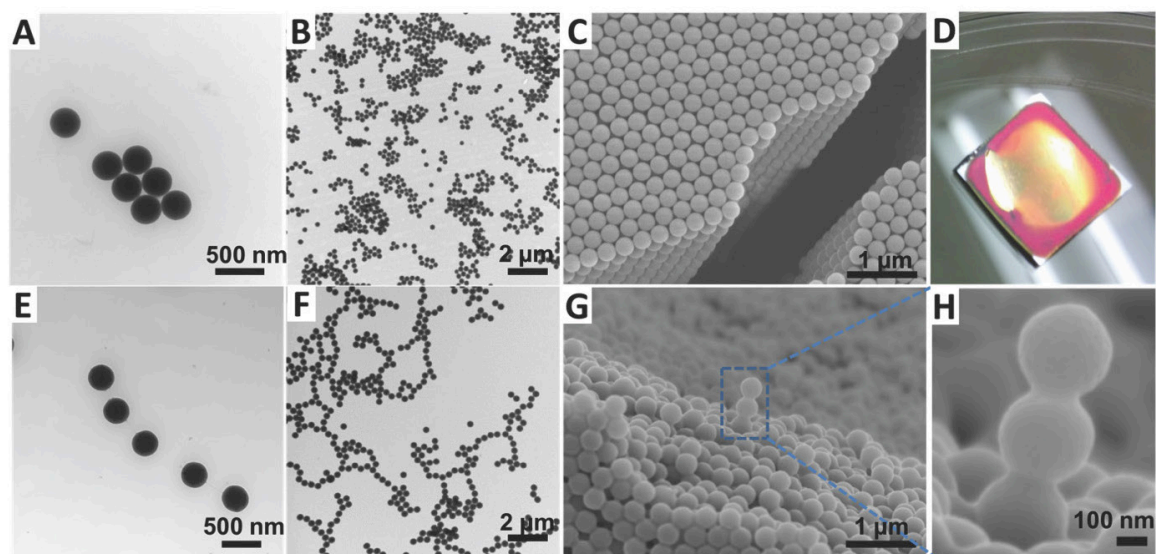


Figure S3. (A and B), TEM images of PS317 seed nanoparticles; (C), SEM image of polystyrene seed nanoparticles; (D), photograph of dried, opalescent polystyrene seed latex on a silicon wafer; (E and F), TEM images of synthesized PS-PB3 nanoparticles; (G) and (H), SEM images of PS-PB3 nanoparticles.

FTIR of Polystyrene-core-poly(*n*-butyl methacrylate)-shell Nanoparticles

The characteristic spectra of PS appeared at 698.00, 756.46, 2924.46, 3000.00, 3026.08, 3060.30, 3082.61 cm^{-1} ,¹ and that of PB appeared at: C=O at 1728.21 cm^{-1} ; C-O at 1272.64, 1241.59, and 1154.33 cm^{-1} ; and $-(\text{CH}_2)_3\text{CH}_3$ at 1067.94, 965.46, and 845.09 cm^{-1} .² As shown in Figure 4, the Fourier-transform infrared (FTIR) spectra of core-shell nanoparticle consisted both of the characteristic spectra of PS and PB, which confirms the existence of PS and PB in core-shell nanoparticle.

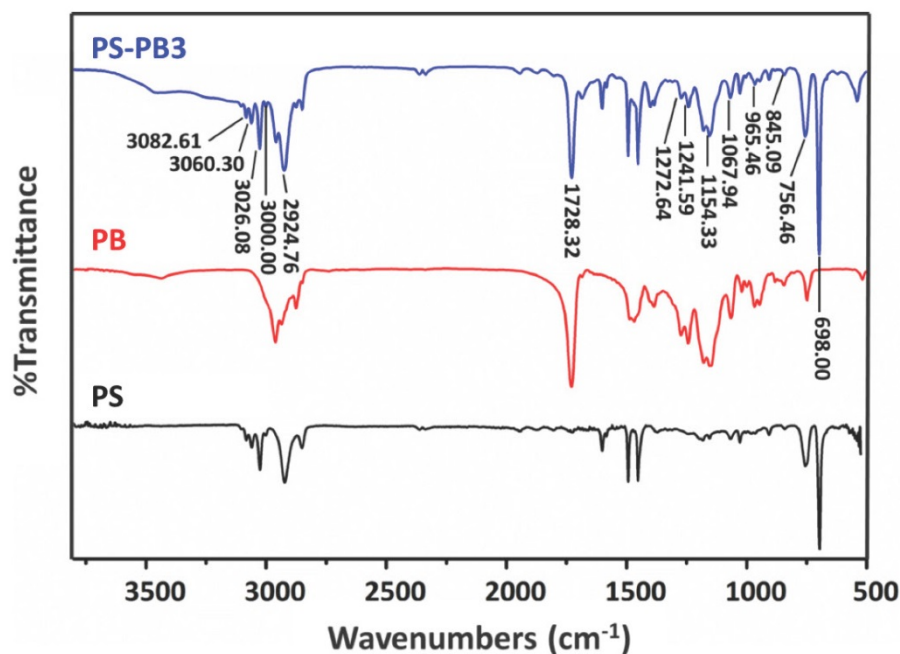


Figure S4. FTIR spectra of polystyrene seed nanoparticles, pure poly *n*-butyl methacrylate and synthesized polystyrene-core-poly(*n*-butyl methacrylate)-shell nanoparticles.

XPS of Nanoparticle Films

The carbon/oxygen atomic ratio of PS and PS-PB nanoparticles are summarized in Table 1. The carbon/oxygen ratio of seed nanoparticle was determined as 100%/0, which agrees with the composition of polystyrene. The oxygen atomic composition of pure poly(n-butyl methacrylate) is 20%. The measured values in Table 1 are slightly less.

Table S1. Atomic composition of PS and PS-PB3 nanoparticles determined by XPS.

Nanoparticle designation	Recorded electron takeoff angle	Carbon Atomic%	Oxygen Atomic%
PS	10°	100	0
PS-PB3	10°	84.3	15.7
	90°	85.4	14.6

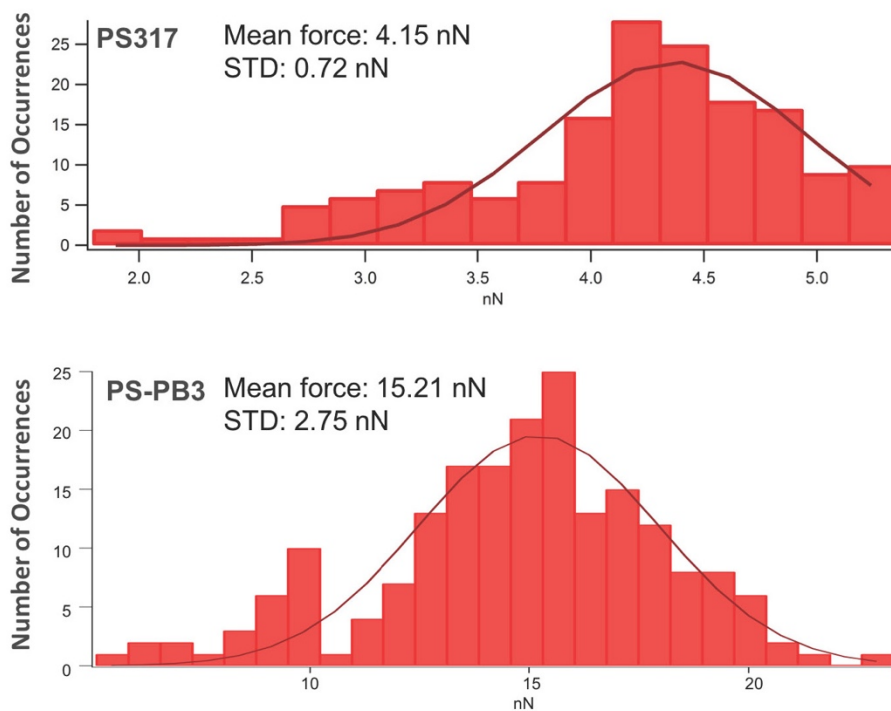


Figure S5. Distributions of the pull-off force based on 155 measurements for PS317 and 196 measurements for PS-PB3. Force was expressed as nano newtons, $\text{nN} = 10^{-9} \text{ N}$.

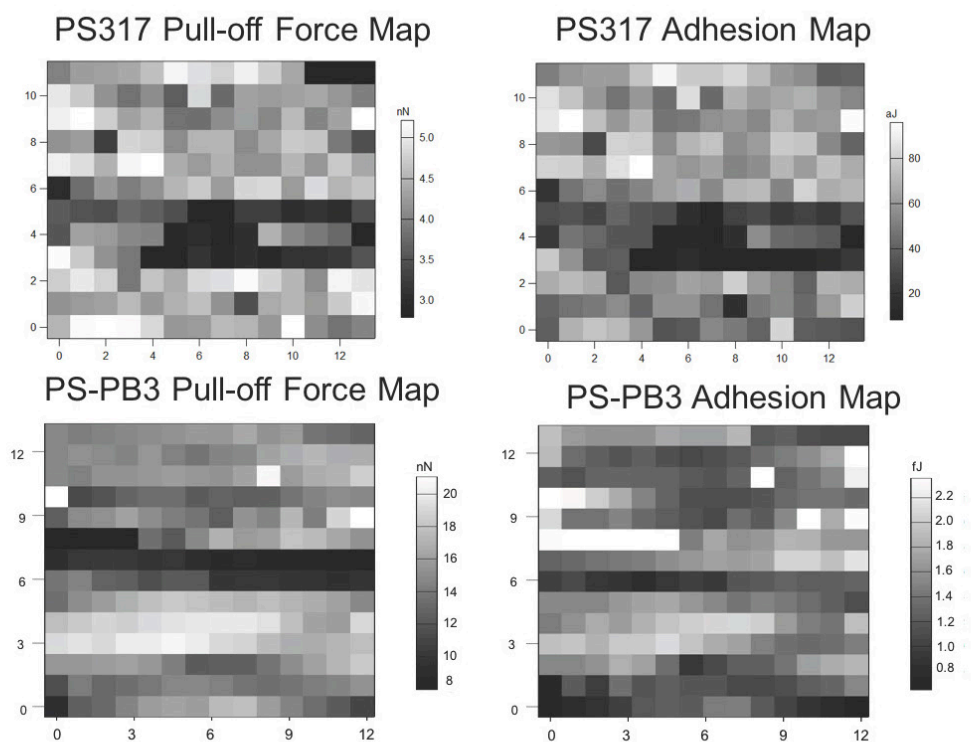


Figure S6. Sequential maps represent the distribution of pull-off force and adhesion work measurements in sequence form start to finish. Square at the top left origin (0,0) represents the first measurement and the square diagonal to the origin at the bottom right represents the last measurement for that set. Force was expressed as nanonewton, $\text{nN} = 10^{-9} \text{ N}$. Work was expressed as attojoules, $\text{aJ} = 10^{-18} \text{ J}$, and femtojoules, $\text{fJ} = 10^{-15} \text{ J}$.

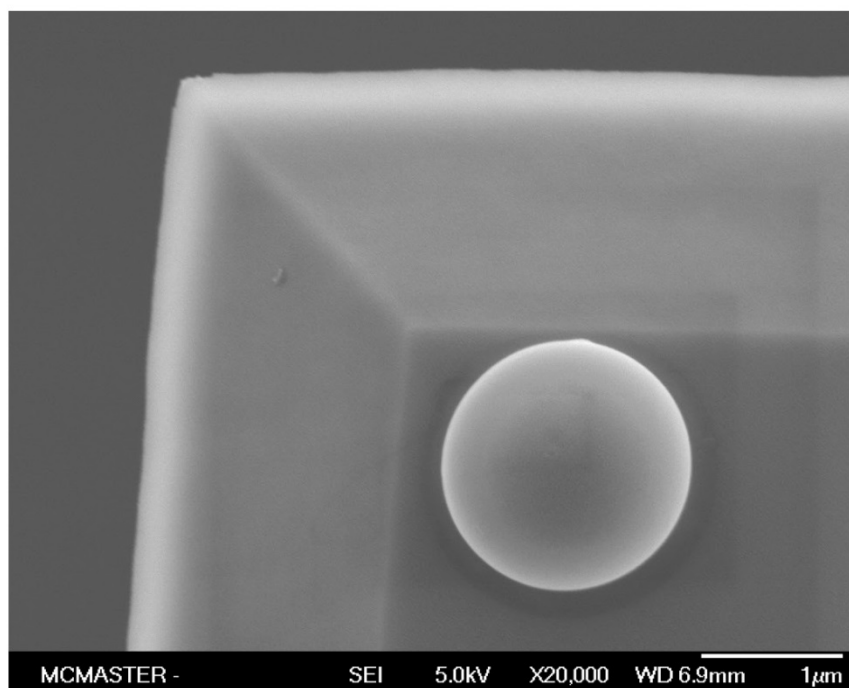


Figure S7. SEM image of AFM colloidal probe after performing over 100 colloidal probe AFM adhesion measurements against a PS-PB3 coated surface.

References

- (1) Liang, C. Y.; Krimm, S., Infrared Spectra of High Polymers. Vi. Polystyrene. *J. of Polym. Sci.* **1958**, *27*, 241-254.
- (2) Peng, H.; Cheng, S.; Fan, Z., Synthesis and Characterization of Poly(N-Butyl Methacrylate)-B-Polystyrene Diblock Copolymers by Atom Transfer Radical Emulsion Polymerization. *J. Appl. Polym. Sci.* **2005**, *98*, 2123-2129.

Chapter 3 Mineral-Mineral Particle Collision During Flotation Remove Adsorbed Nanoparticle Flotation Collectors

In chapter 3, flotation experiments were conducted by myself with the assistance of Marie Price who worked with me as a summer student. The rest of the experiments were conducted by myself. I plotted all experimental data. Dr. Pelton developed the nano-scale ball milling model, did the calculation in Mathcad and plotted the simulation data. Dr. Dai and Dr. Xu contributed useful discussions and gave useful advices on this paper. I wrote the manuscript, and Dr. Pelton edited it into this final version. This work was submitted to *International Journal of Mineral Processing* on July 30, 2016¹²⁶.

Mineral-Mineral Particle Collisions During Flotation Remove Adsorbed Nanoparticle Flotation Collectors

Xiaofei Dong[†], Marie Price[†], Zongfu Dai[‡], Manqiu Xu[‡], and Robert Pelton^{†*},

[†]Department of Chemical Engineering, McMaster University, 1280 Main Street West, Hamilton, Ontario, Canada L8S 4L7

[‡]Vale Base Metals Technology Development, 2060 Flavelle Blvd., Mississauga, Ontario, Canada L5K 1Z9

*Corresponding author: peltonrh@mcmaster.ca

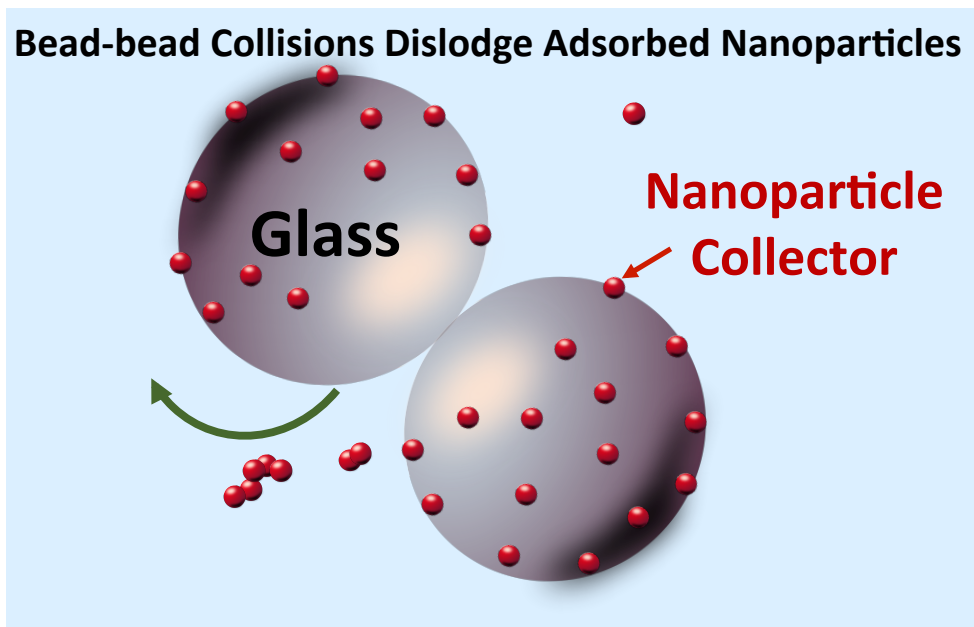
Keywords

Serpentines, pentlandite, flotation, nanoparticles, collectors, conditioning time

Abstract

Flotation of 43 μm diameter, hydrophilic glass beads with hydrophobic cationic polymeric nanoparticle flotation collectors revealed that bead-bead collisions during conditioning and flotation caused the irreversible erosion of the adsorbed nanoparticles – nano-scale ball milling. The eroded particles were present in the suspension as large aggregates. A phenomenological model of the erosion dynamics helps explain the roles of nanoparticle size and concentration.

Table of Contents



Introduction

Over the last seven years we have been attempting to develop nanoparticle flotation collectors based on polymer (latex) nanoparticles. Because our nanoparticles are much larger than conventional molecular collectors such as PAX (potassium amyl xanthate), we hypothesized that nanoparticles may offer advantages for mineral particle suspensions with surfaces contaminated with nanometer scale contaminants, such as serpentine minerals. Polymer latexes have been used before in mineral and coal processing, mainly as flocculating agents (Lyadov et al., 1979) (Attia and Yu, 1991; Laskowski and Yu, 2000; Laskowski et al., 1995; Littlefair and Lowe, 1986; Palmes and Laskowski, 1993) Although most of these studies did not involve flotation, Zhan's thesis reported apatite flotation in the presence of poly(methyl acrylate-co-acrylic acid) copolymer latex, with and without an oleic acid collector (Zhan, 1999).

Our nanoparticle flotation collector development efforts have involved two types of experiments – pentlandite flotation experiments mainly conducted in the pilot facilities of our industry partner Vale, and small scale laboratory flotation of a simplified system, consisting of negatively charged, hydrophilic glass beads, as a model for the mineral particles. Simple cationic polystyrene latexes were used for most of the glass bead flotation studies, whereas more complex particle surface chemistries were used for the pentlandite studies.

The pentlandite experiments were used to assess the commercial feasibility of nanoparticle collectors, assessing both recovery and grade. By contrast, the model glass bead experiments answered specific mechanistic and nanoparticle design questions, such as the role in flotation of nanoparticle diameter, hydrophobicity, softness, and extent of adsorption of the nanoparticles on the glass beads.

The main findings from the model glass bead experiments were: small nanoparticles (~50 nm diameter) were far more effective than larger (> 100 nm) particles (Yang et al., 2012a); the nanoparticles must be sufficiently hydrophobic – there is little scope to deviate from pristine polystyrene without losing flotation efficiency (Yang and Pelton, 2011); incorporation of comonomers giving either uniform softer particles (Yang et al., 2013b), or core-shell particles with a soft shell (Dong et al., 2016) were superior. One of the most important findings from the glass bead experiments was that when using an effective nanoparticle flotation collector, as little as 10% coverage of the glass bead surface was sufficient to give good flotation (Yang et al., 2011), showing that with optimized particles, nanoparticle flotation collectors could be commercially feasible.

Our published pentlandite flotation studies show that nanoparticles can sometimes give better flotation than PAX (Yang et al., 2012b) (Yang et al., 2013a) The selective deposition of nanoparticles onto nickel-rich surfaces was obtained by incorporating amine, imidazole and other nickel affinity ligands as surface functional groups on the nanoparticles. None of our existing nanoparticles was sufficiently promising for commercial application because the required

nanoparticle dosages were too high. We believe that nanoparticle aggregation in the flotation liquor was competing with nanoparticle deposition onto the mineral particle surfaces. A fine balance is required in the design of the nanoparticle surface chemistry. Substituents that increase colloidal stability or affinity to the pentlandite are hydrophilic and can easily render the nanoparticle too hydrophilic to induce flotation. We are currently employing a combinatorial synthesis plus high throughput screening strategy to optimize nanoparticle surface chemistry to give sufficient colloidal stability, hydrophobicity and pentlandite selectivity (Abarca et al., 2015) (Abarca et al., 2016).

In trying to understand why smaller and softer particles are more effective, we recently concluded that high nanoparticle adhesion to the glass bead surfaces was a requirement for nanoparticle flotation collectors (Dong et al., 2016). Furthermore, direct measurement of nanoparticle/silica adhesion suggested that hydrodynamic forces in our flotation experiments were too low to dislodge adsorbed nanoparticles. Instead, we proposed that mixing induced bead-bead collisions removed adsorbed nanoparticles in what we called “nano-scale ball milling”.

In this paper, we present direct evidence for the nano-scale ball milling effect. One the most revealing experiments shown herein involves measuring flotation recovery as a function of conditioning time. Laboratory flotation studies often involve a conditioning step where dispersed mineral particles are mixed with the flotation collector, giving time for the collector to adsorb before initiation gas flow. The flotation literature deals with a large variety of minerals and collector chemistries. However, with the exception of kerosene or other mineral oil emulsion, all the collector chemistries are small molecules that can rapidly diffuse to surfaces. (Fuerstenau et al., 2007) The flotation literature yields no general conclusions regarding the role of conditioning time after collector addition. For example, coal recovery decreases with increasing conditioning time because of coal surface oxidation (Xia et al., 2014) whereas other systems can give higher recoveries after a long conditioning time. (Hadler et al., 2005) (Kuopanportti et al., 2000) In summary, it seems fair to conclude that in conventional flotation systems, post-collector conditioning time is not a sensitive parameter, and is not often studied. In contrast, nanoparticles are much larger than molecular collectors; we anticipated that longer conditioning times would be required. However, herein we show that with excessive conditioning the nanoparticle collectors become completely ineffective. We present evidence supporting the conclusion that bead-bead collisions remove nanoparticle flotation collectors.

Experimental Section

Materials. Glass beads with a mean diameter of 43 μm were purchased from Polysciences Inc. and used as supplied. The flotation frother, UniForth 250C (>99%), a mixture of monomethyl polypropylene glycol, 250kDa and dipropylene glycol monomethyl ether, was donated by VALE

INCO Canada (Mississauga, ON) and used as supplied. All water used was processed with a Barnstead Nanopure Diamond System (Thermo Scientific) and had a resistance over 18M Ω .

Characterization. The hydrodynamic diameters of synthesized nanoparticles were determined by dynamic light scattering (Brookhaven Instruments Corporation) with a detector angle of 90°. Latex samples were diluted with 5 mM NaCl solution to give a scattering intensity between 100 and 150 kcps. Dispersions were equilibrated to 25°C for 3 min before analyzing. The duration of each measurement was set as 3 min. Three sets of measurements were undertaken for each sample. The results were analyzed by BIC dynamic light scattering software (Windows 9KDLSW version 3.34) using the cumulants model, whereas the CONTIN model was used to generate the particle size distribution, expressed as a polydispersity index (PDI).

Electrophoretic mobility (EM) measurements were performed on a Zeta PALS instrument (Brookhaven Instruments Corporation) at 25°C in the phase analysis light scattering mode. 1.5 mL dilute nanoparticle dispersion in 5 mM NaCl were dispensed into a clear cuvette and thermally equilibrated to 25°C before analyzing. The reported EM values were the average of 10 runs with each consisting of 15 scans.

Water sessile drop contact angles on glass slides coated with nanoparticles were measured with a Krüss Drop Shape Analysis System DSA 10 running DSA software (version 1.80.0.2). In a typical water contact angle experiment, pre-cut glass slides (1 cm squares, Gold Line Microscope Slides, VWR) were cleaned in ethanol with sonication for 30 min, followed by rinsing with water and treating with UV-Ozone (UV-Ozone ProCleaner, Bio Force Nanosciences, Ames, IA, USA) for 20 min. Cleaned glass slides were immersed in 0.5 wt % nanoparticle dispersion in 5 mM NaCl for 30 min, and then dipped into 5 mM NaCl solution to rinse off unbound nanoparticles. The slides were dried in air at room temperature. The properties of the synthesized nanoparticles are summarized in the supporting information file (SI Table 1).

Conditioning. The conditioning and flotation experiments were performed in the same vessel, a polypropylene 125 mL beaker (Nalgene® 1201-0100, ThermoFisher Scientific) with an average inner diameter of 53 mm, sitting on a 150 mm plastic Petri dish (430599, Corning). A 25×9 mm cross shape magnetic stirring bar (SEOH PTFE Stirrer Bar, Cross 25×9 mm, Scientific Equipment of Houston, USA), was driven by a Corning PC-610 stirrer plate. To the beaker were added 125 mL of 5 mM NaCl solution, nanoparticle dispersion, and 2 g of glass beads (a model for mineral particles). Unless stated otherwise, the nanoparticle dose was 2 mg (dry) from stock dispersions, typically 3.5 % solids. The magnetic stirrer was operated at 600 RPM for times between 1 and 240 minutes. After conditioning, the glass beads were isolated for electron microscopy (JEOL 7000F SEM, JEOL Ltd., Japan) by sedimentation. 100 mL of the supernatant latex dispersion was used to measure the latex particle size distribution in a Malvern Mastersizer 2000 using a HeNe laser operating at 633 nm. The reported particle sizes were taken to be the mean values of volume diameters from three replicated measurements.

Flotation. In some cases conditioning was immediately followed by flotation. After conditioning, 0.125 mL UniFroth (1 wt%) was added to the flotation giving a frother concentration of 10 mg/L. After 30 seconds mixing, the stirring speed was increased to 900 rpm and the nitrogen flow to the frit (Corning Pyrex, consisting a 30 mm coarse glass frit attached by a 90 degree elbow, purchased from Fisher Scientific) was initiated at a rate of 2.0 L/min. Froths forming on the top of the beaker were scraped over the side to be caught in the Petri dish. After typically 2 minutes, the gas flow was stopped and the wet and dry masses in the Petri dish were measured. A minimum of three replicates was performed for each condition.

Quiescent Nanoparticle Deposition. PS317 latex (0.556 mL, 3.6 wt %) or PS63 latex (0.185 mL, 3.5 wt %) was dispersed into a plastic beaker filled with 125 mL of 5 mM NaCl solution, and 2 grams of glass beads. After 10 minutes adsorption time, the beads were rinsed with excess salt solution and examined by SEM. Dried beads were placed on a conductive carbon tape and sputtering coated with 5 nm platinum. Measurements were made with a JEOL JSM 7000F SEM at a working distance less than 10 mm and accelerating voltages of 2.8-5 kV

Results

Cationic polystyrene latexes were prepared by surfactant-free emulsion polymerization (Goodwin et al., 1979) and the surface properties are summarized in Table 1. Long used as model colloids, these nanoparticles are monodisperse with pristine polystyrene surfaces, decorated with cationic amidine groups originating from polymerization initiator. The nanoparticles are hard spheres at room temperature flotation conditions because the glass transition temperature of polystyrene is around 100 °C. The water contact angles on glass surfaces saturated with adsorbed nanoparticles, indicate that both nanoparticles in Table 1 were sufficiently hydrophobic to promote flotation (Yang and Pelton, 2011).

Table 1 Properties of surfactant-free, cationic polystyrene nanoparticle flotation collectors for glass bead flotation.

Nanoparticle Designation	Diameter (PDI), nm	Water Contact Angle	Electrophoretic Mobility (SE) $\times 10^{-8} \text{ m}^2 \text{ s}^{-1} \text{ V}^{-1}$
PS63	62.9 (0.035)	76.0±1.1	1.90 (0.36)
PS317	317.2 (0.002)	56.7±1.5	4.53 (0.14)

A series of glass bead (43 μm mean diameter) flotation experiments was conducted in which the conditioning time was varied. The mixing was sufficiently vigorous to keep the heavy beads in suspension. After conditioning, frother was added, a gas sparging tube was introduced and the nitrogen flow was initiated. Figure 1 shows the glass bead recoveries as functions of

conditioning time for the small and large nanoparticles. The PS63 high dosage curve (5 mg, $\Gamma_{\max} = 0.89$) gave maximum recovery after only 1 minute of conditioning. With lower PS63 dosage, the maximum recovery occurred after 5 minutes conditioning. At long conditioning times the PS63 nanoparticles did not promote glass bead flotation.

The larger PS317 particles were completely ineffective as flotation collectors. These results clearly show that the effectiveness of nanoparticle flotation collectors deteriorated with conditioning. Presented below is evidence that conditioning removes adsorbed nanoparticles.

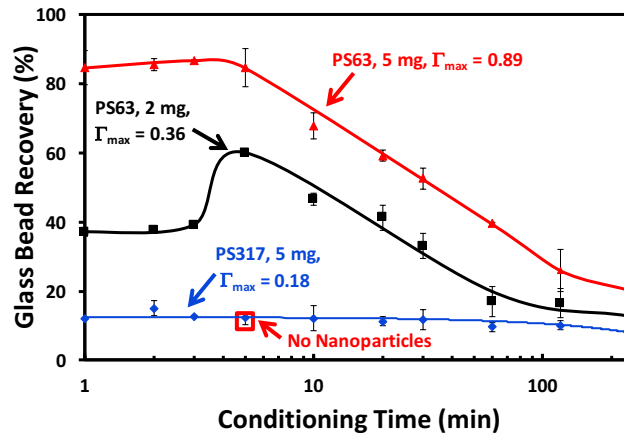


Figure 1 Experimental glass bead flotation recoveries as functions of the conditioning time. Γ_{\max} values are the theoretical fraction of the bead surface areas covered if all of the added nanoparticles adsorbed on the glass surfaces. Flotation measurements were performed in triplicate, and the error bars give the standard deviation. 5 mg nanoparticle gives a collector dosage of 2.5 kg/t and 2 mg gives 1 kg/t nanoparticle collector dosage. Solid lines are the lines drawn to guide the eye. Conditioning time of control experiment is 5 minutes.

One of the advantages of nanoparticle flotation collectors is that they are easily observed by electron microscopy. Figure 2 shows a series of SEM images of glass bead surfaces as functions of conditioning time. The first micrograph for each latex show particles surfaces that were prepared by quiescent mixing of the beads with the nanoparticles. In this case there were no bead-bead collisions and both sizes of cationic nanoparticles readily adsorbed onto negatively charged glass bead surfaces. However, with conditioning the two types of nanoparticles behaved differently. The coverage of the large PS317 nanoparticles was very low at all conditioning times. By contrast the PS63 gave high coverages at short conditioning times, whereas most of the PS63

particles were removed at long times. The densities of the adsorbed nanoparticle micrographs in Figure 2 are directly correlated with the recovery results in Figure 1. In other words, the micrographs confirm that conditioning dislodges nanoparticles adsorbed on glass bead surfaces.

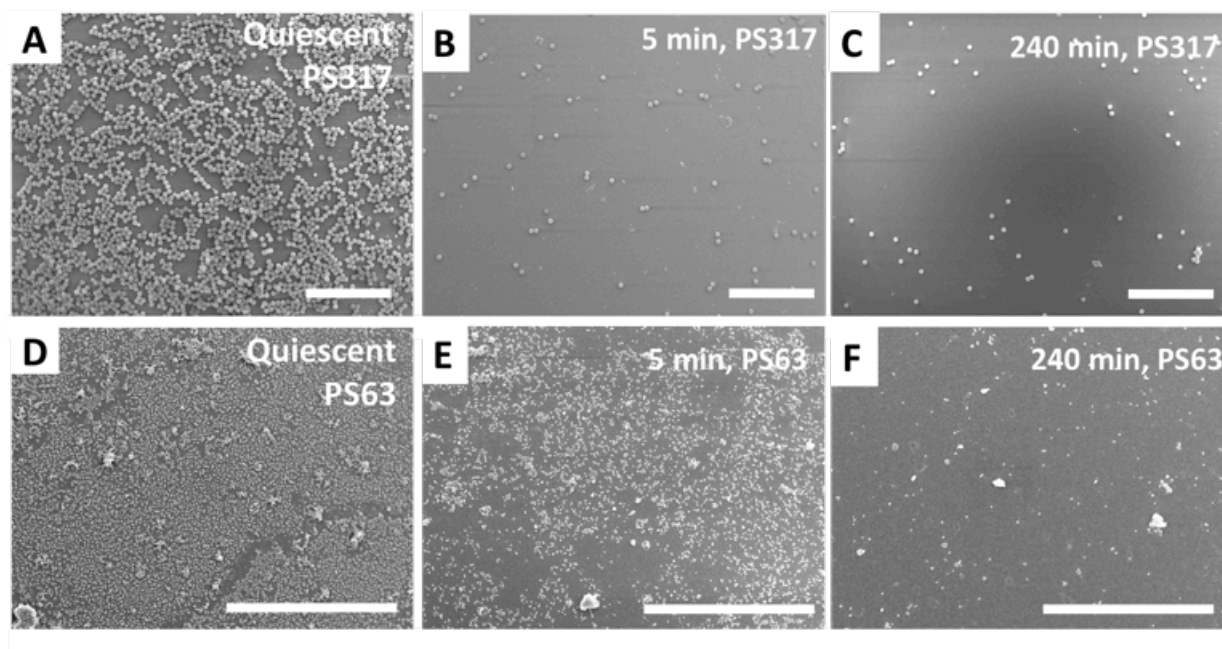


Figure 2 SEM images of glass bead surfaces as functions of conditioning time with two sizes of polystyrene nanoparticles. The first micrographs in each row show bead surfaces exposed to nanoparticles under quiescent conditions with no bead-bead collisions. The second column (B & E) images correspond to 5 min conditioning, whereas the third column (C&F) images were taken after 240 min conditioning. The scale bars correspond to 5 μm .

We also explored the fate of nanoparticles dislodged from the glass bead surfaces. After conditioning, the heavy glass beads were allowed to settle and the particle size distributions of the supernatant suspension were measured with a Malvern Mastersizer. Figure 3 shows two series of bead-free supernatant particle size distributions as functions of conditioning time. For both nanoparticle types, the distributions were bimodal, with the sub micrometer diameter peak corresponding to the nanoparticles. The larger peak around 50 μm suggests very large nanoparticle aggregates. For conditioning times of 60 min or longer, the small peak completely disappeared, meaning individual nanoparticles were either adsorbed on the beads or were aggregated.

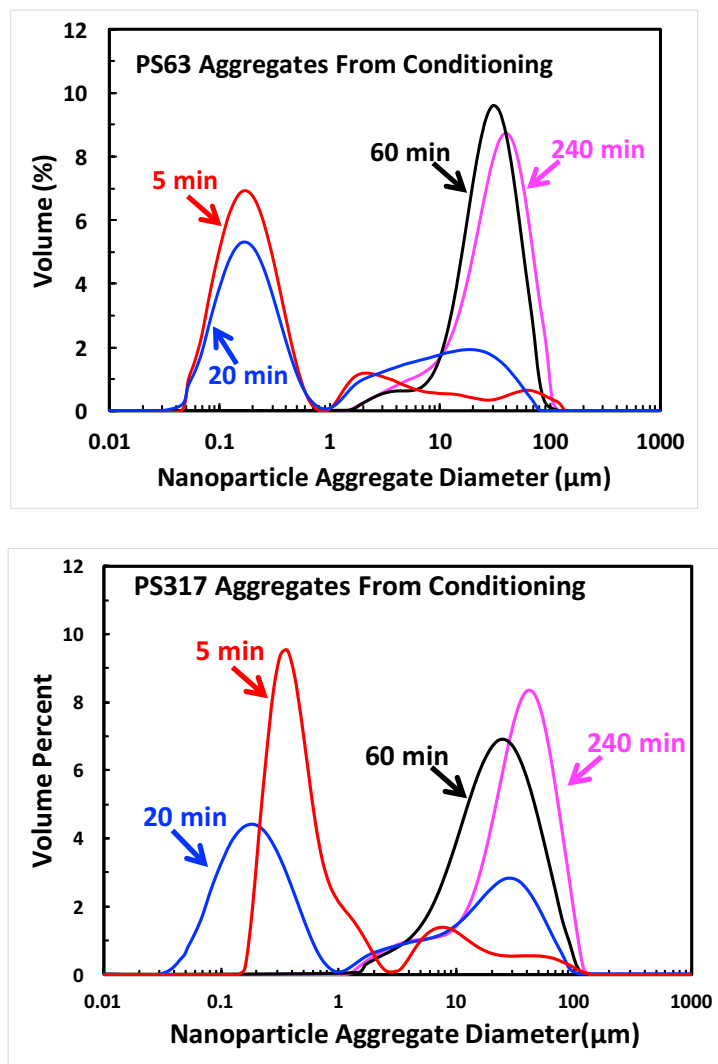


Figure 3 Particle size distributions for the supernatant suspension after the glass beads were removed by sedimentation. The nanoparticle dosages were 2.5 kg/t corresponding to Γ_{\max} values of 0.89 for PS63 and 0.18 for PS317.

Further evidence for large aggregates of nanoparticles was obtained by SEM analysis of the floated glass beads. Figure 4 shows that along with the collected beads after flotation, very large nanoparticle aggregates were present with the beads. Although some of these may have formed during sample preparation, this photograph, together with the size distributions in Figure 3, suggests significant nanoparticle aggregation. Furthermore we emphasize that the ionic strength was low (5 mM NaCl) and the electrophoretic mobilities were high (Table 1); conditions where the nanoparticle dispersions were stable. Additionally, in an agitated flotation cell without beads, both PS63 and PS317 were stable and no aggregates were observed, see supporting information file (Figure S1).

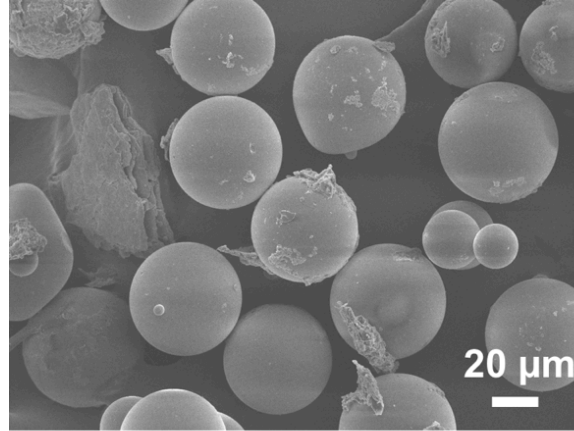


Figure 4 SEM micrographs of glass beads collected in the froth after 240 minutes conditioning. The flotation employed 5 mg PS63 nanoparticles and 2 g glass beads ($\Gamma_{\max} = 0.89$).

Modeling Nanoparticle Deposition and Removal During conditioning

In the following paragraphs we present a simplified model that we propose demonstrates the key features of the nano-scale ball milling mechanism. The key equations are given below. A detailed derivation and example calculations are shown in the Supplementary Information file. The overall goal is to calculate the coverage Γ , the fraction of the glass bead surface area covered with adsorbed nanoparticles, as functions of the conditioning time.

Nanoparticle deposition. The rate of nanoparticle deposition is given by the following expression (Eq. 1) and the terms are described in Table 2. The equation does not account for the blocking by existing deposited particles, and thus is most applicable at low coverage. Every parameter is known except the rate constant, k_d , which accounts for all of the mass transfer and colloidal interactions. Example plots of coverage, Γ , versus conditioning time are shown in Figure 5 for a series of varying nanoparticle radii at constant nanoparticle mass dosage. Parameter values are given in Table 2, except for the radii which are shown on the figure. Γ is >1 for the smallest nanoparticles at long times because blocking was not accounted for in Eq. 1.

$$\frac{d}{dt}\Gamma = ce^{-bt} \quad \text{where} \quad b = k_d C_b \quad c = \frac{r_p^2}{4r_b^2} C_{po} k_d$$

Eq. 1

Table 2 Definition of model parameters and the “base case” parameters values.

Parameters	Description
$r_p = 25 \text{ nm}$	Nanoparticle radius, m.
$\rho_{ps} = 1050 \text{ kg/m}^3$	Nanoparticle density
$r_b = 21.5 \text{ }\mu\text{m}$	Glass bead average radius
$\rho_b = 2200 \text{ kg/m}^3$	Glass bead density
$C_b = 16.7 \text{ g/L}$	Glass bead concentration
t	Conditioning time, s
$k_d = 3.16 \times 10^{-14} \text{ m}^3/\text{s}$	Deposition rate constant, an unknown constant
$C_{po} = 7.28 \times 10^{17} \text{ m}^{-3}$	Initial concentration of nanoparticles, m^{-3}
$X = 3.16 \times 10^{-11} \text{ m}^3/\text{s}$	Bead-bead collision rate constant, an unknown constant
$c_p = 50 \text{ mg/L}$	Mass concentration of added nanoparticles.
Γ	Coverage - fraction of bead surface covered with nanoparticles
Γ_{max}	Maximum possible coverage assuming all of the added nanoparticles adsorb onto glass bead surfaces.
Γ_{crit}	The minimum coverage required for bead attachment to air bubbles.

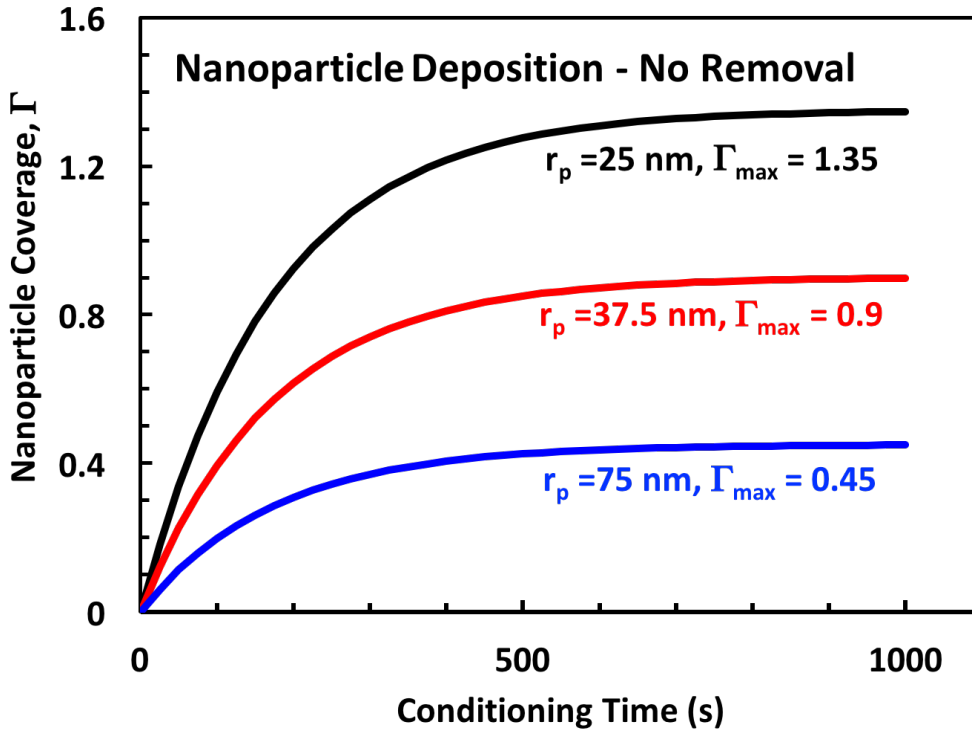


Figure 5 Fraction of bead surface area covered versus conditioning time. The labels besides the curves give the nanoparticle radii and the maximum theoretical coverage. All other parameters are given in Table 2 except the $X = 0$ (i.e. no nanoparticle removal).

Nanoparticle removal. During turbulent mixing, bead-bead collisions will occur. We assume that when the surface of one bead rubs across another, within the area of contact, the nanoparticles on both beads are scraped to form aggregates that are irreversibly dislodged from the bead surfaces. The experimental results in Figure 3 suggest that many of the nanoparticles aggregates are in suspension completely dislodged from the glass bead surfaces. Figure 6 illustrates that upon bead-bead contact, the areas on both bead surfaces subject to nanoparticle removal consist of spherical caps whose areas are proportional the nanoparticle diameter. Using expressions for these areas, the rate of nanoparticle removal is given by Eq. 2 where X the bead-bead collision frequency is an unknown parameter. See the supporting information file for details of the derivation.

$$\frac{d}{dt}\Gamma = -a\Gamma \quad \text{where} \quad a = XC_b \frac{r_p}{r_b} \quad \text{Eq. 2}$$

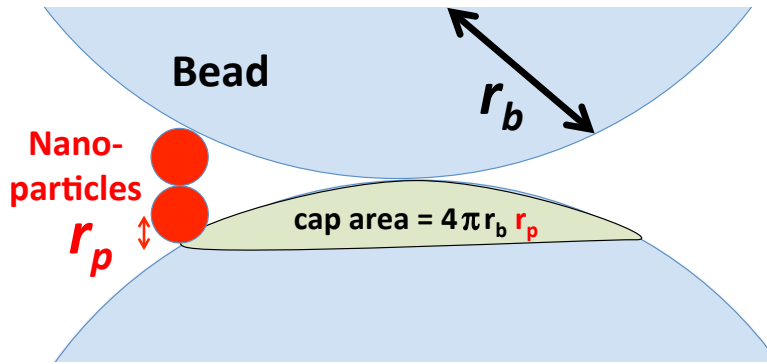


Figure 6 The geometry of two nanoparticle coated glass beads in contact. The areas of interaction are two spherical caps on the beads. The areas of each cap = $4 \pi r_b r_p$.

Note that this mechanism alone does not explain the very large nanoparticle aggregates observed with conditioning time – see Figure 3. For example, if the glass beads are saturated with 63 nm diameter nanoparticles, the total number of particles present in two spherical caps is ~ 5400 . If we assume that all the particles on two caps form a single aggregate and that the aggregate has a 50% void fraction, the aggregate size is about 700 nm. Subsequent aggregation processes in suspension are required to generate the very large aggregates that we have observed.

Absorption and removal. Combining rates of deposition (Eq. 1) with removal (Eq. 2) and integrating gives Eq. 3 for the time dependent coverage during conditioning. The terms a , b , and c are collections of parameters that do not vary with time. The model has only two unknown parameters k_d and X ; values assigned to these parameters were arbitrarily chosen. An increase of k_d will increase the peak surface coverage value and decrease the conditioning time required to achieve peak coverage, whereas an increase of X will diminish the peak surface coverage value and increase the conditioning time required to achieve peak coverage. Figure 7A shows the predicted coverage versus conditioning time for three nanoparticle radii. In all cases the initial deposition is rapid. However, at longer times, particle removal takes over. In this case, the mass concentration of nanoparticles was assumed to be constant, resulting in the smallest particles giving the highest peak coverage and the most sustained coverage.

$$\Gamma = \frac{c}{a-b} e^{-at} (e^{(a-b)t} - 1) \quad \text{Eq. 3}$$

Although the simulated results in Figure 7A look superficially like the recovery versus conditioning time curves in Figure 1, we emphasize that the model simulates conditioning, whereas our results reflect the flotation behaviors. One way to link the model calculations to

predict flotation trends is as follows. We have published a few curves showing glass bead recovery versus the percent nanoparticle coverage. One of our most effective nanoparticles for glass bead flotation gave high recoveries if more than 10% of the bead surfaces were covered with nanoparticles (i.e. $\Gamma_{\text{crit}} \geq 0.1$) (Yang et al., 2011). When we apply this criterion to a curve in Figure 7A, we define two times, t_1 and t_2 for each simulated curve. According to the $\Gamma_{\text{crit}} = 0.1$ criteria, flotation can only occur over the time period, $t_1 < t < t_2$. In other words, the longest effective flotation time, and presumably the highest recovery, corresponds to maximum values of $\Delta t = t_2 - t_1$.

Figure 7B shows the corresponding Δt as a function of nanoparticle radius, based on the criteria $\Gamma \geq \Gamma_{\text{crit}} = 0.1$. The available time for flotation, Δt , decreases almost linearly with nanoparticle radius assuming a constant mass dosage of nanoparticles.

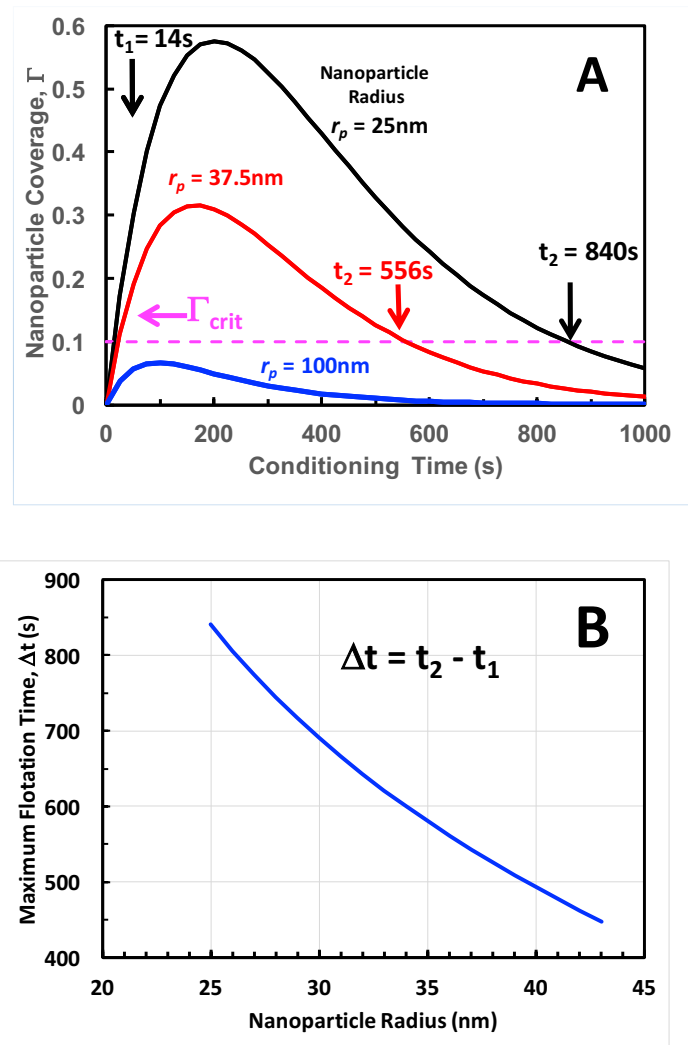


Figure 7 A: The influence of nanoparticle radius on glass bead coverage. Base case parameters

are given in Table 2. B: The corresponding Δt for $\Gamma_{\text{crit}} = 0.1$, as a function of particle radius.

We employed the model to explore the role of nanoparticle dosage. Figure 8 shows Δt as a function of the nanoparticle dosage expressed as Γ_{max} , the coverage on the beads assuming all of the nanoparticles adsorb and do not come off. Up to a dosage of $\Gamma_{\text{max}} = 0.25$ there is no time where the surface coverage, Γ , is greater than 0.1 so $\Delta t = 0$. At higher dosages, Δt increases dramatically. This simulation illustrates a key point in this paper; although low coverage values can promote flotation, the required nanoparticle dosages are high to compensate for the loss of particles if nano-scale ball milling is rapid.

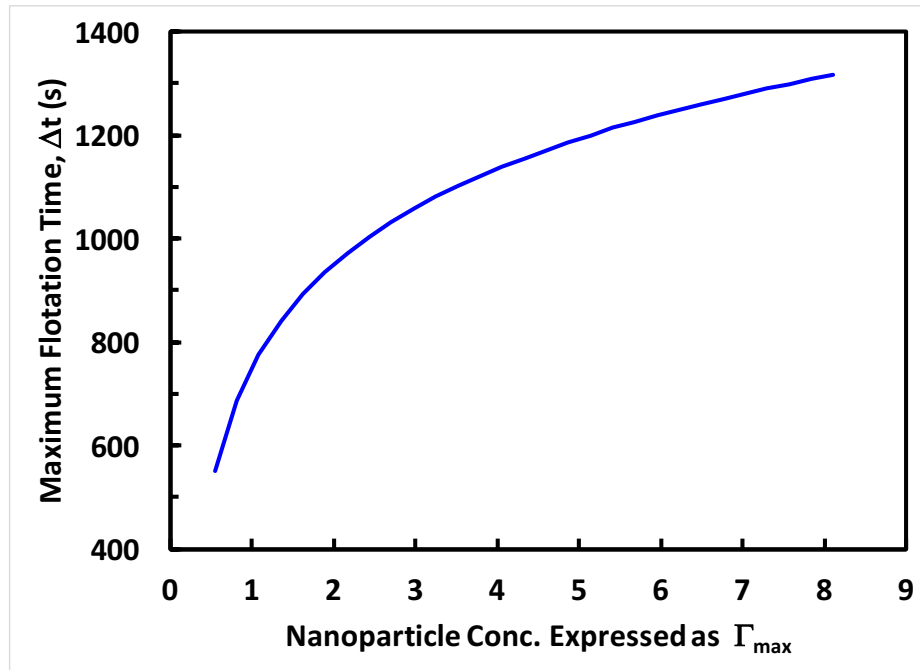


Figure 8 Δt , for $\Gamma_{\text{crit}} = 0.1$, as a function of nanoparticle concentration expressed as the maximum coverage, Γ_{max} . All parameters are given in Table 2 except the nanoparticle concentration that varied from 0.01 to 0.3 g/L

Discussion

Our results demonstrate that turbulent mixing induces bead-bead collisions, which can dislodge nanoparticle aggregates. This concept is not foreign to the mineral processing industry which

has employed high intensity mixing to remove adsorbed slime particles on the surfaces of ultramafic ores. (Chen et al., 1999a, b) There is no evidence in the literature that nano-scale ball milling is important for conventional molecular collectors. Whether present as adsorbed monolayers or hemi-micelles, we believe molecular collectors are simply too small to suffer significant damage during impacts between mineral particles.

Does nano-scale ball milling prevent the development of commercially significant nanoparticle flotation collectors? We have recently shown that core-shell nanoparticles with soft shells require more energy to detach from a surface compared to the hard nanoparticles used in the current work (Dong et al., 2016). Also both our model and our results show that smaller particles are removed more slowly. Finally, when considering pilot or full-scale trials of nanoparticles, this work suggests that nanoparticle flotation collectors should be added just before the flotation cells, minimalizing particle-particle interactions.

From a mechanistic perspective, nano-scale ball milling explains the influence of nanoparticle size – see Figure 7. From the earliest stages of our research, we have consistently observed that smaller nanoparticles are more effective than larger particles, even when the number concentrations are adjusted to give the same maximum coverage of adsorbed particles on the beads. We have argued in the past that many adsorbed small hydrophobic particles are superior to fewer, larger nanoparticles covering the same area because expansion of the three phase contact line is easier with smaller but more closely spaced particles during the attachment of mineral particles to air bubbles (Yang et al., 2012a). However, based on conditioning time studies described herein, nano-scale ball milling is an alternative explanation. Finally, in future work we will present results showing the nano-scale ball milling of core-shell particles with soft shells. In this case, nanoparticle adhesion is greater. However when they are removed by nano-scale ball milling, remnants of the soft shell polymer are left on the glass bead surfaces - footprints.

Conclusions

The main conclusions from this work are:

1. Bead-bead collisions during conditioning and flotation erode deposited nanoparticles (nano-scale ball milling) leading to a dramatic loss in flotation recovery with conditioning time.
2. The scraping of bead surfaces during bead-bead collisions produces large nanoparticle aggregates that do not promote flotation.
3. Larger particles are more susceptible to removal by nano-scale ball milling. The impact area on glass surfaces where deposited nanoparticles could be removed in a single bead-bead collision, increases linearly with nanoparticle diameter.

4. The coverage of nanoparticles adsorbed on glass versus conditioning time results were modeled by combining two exponential functions of time, one describing the nanoparticle deposition and the other describing particle removal by nano-scale ball milling.

Acknowledgments

We thank Drs. Carlos Filipe and Erlita Mastan for mathematical help, and Dr. Songtao Yang from AuTec Innovative Extractive Solutions Ltd. We thank the Natural Sciences and Engineering Research Council of Canada (NSERC) and VALE Base Metals for funding this project. Some measurements were performed in the McMaster Biointerfaces Institute funded by the Canadian Foundation for Innovation. R.P. holds the Canada Research Chair in Interfacial Technologies.

References

- Abarca, C., Ali, M.M., Yang, S., Dong, X., Pelton, R.H., 2016. A Colloidal Stability Assay Suitable for High-Throughput Screening. *Anal. Chem.* 88, 2929-2936.
- Abarca, C., Yang, S., Pelton, R.H., 2015. Towards high throughput screening of nanoparticle flotation collectors. *J. Colloid Interface Sci.* 460, 97-104.
- Attia, Y., Yu, S., 1991. Adsorption thermodynamics of a hydrophobic polymeric flocculant on hydrophobic colloidal coal particles. *Langmuir* 7, 2203-2207.
- Chen, G., Grano, S., Sobieraj, S., Ralston, J., 1999a. The effect of high intensity conditioning on the flotation of a nickel ore, part 2: Mechanisms. *Miner. Eng.* 12, 1359-1373.
- Chen, G., Grano, S., Sobieraj, S., Ralston, J., 1999b. The effect of high intensity conditioning on the flotation of a nickel ore. Part 1: Size-by-size analysis. *Miner. Eng.* 12, 1185-1200.
- Dong, X., Marway, H.S., Cranston, E.D., Pelton, R.H., 2016. Relating nanoparticle shape and adhesiveness to performance as flotation collectors. *Industrial & Engineering Chemistry* submitted.
- Fuerstenau, M., Jameson, G., Yoon, R., 2007. Froth flotation: a century of innovation. Society for Mining, Metallurgy, and Exploration, Littleton, Colorado.
- Goodwin, J.W., Ottewill, R.H., Pelton, R., 1979. Studies on the Preparation and Characterization of Monodisperse Polystyrene Lattices .5. Preparation of Cationic Lattices. *Colloid Polym. Sci.* 257, 61-69.
- Hadler, K., Aktas, Z., Cilliers, J.J., 2005. The effects of frother and collector distribution on flotation performance. *Miner. Eng.* 18, 171-177.
- Kuopanportti, H., Suorsa, T., Dahl, O., Niinimäki, J., 2000. A model of conditioning in the flotation of a mixture of pyrite and chalcopyrite ores. *Int. J. Miner. Process.* 59, 327-338.
- Laskowski, J.S., Yu, Z., 2000. Oil agglomeration and its effect on beneficiation and filtration of low-rank/oxidized coals. *Int. J. Miner. Process.* 58, 237-252.
- Laskowski, J.S., Yu, Z., Zhan, Y., 1995. Hydrophobic agglomeration of fine coal, in: Laskowski, J.S., Poling, G.W. (Eds.), *Proceedings of the 1st UBC-McGill Bi-Annual International Symposium on Fundamentals of Mineral Processing*. Metal Society of CIM, Vancouver, p. 245.
- Littlefair, M.J., Lowe, N.R.S., 1986. On the selective flocculation of coal using polystyrene latex. *Int. J. Miner. Process.* 17, 187-203.
- Lyadov, V.V., Gryanko, V.I., Nikitin, I.N., Prebobrazhenskii, B.P., 1979. Selective flocculation of coal slurries using latexes. *Coke Chemistry* 9, 12.
- Palmes, J.R., Laskowski, J.S., 1993. Effect of the properties of coal surface and flocculant type on the flocculation of fine coal. *Miner. Metall. Proc.*, 218-222.

- Xia, W.C., Yang, J., Liang, C., Zhu, B., 2014. The Effects of Conditioning Time on the Flotation of Oxidized Coal. *Energy Sources, Part A: Recovery, Utilization, and Environmental Effects* 36, 31-37.
- Yang, S., Pelton, R., 2011. Nanoparticle Flotation Collectors II: The Role of Nanoparticle Hydrophobicity. *Langmuir* 27, 11409–11415.
- Yang, S., Pelton, R., Abarca, C., Dai, Z., Montgomery, M., Xu, M., Bos, J.-A., 2013a. Towards nanoparticle flotation collectors for pentlandite separation. *Int. J. Miner. Process.* 123, 137-144.
- Yang, S., Pelton, R., Montgomery, M., Cui, Y., 2012a. Nanoparticle Flotation Collectors III – The Role of Nanoparticle Diameter. *ACS Appl. Mater. Inter.* 4, 4882–4890.
- Yang, S., Pelton, R., Raegen, A., Montgomery, M., Dalnoki-Veress, K., 2011. Nanoparticle Flotation Collectors – Mechanisms Behind a New Technology. *Langmuir* 27, 10438–10446.
- Yang, S., Pelton, R., Xu, M., Dai, Z., 2012b. Nanoparticle Flotation Collectors for Pentlandite, Proceedings of the 44th Annual Canadian Mineral Processors Conference. Canadian Institute of Mining Metallurgy and Petroleum, Ottawa, pp. 225-236.
- Yang, S., Razavizadeh, B.M., Pelton, R., Bruin, G., 2013b. Soft Nanoparticle Flotation Collectors. *ACS Appl. Mater. Inter.* 5, 4836–4842.
- Zhan, Y., 1999. Latices as flocculants in selective flocculation of mineral suspensions, Department of Mining and Mineral Processing. University of British Columbia, Vancouver, Canada.

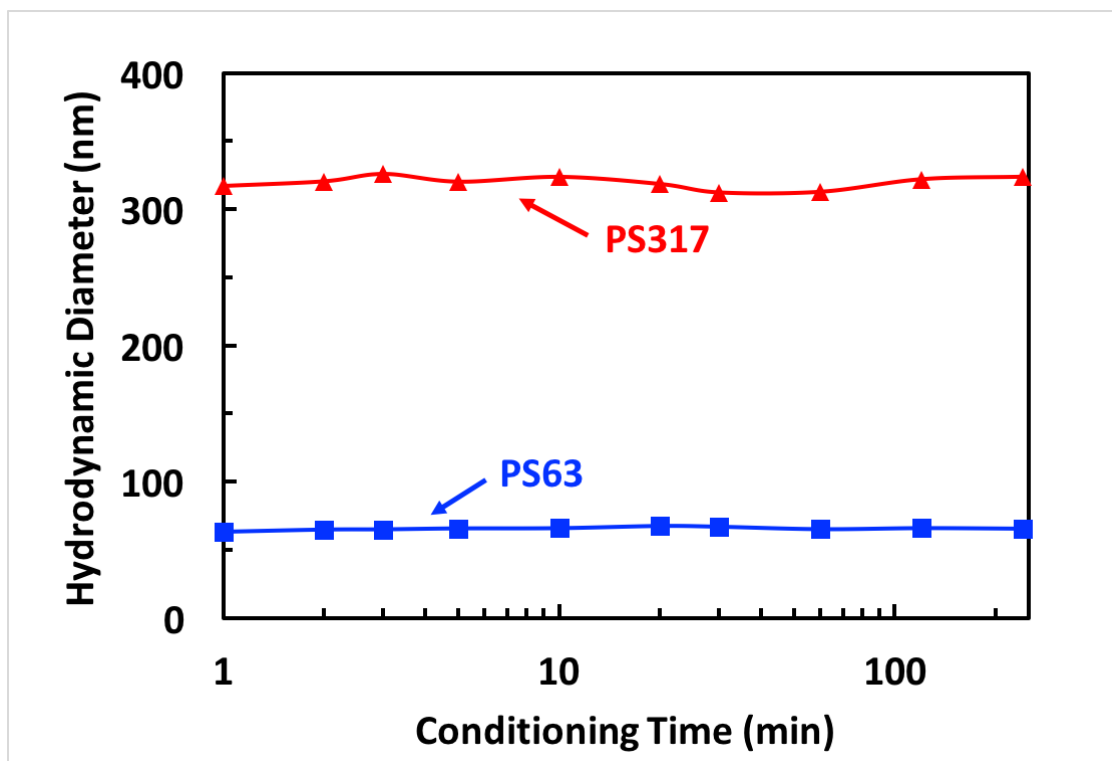
Appendix: Supporting Information for Chapter 3

Figure S1 Nanoparticle size distributions for the suspension in an agitated flotation cell without glass beads. Solid lines are the lines drawn to guide the eye.

This model simulates the adsorption and removal of nanoparticles from glass bead surfaces during conditioning, a process was termed as nano-scale ball milling.

Modeling by R. Pelton 2015-2016

Symbols

Γ	Fraction of glass beads covered with nanoparticles
C_p	Concentration of individual nanoparticles in solution, $1/m^3$
C_{po}	Initial nanoparticle concentration
C_{ad}	Concentration of adsorbed nanoparticles
C_b	Concentration of glass bead
k_d	Rate constant of nanoparticle deposition, m^3/s
r_p	Radius of nanoparticle
r_b	Radius of glass bead
$X \cdot C_b^2$	Number of bead-bead collisions per second

Deposition rate - no removal, assume coverage is low - no blocking

$$\Gamma = \frac{C_{ad} \cdot \pi \cdot r_p^2}{C_b \cdot 4 \cdot \pi \cdot r_b^2} = \alpha \cdot C_{ad} \quad \text{Defining coverage of glass spheres with nanoparticles}$$

$$\frac{d}{dt} \Gamma = \alpha \frac{d}{dt} C_{ad} \quad \alpha = \frac{r_p^2}{4 \cdot C_b \cdot r_b^2}$$

$$\frac{d}{dt} C_p = -k_d \cdot C_p \cdot C_b$$

$$\frac{d}{dt} \ln(C_p) = -k_d \cdot C_b \quad \text{NP conc. in solution decreases exponentially with time}$$

$$C_p(t) = C_{po} \cdot \exp(-k_d \cdot C_b \cdot t) \quad C_p = C_{po} \quad \text{when } t = 0$$

$$C_{ad}(t) = C_{po} - C_p(t)$$

$$\Gamma_d(t) = \alpha \cdot C_{po} \cdot (1 - \exp(-k_d \cdot C_b \cdot t))$$

$$\frac{d}{dt} \Gamma_d = \alpha \cdot C_{po} \cdot k_d \cdot C_b \cdot \exp(-k_d \cdot C_b \cdot t)$$

Simplifying where b and c are independent of time

$$\frac{d}{dt} \Gamma_d = c \cdot \exp(-b \cdot t) \quad \text{Equation 1}$$

where the following are constants for a given experiment

$$b = k_d \cdot C_b$$

$$c = \alpha \cdot C_{p0} \cdot k_d \cdot C_b = \frac{r_p^2}{4 \cdot C_b \cdot r_b^2} \cdot C_{p0} \cdot k_d \cdot C_b = \frac{r_p^2}{4 \cdot r_b^2} \cdot C_{p0} \cdot k_d$$

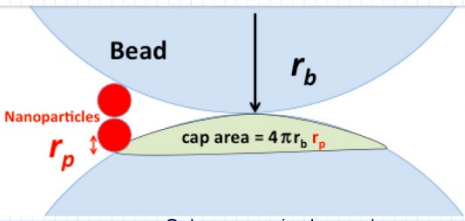
$$c = \frac{r_p^2}{4 \cdot r_b^2} \cdot C_{p0} \cdot k_d$$

$$\Gamma_d(t) = \frac{r_p^2}{4 \cdot C_b \cdot r_b^2} \cdot C_{p0} \cdot (1 - \exp(-k_d \cdot C_b \cdot t))$$

Particle removal

Assume when two beads collide, the adsorbed nanoparticles on each bead that are in the interaction zone are rubbed off (eroded) and are deactivated

The interaction zone on each bead is assumed to be a spherical cap with a height equal to the nanoparticle radius.



Only one cap is shown above, however, np on caps of both beads are assumed to be eroded when two beads collide.

$A_c = 2 \pi \cdot r_b \cdot 2 r_p$ area of spherical cap - ref Wolfram

$A_T = 4 \pi \cdot r_b^2 \cdot C_b$ total bead area per m³

$\frac{A_c}{A_T} = \frac{2 r_p}{2 \cdot r_b \cdot C_b}$ This is the area of one spherical cap divided by total bead area

$X := \frac{m^3}{s}$ Rate constant for bead/bead collisions

$X \cdot C_b^2$ Rate of bead/bead collisions

$\frac{d}{dt} C_{ad} = -X \cdot C_b^2 \cdot 2 \cdot \frac{A_c}{A_T} \cdot C_{ad}$ Rate of removal of adsorbed nanoparticles

$$\frac{d}{dt}\Gamma = -X \cdot C_b^2 \cdot 2 \cdot \frac{A_c}{A_T} \cdot \Gamma$$

$$\frac{d}{dt}\Gamma = -a \cdot \Gamma \quad \text{Equation 2}$$

where $a = X \cdot C_b^2 \cdot 2 \cdot \frac{A_c}{A_T} = X \cdot C_b \cdot \frac{2 r_p}{r_b}$ a is a collection of terms independent of time

Combining deposition, Equation 1, and removal, Equation 2.

$$\frac{d}{dt}\Gamma = c \cdot \exp(-b \cdot t) - a \cdot \Gamma \quad \text{Equation 3}$$

a , b , and c are constants for a given experiment

$$\Gamma = \frac{c}{a-b} \cdot e^{-a \cdot t} \cdot (e^{(a-b) \cdot t} - 1) \quad \text{Equation 4 Integrated form}$$

At peak of Γ vs t , slope = 0

$$\Gamma_{max} = \frac{-a \cdot b \cdot C_{po} \cdot \exp(-b \cdot t_{max})}{a}$$

substituting for a , b , c

$$\Gamma_{max} = \frac{\frac{r_p}{r_b} \cdot k_d \cdot C_{po}}{-X \cdot C_b} \cdot \exp(-(k_d \cdot C_b) \cdot t_{max})$$

5 Ball milling July 20.mcdx 07/25/2016

Non-Commercial Use Only

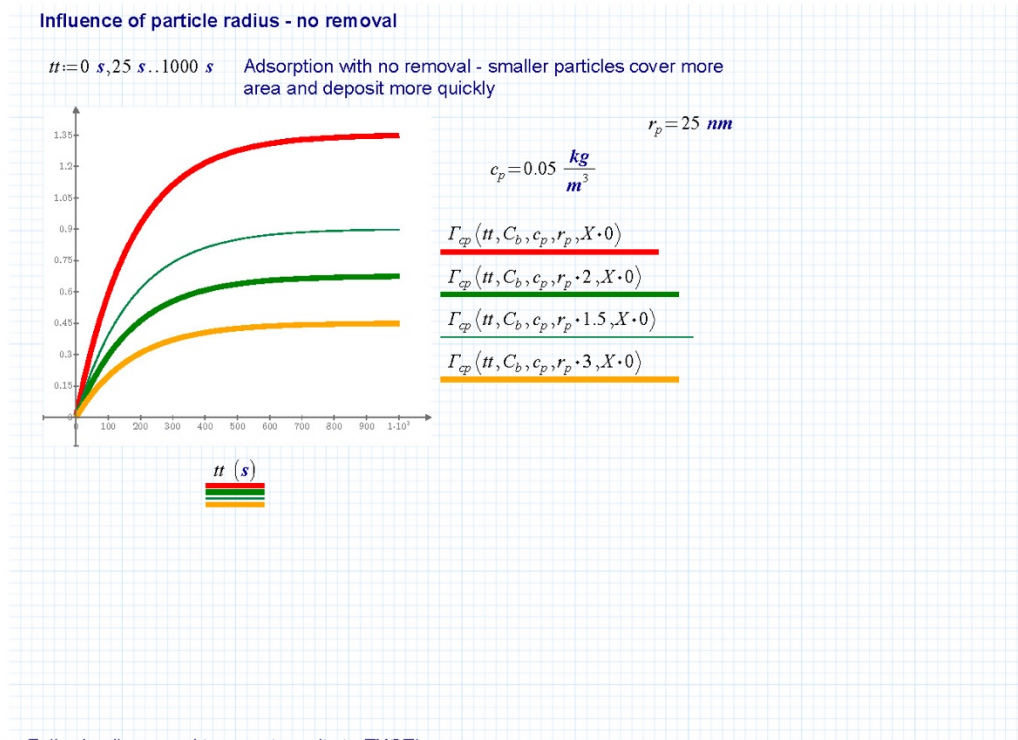
Numerical evaluation

Beads		nanoparticles	
$r_b := 21.5 \mu\text{m}$	radius	$r_p := 25 \text{ nm}$	radius
$\rho_b := 2.2 \frac{\text{gm}}{\text{mL}}$	density	$c_p := 0.05 \frac{\text{gm}}{\text{L}}$	dose
$m_b := 2 \text{ gm}$	mass added	$\rho_{ps} := 1.05 \frac{\text{gm}}{\text{mL}}$	density
$V := 120 \text{ mL}$	liquid volume		
$C_b := \frac{m_b}{\rho_b \cdot \frac{4}{3} \pi \cdot r_b^3 \cdot V} = (1.8198 \cdot 10^{11}) \frac{1}{\text{m}^3}$	initial bead conc.	$C_{po} := \frac{c_p}{\rho_{ps} \cdot \frac{4}{3} \pi \cdot r_p^3} = (7.2757 \cdot 10^{17}) \frac{1}{\text{m}^3}$	initial nanoparticle conc.
$\Gamma_{max}(C_b, c_p, r_p) := \frac{\frac{c_p}{\rho_{ps} \cdot \frac{4}{3} \pi \cdot r_p^3} \cdot \pi \cdot r_p^2}{C_b \cdot 4 \pi \cdot r_b^2}$	Maximum Γ assuming all nanoparticles adsorb	$X := \frac{\text{m}^3}{\text{s}} \cdot 10^{-11}$	rate constant for bead/bead collisions
Equation 4 coded as a function		$k_d := \frac{\text{m}^3}{\text{s}} \cdot 10^{-13.5}$	rate constant for bead/nanoparticle collisions

$$\Gamma_{ep}(t, C_b, c_p, r_p, X) := \frac{\frac{k_d}{4 \cdot r_b^2} \cdot \frac{c_p}{\rho_{ps} \cdot \frac{4}{3} \pi \cdot r_p^3}}{X \cdot C_b \cdot \frac{2 \cdot r_p}{r_b} - k_d \cdot C_b} \cdot \exp\left(-X \cdot C_b \cdot \frac{2 \cdot r_p}{r_b} \cdot t\right) \cdot \left(\exp\left(\left(X \cdot C_b \cdot \frac{2 \cdot r_p}{r_b} - k_d \cdot C_b\right) \cdot t\right) - 1\right)$$

6 Ball milling July 20.mcdx 07/25/2016

Non-Commercial Use Only



7 Ball milling July 20.mcdx 07/25/2016

Non-Commercial Use Only

Following lines used to export results to EXCEL

```

i:=1,2..40
te := i · 25
a := WRITEEXCEL ("a.xls", te)
c1i := Γcp (te · s, Cb, cp, rp, X)
b := WRITEEXCEL ("b.xls", c1)
c2i := Γcp (te · s, Cb, cp, rp · 1.5, X)
c := WRITEEXCEL ("c.xls", c2)
c3i := Γcp (te · s, Cb, cp, rp · 2, X)
d := WRITEEXCEL ("d.xls", c3)
c4i := Γcp (te · s, Cb, cp, rp · 4, X)
e := WRITEEXCEL ("eee.xls", c4)

```

$1.5 \cdot r_p = 37.5 \text{ nm}$

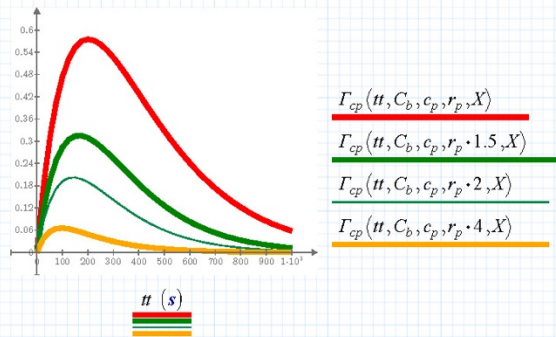
$2 \cdot r_p = 50 \text{ nm}$

$4 \cdot r_p = 100 \text{ nm}$

8 Ball milling July 20.mcdx 07/25/2016

Non-Commercial Use Only

Adsorption plus removal. Increasing the np size at constant mass concentration lowers the peak coverage and slightly shifts the curves to the left.



Increasing the bead concentration lowers the peak coverages and shifts it to shorter times

Calculating t_1 and t_2 , the times where coverage equals a critical value

$\Gamma_{crit} := 0.1$ The assumed minimum coverage for flotation

Calculating the times corresponding to Γ_{crit}

$t := 802 \text{ s}$

$t_2(C_b, c_p, r_p) := \text{root}(\Gamma_{crit} - \Gamma_{cp}(t, C_b, c_p, r_p, X), t)$

$t_2(C_b, c_p, 1.5 \cdot r_p) = 556.2978 \text{ s}$

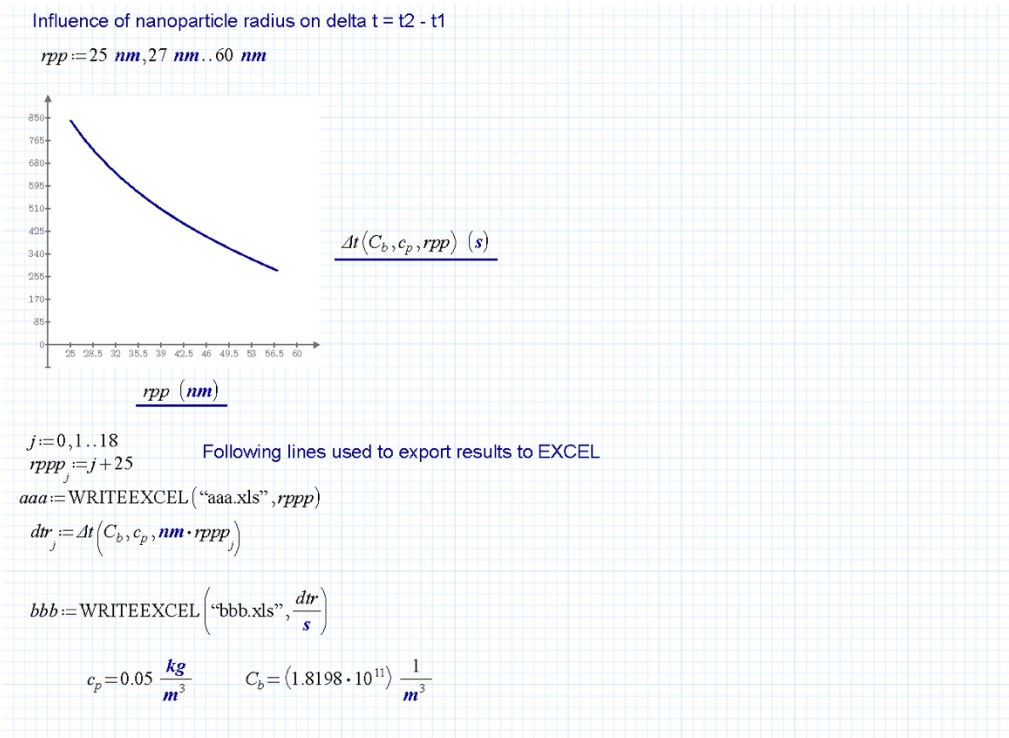
$t_1(C_b, c_p, r_p) := \text{root}(\Gamma_{crit} - \Gamma_{cp}(t, C_b, c_p, r_p, X), t, 0 \text{ s}, 150 \text{ s})$

$t_1(C_b, c_p, r_p) = 13.7736 \text{ s}$

$\Delta t(C_b, c_p, r_p) := t_2(C_b, c_p, r_p) - t_1(C_b, c_p, r_p)$

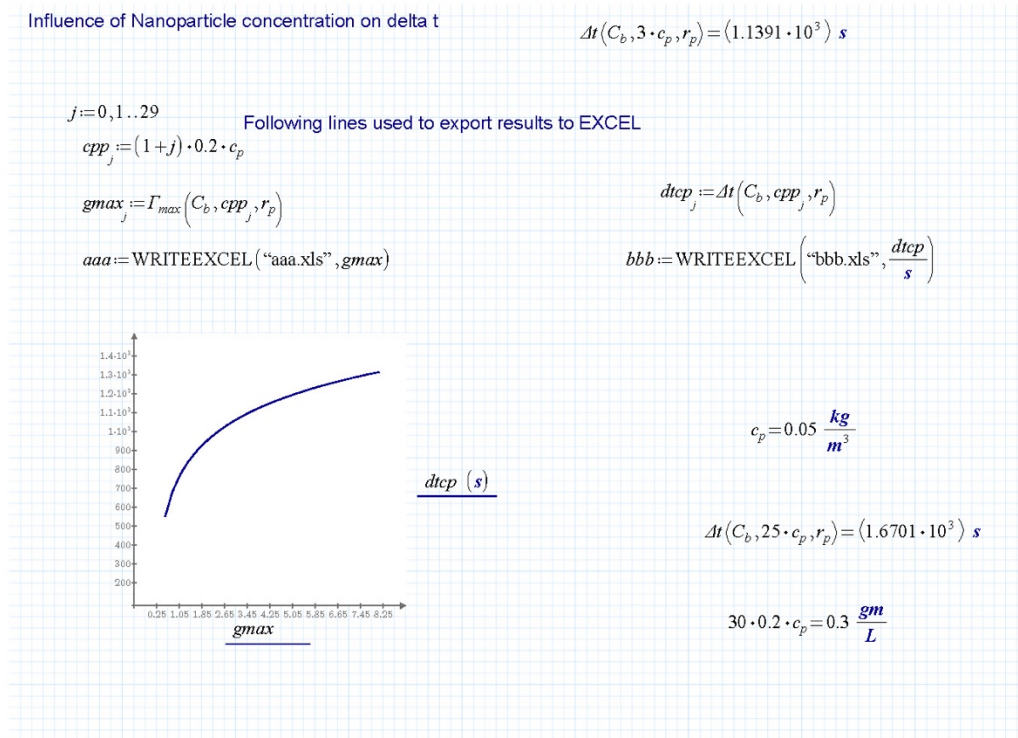
$\Delta t(C_b, c_p, r_p) = 840.5191 \text{ s}$

[Browse for Image...](#)



11 Ball milling July 20.mcdx 07/25/2016

Non-Commercial Use Only



12 Ball milling July 20.mcdx 07/25/2016

Non-Commercial Use Only

Maximum number of nanoparticles adsorbed on two caps

$$N_{max}(r_p) := 2 \frac{4 \pi \cdot r_p \cdot r_b}{\pi \cdot r_p^2}$$

Maximum number of adsorbed nanoparticles on two patches

$$N_{max}(32 \text{ nm}) = 5.375 \cdot 10^3$$

$$Vm(r_p) := N_{max}(r_p) \cdot \frac{4}{3} \pi \cdot r_p^3$$

$$\left(\frac{2 \cdot Vm(32 \text{ nm})}{\frac{4}{3} \pi} \right)^{\frac{1}{3}} = 706.2408 \text{ nm}$$

Corresponding diameter of spherical aggregate with 50% void volume

Chapter 4 Effects of Nano-scale Ball Milling on Soft Nanoparticle Collectors

In chapter 4, flotation experiments were conducted by myself with the assistance of Marie Price who worked with me as a summer student. I prepared the AFM sample. The AFM imaging and AFM data processing were performed by Dr. Gustafsson who work with Dr. Pelton as a post-doctoral fellow. The rest of the experiments were conducted by myself. I plotted all experimental data. I wrote the manuscript, Dr. Gustafsson added the experimental description of AFM imaging, and edited my first draft. Dr. Pelton helped to analyze data, gave useful advice on particle-bubble attachment test, and edited the manuscript into this final version. This chapter is in preparation for submission.

Effects of Nano-scale Ball Milling on Soft Nanoparticle Collectors

Xiaofei Dong[†], Emil Gustafsson[†], Marie Price[†], and Robert Pelton^{†*},

[†]Department of Chemical Engineering, McMaster University, 1280 Main Street West, Hamilton, Ontario, Canada L8S 4L7

Introduction

With high corrosion resistance and non-toxic properties, nickel and nickel alloys have been widely used in steels industry, coinage, food handling and pharmaceutical equipment ¹. Separation of Pentlandite (Pn, Ni_{4.5}Fe_{4.5}S₈), the principal formula of nickel, from associated slimes is usually achieved by froth flotation, where hydrophobic solids are carried to the surface with rising air bubbles overflowing the flotation cell into the collector launder, whereas the unwanted hydrophilic slimes are left on the bottom of the cell to be discharged ². The surface of natural Pn particles is hydrophilic and therefore it is necessary to increase the hydrophobicity of the surface prior to flotation. In commercial Pn flotation practices, a molecular xanthate collector such as potassium amyl xanthate (PAX), is frequently employed in the conditioning step to impart hydrophobicity to Pn particles ³.

As a result of decreasing high grade nickel ore reserves, increasing efforts are directed towards the processing of disseminated ultramafic deposits ^{4,5}. However, extraction of nickel from ultramafic ore faces the technical challenge that serpentine fibers, typically with a diameter of 20 nm, are present on the ore surface ^{6,7}, acting as a surface barrier that interferes with bubble attachment ^{8,9} and thereby limits the nickel recovery. In addition, the continued use of xanthate has raised ever increasing environmental concerns, as carbon disulfide is readily emitted when xanthate decomposes and excess xanthate in discharge waters is a threat to aquatic life ¹⁰. There are both economic and environmental reasons to find a replacement for xanthate collectors ¹¹.

Over the past few years, we have explored using polymeric nanoparticles as flotation collectors. The potential advantage of nanoparticle collectors over molecular collectors for nickel ultramafic ore separation is that the efficiency of relatively large nanoparticles adsorbed between serpentine

surface fibers is less suppressed by the fibers than the 1 nm patches of conventional xanthate collector. Laboratory scale flotation experiments, using glass beads as a model of Pn particles, have demonstrated that cationic hydrophobic nanoparticles can adsorb on negatively charged glass bead surfaces and facilitate the attachment of air bubbles in flotation¹²⁻¹⁵. In addition, Pn flotation studies showed that a polystyrene based nanoparticle collector with an imidazole functionalized surface can sometimes give better Pn recovery than PAX¹⁶.

We have previously shown that soft particles give substantially higher adhesion to glass beads, the model of mineral particles, than corresponding rigid particles¹⁷. Studies of the recovery as a function of conditioning time of rigid nanoparticle collectors revealed that bead-bead collisions (nano-scale ball milling) during the conditioning dislodge adsorbed polystyrene nanoparticles, and small nanoparticle collectors were less susceptible to erosion than larger particles¹⁸. We speculate that small nanoparticle size and high nanoparticle/glass adhesion are two key parameters to minimize the negative impact of nano-scale ball milling on the flotation performance.

In this paper, we report the flotation performance for soft nanoparticle collectors as a function of conditioning time. The glass beads flotation results of a 356 nm soft shelled polystyrene-poly(*n*-butyl methacrylate) nanoparticle, and two soft-lobed Janus nanoparticles with diameters of 317 nm and 92 nm are compared. Electron microscopy was used to assess the effect of the suggested nano-scale ball milling on the soft nanoparticle collectors. In addition, we present the concept of footprints, which provide direct evidence supporting the removal of adsorbed nanoparticles from bead surfaces, and their potential for improving flotation is discussed.

Experimental Section

Materials. Sodium chloride (>95%) and ethanol (>95%) were purchased from Fisher Scientific and used as received. Glass beads with an average diameter of $43 \pm 11 \mu\text{m}$, determined using a Malvern Mastersizer 2000, were purchased from Polysciences Inc. and used as supplied. The flotation frother, UNIFROTH 250C (>99%), a mixture of monomethyl polypropylene glycol, 250kDa and dipropylene glycol monomethyl ether, was donated by VALE Canada Limited (Mississauga, ON) and used as supplied. Water type 1 (as per ASTM D1193-6²⁰, resistivity 18 M Ω cm, from Barnstead Nanopure Diamond system) were used in all the experiments.

Nanoparticles. Cationic polystyrene-core-poly (*n*-butyl methacrylate)-shell (PS-PB) nanoparticles and polystyrene-poly (*n*-butyl methacrylate) Janus nanoparticles were prepared by two-step seeded emulsion polymerization procedures¹⁷ and the recipes were included in the supporting information file (Table S 1). The hydrodynamic diameter was determined by dynamic light scattering (Brookhaven Instruments Corporation, USA) at a 90° detector angle. The test samples were prepared with 5 mM NaCl solution and diluted to give a scattering intensity between 100 and 150 kcps. The dispersions were equilibrated at 25°C for 3 min before analyzing and the duration of each subsequent measurement was 3 min. Three sets of

measurements were undertaken for each sample and the results were analyzed using BIC dynamic light scattering software (Windows 9KDLSW version 3.34) using the cumulants model, whereas the CONTIN model was used to generate the particle size distribution, expressed as a polydispersity index (PDI).

Electrophoretic mobility (EM) measurements were performed on a Zeta PALS instrument (Brookhaven Instruments Corporation, USA) at 25°C in the phase analysis light scattering mode. 1.5 mL dilute nanoparticle dispersion in 5 mM NaCl were dispensed into a clear cuvette and thermally equilibrated to 25°C before analyzing. The reported EM values were the average of 10 runs, each consisting of 15 scans.

Water sessile drop contact angles on glass slides coated with nanoparticles were measured with a Krüss Drop Shape Analysis System DSA 10 running DSA software (version 1.80.0.2). In a typical water contact angle experiment, pre-cut glass slides (1 cm squares, Gold Line Microscope Slides, VWR) were cleaned in ethanol with sonication for 30 min, followed by rinsing with water. Washed slides were dried with compressed air and then treated with UV-Ozone (UV-Ozone ProCleaner, Bio Force Nanosciences, USA) for 20 min. Cleaned glass slides were immersed for 30 min in 0.5 wt % nanoparticle dispersion in 5 mM NaCl, and then dipped into 5 mM NaCl solution to gently rinse off excess nanoparticles. The slides were dried in air at room temperature.

Flotation. Flotation experiments were performed in a polypropylene 125 mL beaker (Nalgene® 1201-0100, ThermoFisher Scientific, USA) with an average inner diameter of 53 mm, sitting on a 150 mm plastic Petri dish (430599, Corning, USA). 125 mL of 5 mM NaCl solution, nanoparticle dispersion, and 2 g of glass beads (a model for mineral particles) were fed into the beaker. Unless stated otherwise, the nanoparticle dose was 5 mg (dry) from stock dispersions, typically 3.5 % solids. The suspension was agitated using a 25×9 mm cross shape magnetic stir bar (SEOH PTFE Stirrer Bar, Cross 25×9 mm, Scientific Equipment of Houston, USA). The magnetic stir bar was driven by a Corning PC-610 stirrer plate with a speed of 600 RPM, and the conditioning time was set between 1 to 240 minutes. After conditioning, 0.125 mL UniFroth (1 wt%) was added to the flotation suspension giving a frother concentration of 10 mg/L. After 30 seconds of mixing, the stirring speed was increased to 900 rpm and the nitrogen flow to the frit (Corning Pyrex, 30 mm coarse glass frit attached by a 90-degree elbow, purchased from Fisher Scientific) was initiated at a rate of 2.0 L/min. Froths forming on the top of the beaker were scraped over the side to be caught in the Petri dish. After typically 2 minutes, the gas flow was stopped. The dry mass of both the beads collected in the froth and remaining in the flotation beaker was measured and the flotation recovery was calculated as the mass fraction of glass beads that were collected in the froth. A minimum of three replicates were performed for each condition.

Surface Characterization of Flotation Products. The topography of glass beads collected in the froth was examined using a scanning electron microscope (SEM) (JEOL 7000F SEM, JEOL

Ltd., Japan). Dried glass beads were placed on a conductive carbon tape and sputter coated with 5 nm platinum prior to analysis. High resolution SEM images were taken at a working distance of less than 10 mm and accelerating voltages of 2.8-5 kV.

Glass bead topography was further analyzed by atomic force microscopy (AFM) using a BioScope Catalyst BioAFM (Bruker). Images were collected in ScanAsyst mode using SCANASYST-AIR cantilevers (Bruker) with a nominal resonance frequency of 70 kHz and a typical spring constant of 0.4 N/m. Glass beads were isolated from the froth and immobilized on a glass slide using double sided tape. The built-in optical microscope was used to position the cantilever on top of an individual glass bead and images with a scan size of 2x2 μm were obtained.

The elemental composition of the footprint was quantitatively analysed using energy dispersive spectroscopy (EDS, Oxford Instrument) equipped with JEOL 7000F SEM running an Oxford Synergy INCA EDS X-ray microanalysis software. SEM micrographs of the footprint areas of interest for EDS analysis, corresponding spectrum and elemental analysis results are included in the Supporting Information File (Figure S 1, Figure S 2 and Table S 2). The reported elemental weight percentage values were the average of three analyzed footprints.

Quantitative Determination of Solid Particles Picked Up by A Captive Air Bubble. An apparatus was designed and built to perform the captive air bubble pick-up test of glass beads with different surface treatments. As shown in Figure 9, the major components of this customized apparatus include: an air bubble generation and size control system (Needle: 14 gauge, Metal Hub NDL, 2 inch, point style 3, 91014, Hamilton Company, USA; Syringe: Tuberculin Syringe, 1 mL, 5202, Cadence Science, USA); an X-Y-Z positioning stage; a clear polycarbonate cell ($L \times W \times H = 36 \text{ mm} \times 27 \text{ mm} \times 50 \text{ mm}$); a particle bed holder ($L \times W \times H = 12.7 \text{ mm} \times 12.7 \text{ mm} \times 44.7 \text{ mm}$, Fluorimeter quartz cuvette, C9167, Sigma-Aldrich, USA); an independent holder for collected particles ($L \times W \times H = 12.7 \text{ mm} \times 12.7 \text{ mm} \times 45.0 \text{ mm}$, BI-SCP Polystyrene, Four sided clear cuvette, Brookhaven Instruments, USA); and a video recording system equipped with Krüss Drop Shape Analysis System DSA 10. The capture rate speed of the Krüss T1C in-built Frame Grabber Camera (DSA10, KRÜSS GmbH Germany) was set as 25 frames per second (fps).

A captive bubble with a diameter of 2.3 mm was generated in 5 mM NaCl solution containing 10 mg/L UniFroth, and held on the needle. A glass bead bed with a height of 2 mm was brought upward through the solution into contact with the stationary captive air bubble, after which it was lowered down to remove from the air bubble. The entire process of particle attachment to the bubble was monitored and recorded using the video recording system. The captive bubble, coated with the picked up glass beads, was moved, through solution, to another holder. After breaking the air bubble, all beads were collected into the empty holder. The particle holder was then isolated from the cell and sealed before it was horizontally loaded onto the working stage of

an optical microscope (M5 Multi Phase 100, SWIFT, USA). No overlap of beads was observed and an example micrograph of collected bead is shown in the Supporting Information (Figure S 3). The number of glass beads was counted manually under the microscope. For each sample, the experiment was run three times at different positions on the bead bed.

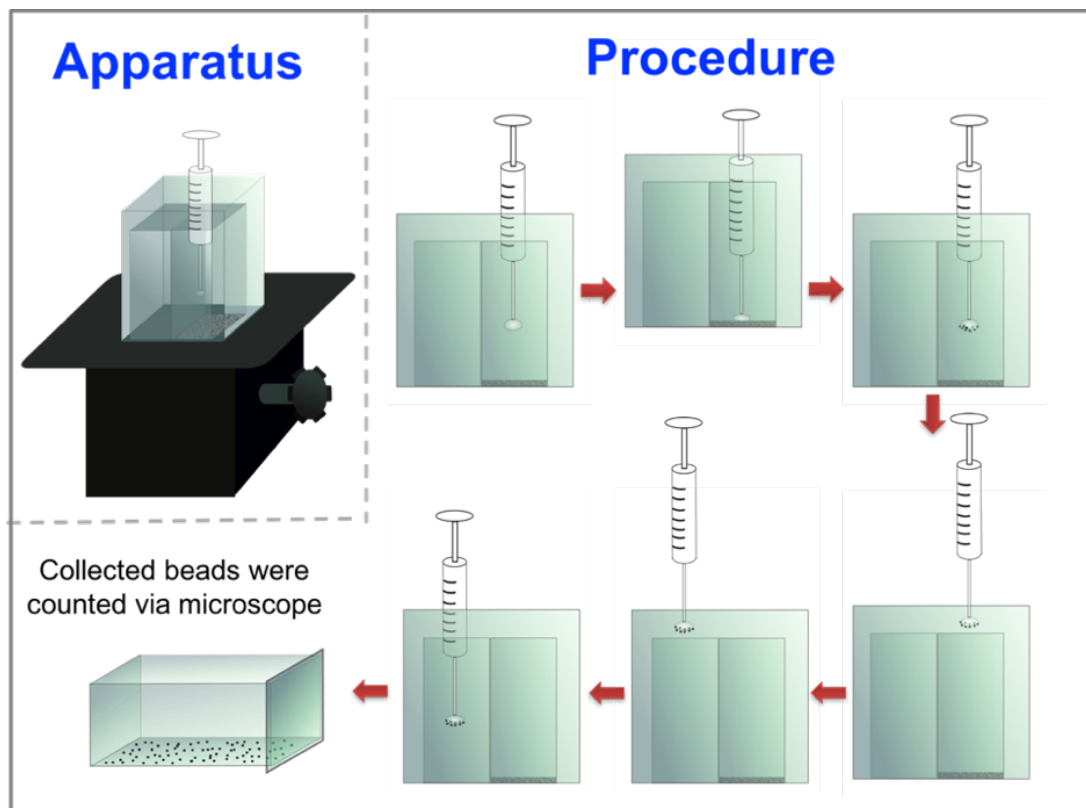


Figure 9 Schematic of the apparatus and experimental procedure of the captive air bubble pick-up test.

Particle-Air Bubble Attachment Test. Figure 10 shows a schematic diagram of the setup for the particle-air bubble attachment test. An air bubble with a diameter of 2.7 mm was generated at the tip of a vertical capillary tube (1/16" OD \times 0.75 mm ID). A suspension of glass bead was fed into a guiding tube (1/16" OD \times 0.75 mm ID) via a syringe pump. Guiding tube was placed 5 mm above the air bubble with the assistance of a micromanipulator (NARISHIGE, MN-151, Japan), which allow individual glass bead drop onto the air bubble surface. This experiment was carried out in a clear polycarbonate cell ($L \times W \times H = 36 \text{ mm} \times 27 \text{ mm} \times 50 \text{ mm}$) filled with 5 mM NaCl solution containing 10 mg/L UniFroth. The entire process of particle-bubble

attachment was monitored and recorded using a Krüss T1C in-built Frame Grabber Camera (DSA10, KRÜSS GmbH Germany) with a recording speed of 25 fps. Example videos can be found in the Supporting Information file (Video S1).

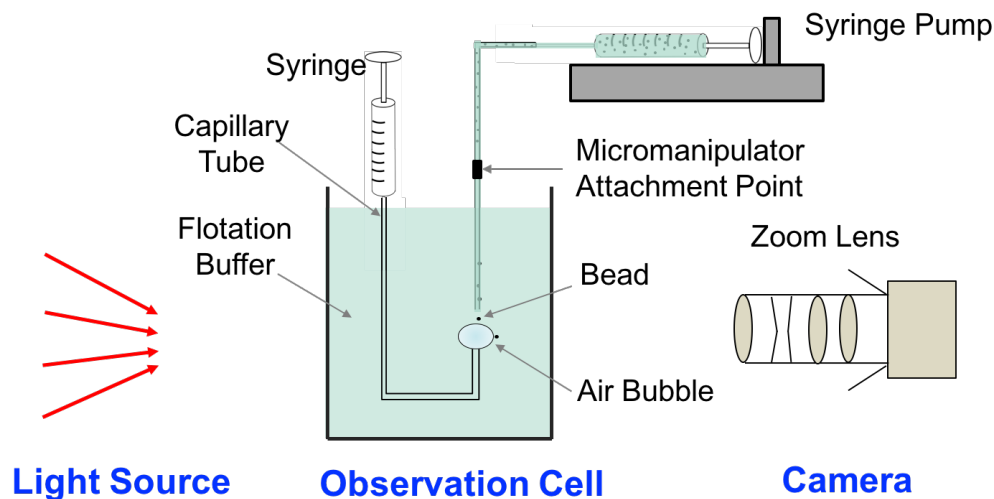


Figure 10 Experimental apparatus of the particle-air bubble attachment test.

Results

Soft core-shell and Janus nanoparticles. Cationic polystyrene-core-poly(*n*-butyl methacrylate)-shell (PS-PB core-shell) and polystyrene/poly(*n*-butyl methacrylate) (PS/PB Janus) nanoparticles were prepared via a two-step seeded emulsion polymerization¹⁷ and the latex properties are summarized in

Table 3. The morphology of the synthesized soft nanoparticles was examined using TEM, and the micrographs are included in the Supporting Information file (Figure S 5). The 356 nm core-shell nanoparticles have a PS core and a PB shell with a thickness of 20 nm, while the 92 nm and 317 nm Janus nanoparticles have a PS lobe on one side and a PB lobe at the opposite side. Both nanoparticles are soft at room temperature since PB has a T_g of 24-31 °C. With surfactant-free surfaces decorated with positively charged amidine groups, derived from the polymerization initiator, the prepared nanoparticles were cationic, and the stock dispersions were colloidally stable. Water contact angle values demonstrated that both nanoparticles are sufficiently hydrophobic to promote flotation¹².

Table 3 Properties of surfactant free, cationic polystyrene-core-poly(*n*-butyl methacrylate)-shell (PS-PB-315 core-shell) and polystyrene/poly(*n*-butyl methacrylate) (PS/PB-92 and

PS/PB-315 Janus) nanoparticles, where the final number on the nanoparticle designation represents the particle hydrodynamic diameter. The electrophoretic mobility (EM) was measured in 5 mM NaCl solution at ambient pH. The standard errors (SE) for the reported EM values were estimated from the average of 10 runs, each consisting of 15 scans. The standard errors (SE) for the contact angle values were calculated from the average of 3 measurements, where the duration for each measurement was 30 seconds.

Nanoparticle	Diameter (PDI), nm	EM (SE), $\times 10^{-8} \text{ m}^2 \text{ s}^{-1} \text{ V}^{-1}$	Water CA (SE), °
PS-PB-356 Core-shell	356.2 (0.016)	4.33 (0.10)	60.0 (1.3)
PS/PB-92 Janus	92.0 (0.036)	1.95 (0.20)	84.1 (1.7)
PS/PB-315 Janus	314.8 (0.021)	4.91 (0.24)	64.7 (0.5)

Flotation Performance. The flotation performance of soft nanoparticles was tested as a function of conditioning time. Flotation experiments were conducted using a laboratory-scale model system where 43 μm diameter glass beads were employed as a model of mineral particles. During the entire flotation operation, the mixture was agitated vigorously to avoid sedimentation of the heavy beads. All flotation experiments, except the control, were performed with a constant nanoparticle dosage of 2.5 kg/t. A dosage of 2.5 kg/t PS-PB-356 can give 16% theoretical surface coverage, expressed as the total projected area of the deposited particles ($n_p \pi d^2 / 4$, where n_p is the nanoparticle number concentration and d is the nanoparticle hydrodynamic diameter) divided by the total surface area of glass beads. The theoretical coverage of 2.5 kg/t of the PS/PB-92 Janus nanoparticle is 62% and that of 2.5 kg/t PS/PB-315 Janus nanoparticle is 18%.

The glass bead recovery as function of conditioning time for the soft core-shell and Janus nanoparticle collectors is summarized in Figure 11. It should be noted that, without any nanoparticle addition, some of the beads were always carried over to the froth phase by a mechanism called hydraulic entrainment. For the PS-PB-356 core-shell nanoparticle, the maximum recovery was 62% and was obtained after 5 minutes of conditioning. For longer conditioning times the recovery decreased and after 60 minutes of mixing only 15% of the glass beads were carried over to the froth phase, indicating that core-shell particles did not promote glass bead flotation at long conditioning times. For the PS/PB-315 Janus nanoparticle, the maximum recovery 90% was obtained after 3 minutes of conditioning. After 30 minutes of conditioning, over 60% of the beads could be collected, whereas at longer conditioning times the PS/PB-315 Janus nanoparticle does not promote flotation. The PS/PB-92 Janus nanoparticle gave a 96% recovery after only 1 minute of conditioning, and the maximum recovery, 99%, was

achieved after 5 minutes of conditioning. The PS/PB-92 Janus nanoparticle was effective for up to 240 minutes of conditioning, after which over 60% of the beads could still be collected.

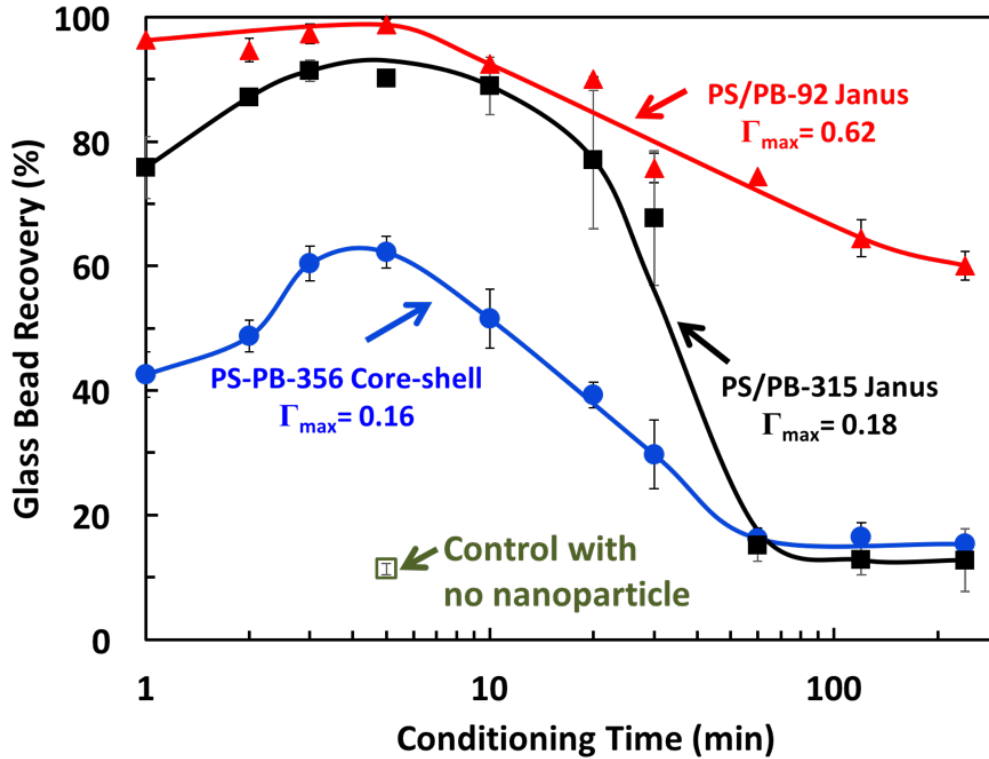


Figure 11 Glass bead flotation recovery as a function of the conditioning time for the PS-PB-356 core-shell, PS/PB-92 Janus and PS/PB-315 Janus nanoparticles. The nanoparticle dosage is 2.5 kg/t. Flotation experiments were performed in triplicate, and the error bars represent the standard deviation. Solid lines are the lines drawn to guide the eye. Conditioning time of control experiment is 5 minutes.

To assess the effect of the suggested nano-scale ball milling on the soft nanoparticle coverage of glass beads, electron microscopy was used to image glass beads that had been conditioned for different times. Figure 12 shows a series of SEM images where the micrographs in left column correlate with 5 minutes of conditioning and those in the right column represent 240 minutes of conditioning. It can be seen that all three soft nanoparticles gave high coverages at short conditioning times. For long conditioning times, nearly all of the large nanoparticles, PS-PB-356 and PS/PB-317, were removed, whereas a significant number of small Janus nanoparticles, PS/PB-92, could be observed after 240 minutes conditioning. This confirmed that extended

conditioning does remove adsorbed particles from the glass bead surfaces but also showed that the small soft nanoparticle, PS/PB-92, was the least susceptible to nano-scale ball milling.

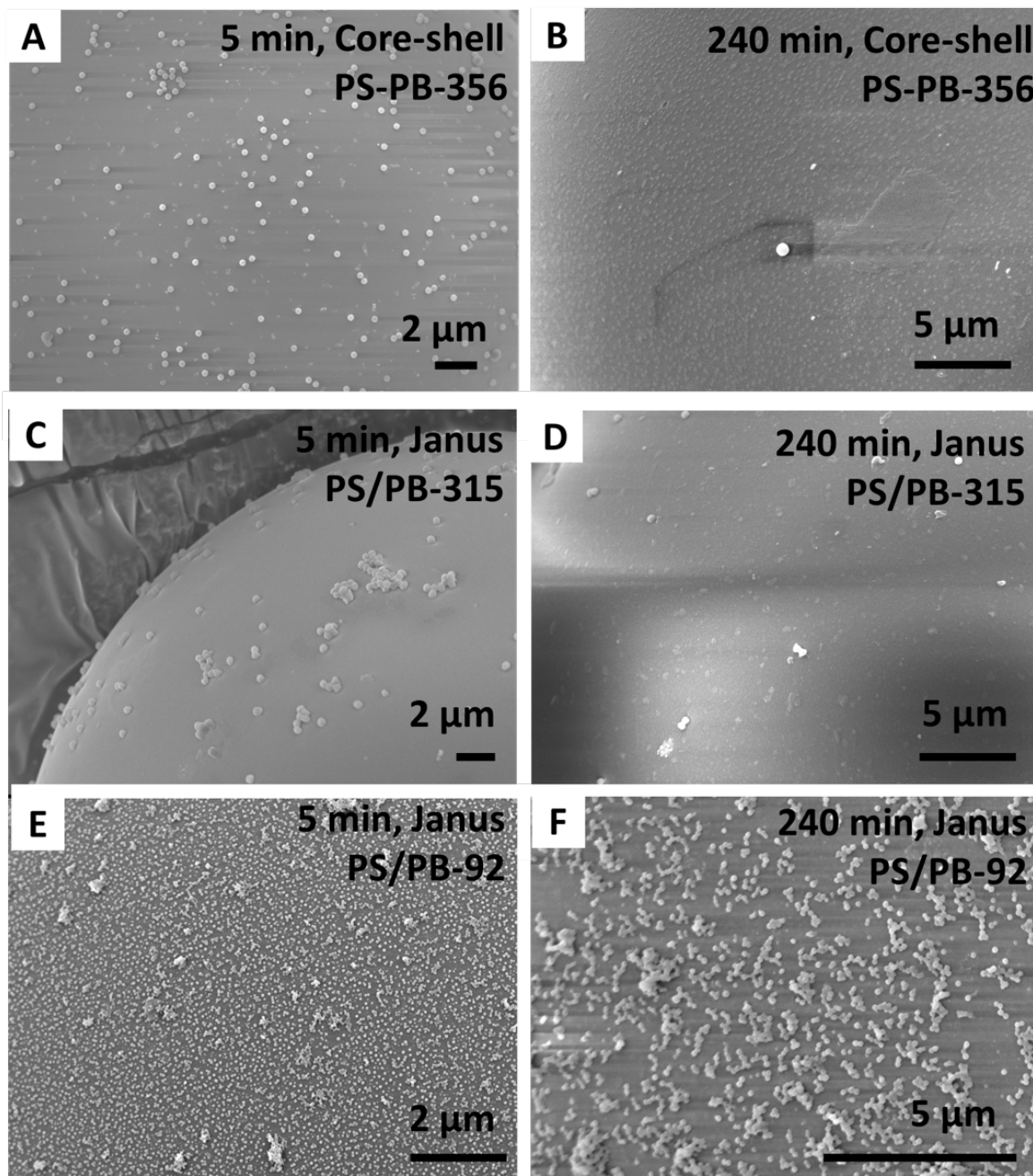


Figure 12 SEM micrographs of PS-PB-356 core-shell, PS/PB-315 Janus and PS/PB-92 Janus nanoparticle coverage on glass bead surfaces for short (5 min) and long (240 min) conditioning time. Micrographs A and B show bead surfaces decorated with PS-PB

core-shell nanoparticles, images C and D show bead surfaces decorated with PS/PB-315 Janus nanoparticles, and images E and F show bead surfaces decorated with PS/PB-92 Janus nanoparticles.

Footprints. Figure 13 shows higher magnification electron micrographs of glass beads after conditioning using the soft shelled nanoparticle collector, PS-PB-356 with a shell thickness of 20 nm. A large number of circular nano-scale patches, significantly smaller than the nanoparticle diameter, can be observed. The typical diameter of these patches is 80 nm, while a few of them have a diameter about 200 nm. The topography of the nano-scale patches on glass beads was also investigated by AFM (Figure 13d). Image analysis determined the height of the patch to be about 20 nm and morphologically these patches are clearly distinguishable from deposited nanoparticles.

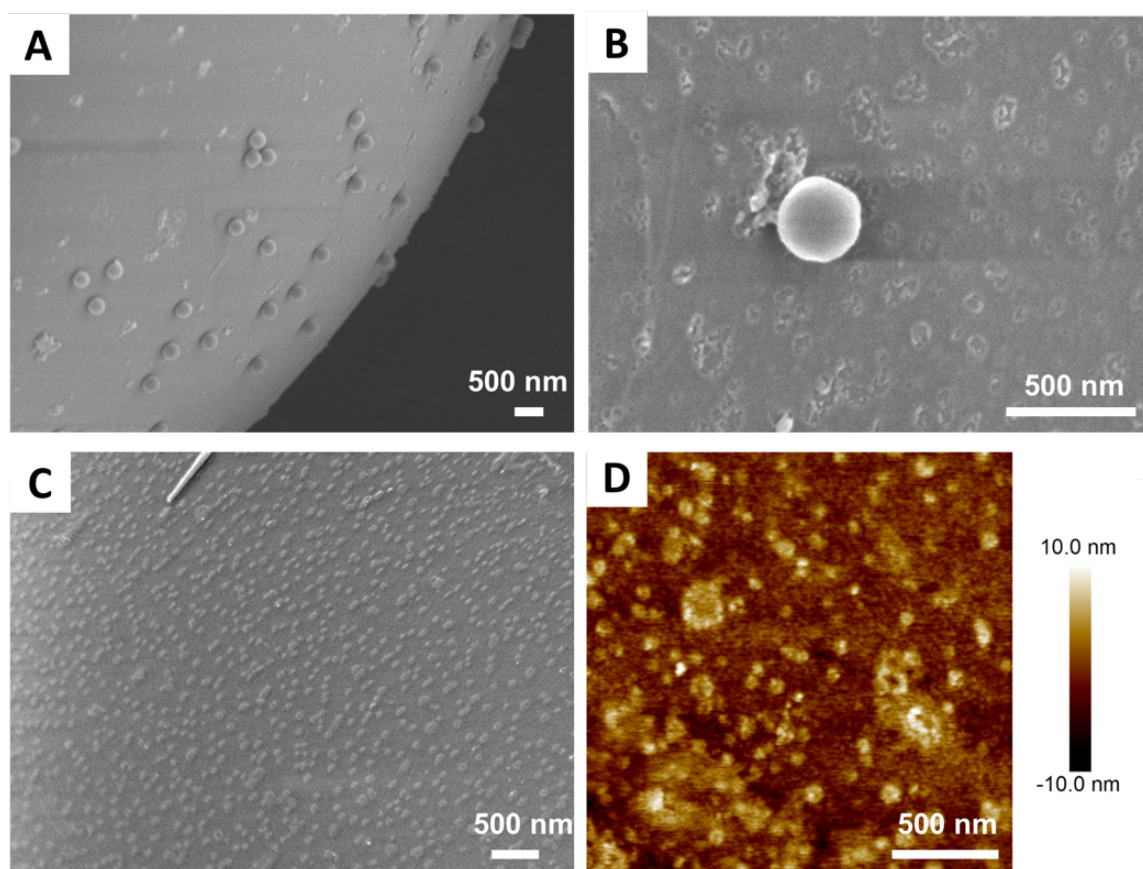


Figure 13 Micrographs of glass beads collected in the froth after 5 minutes (A and B) and 240 minutes (C and D) of conditioning using 2.5 kg/t PS-PB of nanoparticle as collector. Images A-C are SEM images, and D is an AFM height image.

The elemental composition of the patches was quantitatively analyzed by EDS, the spectrums are included in the supporting information file (Figure S 1, Figure S 2 and Table S 2). The analysis showed that the composition of the patches was 72.11 ± 3.44 wt% carbon and 27.89 ± 3.44 wt% oxygen, which is in good agreement with the composition of the shell polymer PB (75 wt% carbon and 25 wt% oxygen), indicating that these patches are remnants of the soft shell polymer. This suggests that when two beads covered with soft shelled nanoparticles collide, adhesive failure occurs in the soft PB polymer shells in the bead-bead contact zone, leaving PB footprints on the bead surfaces after nanoparticle removal.

Based on the hydrophobic nature of PB, with a water contact angle of 92° ¹⁹, footprints are expected to contribute positively to flotation. Captive air bubble pick-up tests (Figure 9) were performed to characterize the hydrophobicity of glass beads following bearing footprints. Two situations where footprints may offer an advantage were investigated. In the first, for short conditioning time, beads were decorated with both nanoparticles and footprints, as seen in the SEM images in Figure 13A and Figure 13B. In the second, as seen in Figure 13C, the conditioning time was sufficiently long that nanoparticles were dislodged and the beads were decorated with footprints only. Hydrophilic plain beads were also tested as a control experiment. Beads picked up by the air bubble were collected and counted under an optical microscope. The results are summarized in Figure 14. The number of beads picked up by an air bubble was 137 ± 7 for plain glass beads, 1760 ± 194 for nanoparticle and footprint decorated beads, and 1287 ± 91 for footprint decorated beads. Solid particles immersed in aqueous solution are more readily picked up by static air bubble contact if their contact angle is higher, thus the captive air bubble pick-up tests suggested that the footprints are sufficiently hydrophobic to promote adhesion.

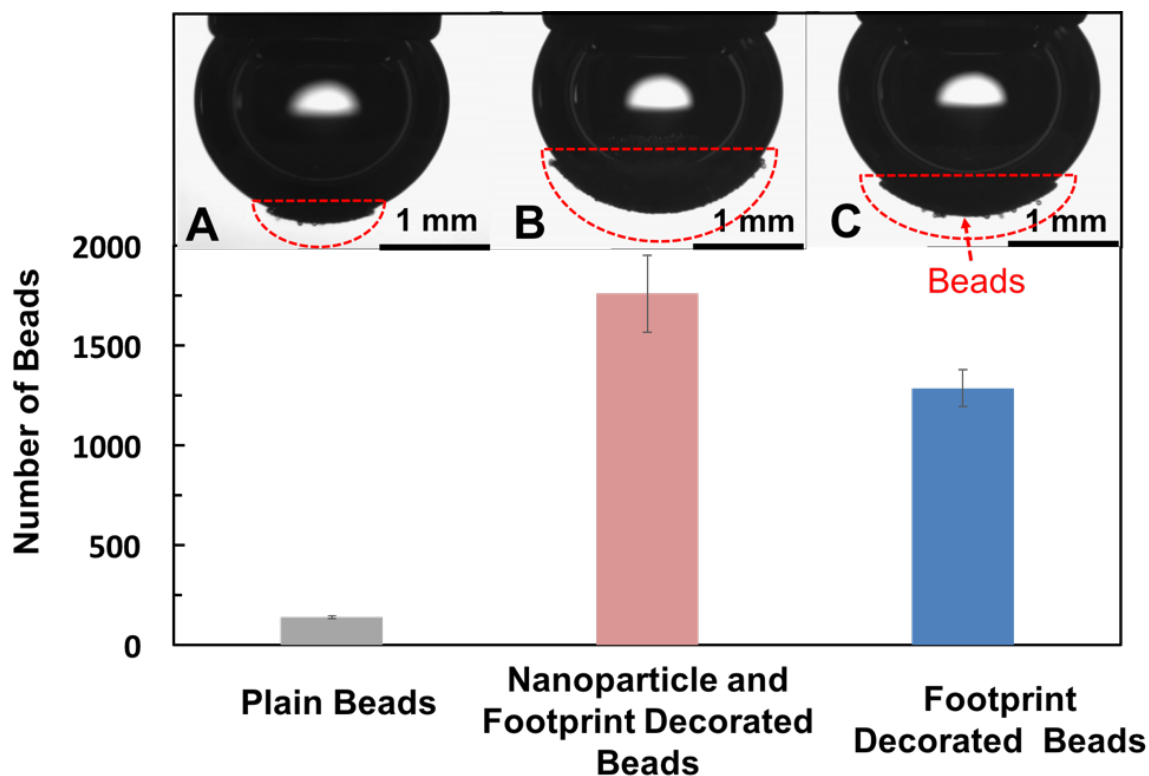


Figure 14 Number of beads picked up by a captive air bubble for A) untreated plain beads, B) nanoparticle and footprint decorated beads, and C) footprint decorated beads. The images are directly correlated with the counted number of beads. Three repeats were made for each sample at different positions on bead bed and the reported number is the average value of the three replicates. The error bars represent the standard deviation of the three replicates.

When considering the potential of using footprints as flotation collectors, the ability of footprints to facilitate the attachment while also preventing the detachment^{20,21} of glass beads from the air bubble surface in an agitated flotation cell need to be addressed. A simplified model flotation apparatus (see Figure 10) based on the work of Xu et. al²² was built to test the ability of glass beads with different surface treatments to adhere to air bubbles in turbulent water flow field. Instead of having air bubbles rising through particles dispersed in a suspension, a single bubble was kept at a fixed position and the suspension of particles was allowed to move against it. The attachment process of glass beads to the air bubble was recorded using a digital camera at a speed of 25 fps and analysed frame by frame. Two example videos can be found in the Supporting Information files (Video S 1 and Video S 2). The trajectories of individual bead on the bubble surface were included in Figure 15. Footprints decorated glass beads were observed to slide and then leave the bubble after passing the equator (Figure 15B). In contrast, beads coated with a combination of nanoparticles and footprints continued to slide on the bubble surface even

after passing the equatorial plane of the bubble (Figure 15A), and a significant number of nanoparticle and footprint decorated beads accumulated on the air bubble surface. Additionally, as illustrated in the supporting information file (Figure S 4), plain bead was also observed to slid off the air bubble surface.

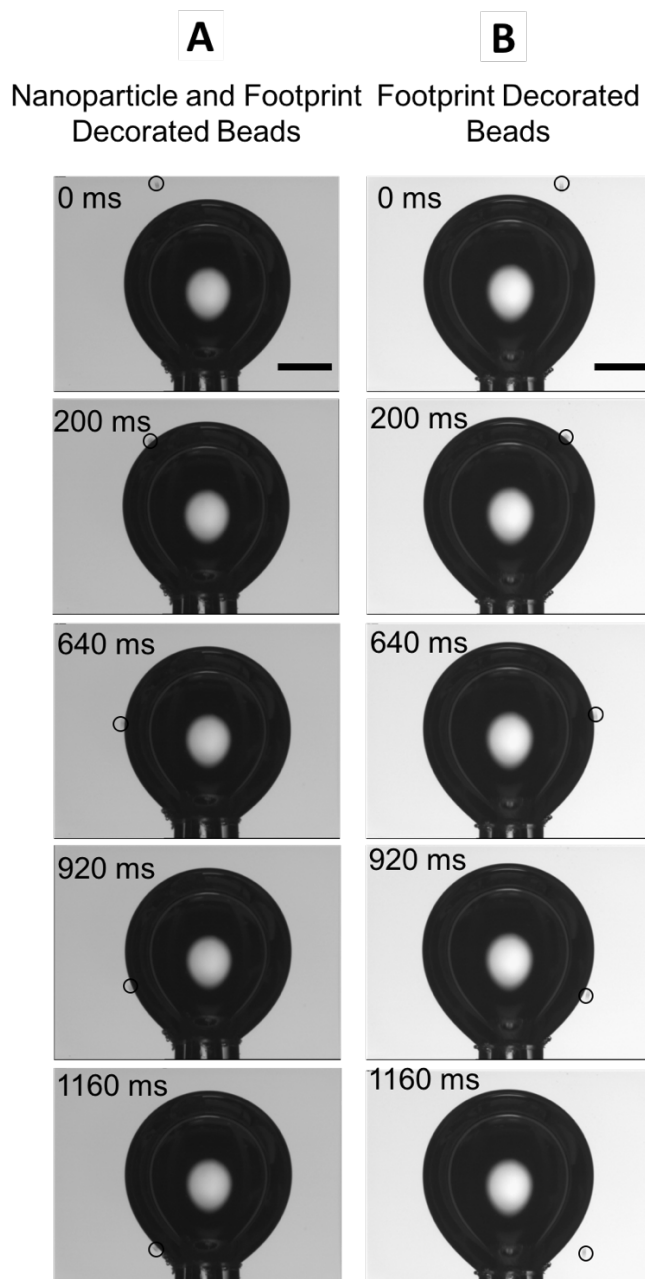


Figure 15 Typical frames shown the attachment processes of the individual glass bead with a static air bubble. The bead indicated in left column (A) was nanoparticle and footprint

decorated bead and the bead in right column (B) was footprint decorated bead. The scale bars represent 1 mm. Note that time 0 ms was denoted as the reference time.

Discussion

The flotation results in Figure 11 show that the small soft nanoparticles (PS/PB-92) were more effective than larger soft nanoparticles (PS/PB-315 and PS-PB-357), especially at long conditioning times. Additionally, compared to the flotation performance of corresponding rigid polystyrene particles of similar size, soft nanoparticles gave higher glass bead recovery for all tested conditioning times. Furthermore, by comparing the surface coverage of PS/PB-92 with a rigid nanoparticles¹⁸ and the large soft nanoparticles shown in Figure 12, we conclude that small nanoparticle size and high nanoparticle/glass bead adhesion minimize the chances of nanoparticle removal by nano-scale ball milling during the conditioning step.

The mass dosage of nanoparticle is a decisive parameter of promoting nanoparticle collectors for commercial application. For a given dosage, the theoretical maximum coverage is inversely related to nanoparticle radius, which indicated that a smaller nanoparticle is therefore a superior collector in terms of reducing dosage. However, considering the severe depression of the molecular collector efficiency by nanoscale surface contaminations, serpentine fibers (typically with a diameter of 20 nm), of nickel ultramafic ores, the minimum diameter of developed nanoparticle collector is 20 nm. Additionally, a small nanoparticle collector is less susceptible to the negative effects of water flow and mixing during conditioning. The Goldman equation²³, Eq. 1, estimates that the lateral displacement force experienced by a particle on a surface in laminar flow increases with the square of the particle radius. The nano-scale ball milling model¹⁸ predicted that a large adsorbed nanoparticle is more likely to be removed than a smaller particle.

$$F_d = 1.7(6\pi\eta r^2 S) \quad \text{Eq. 1}$$

* In Eq. 1 F_d is the lateral displacement force, S is the shear rate, r is the nanoparticle radius, and η is the viscosity.

The observation of footprints is important because it provides direct evidence that the nanoparticles are dislodged from the surface. In addition, as shown in Figure 13, the number of footprints increased dramatically when the conditioning time increased from 5 minutes to 240 minutes. This confirms the prediction of the nano-scale ball milling model¹⁸, that nanoparticle removal rate takes over at long conditioning times.

The morphology and composition characterization indicated that footprints are formed during the nano-scale ball milling of glass beads decorated with soft shell nanoparticles. We suggest two

possible scenarios, schematically represented Figure 16: (A) Two PS-PB soft shell nanoparticle decorated beads collide, and the shell polymer of some nanoparticles are partially scratched off and deposited in the form of a small footprint, 80 nm, on a bare patch on the other bead surface, without knocking the parent nanoparticle off, and (B) At higher collision force the PS-PB nanoparticle is knocked off completely, leaving a relative large footprint, 200 nm, on its original bead. The contact patch diameter of a PS-PB-356 soft shell nanoparticle on a flat surface can be calculated to be 164 nm, see supporting information file (Figure S 6) for the calculation. This value is in good agreement with the size of the observed large footprint further suggesting that it originates from a dislodged parent nanoparticle.

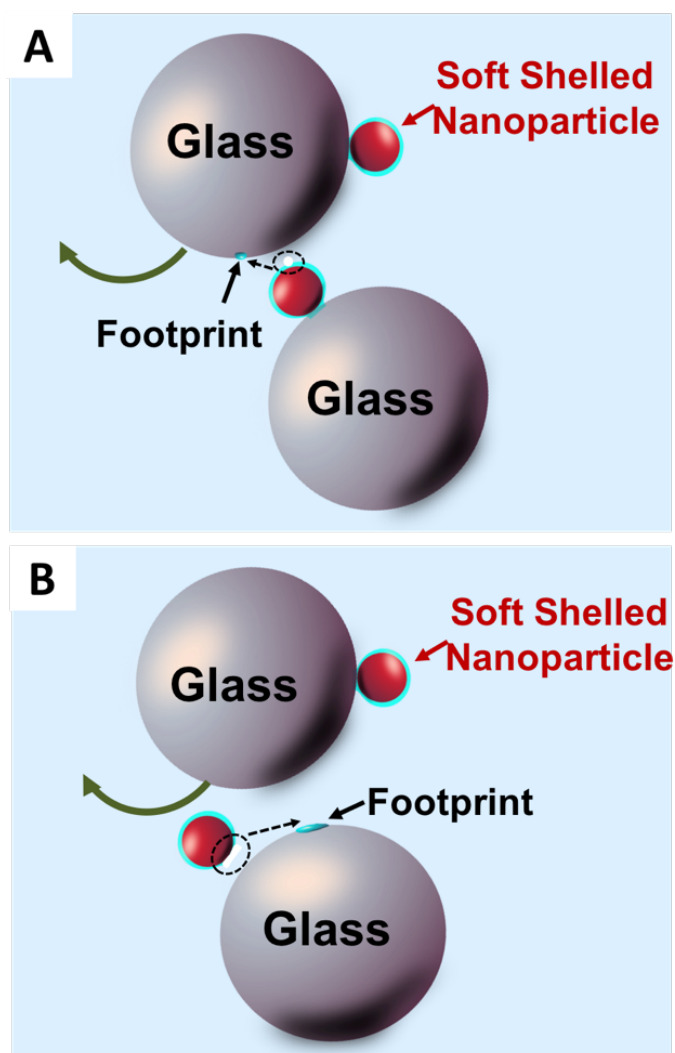


Figure 16 Schematic drawing of the proposed mechanisms of footprint formation, where scenario A) represents the small footprint and B) the large footprint.

Footprints were observed on glass bead surfaces also when soft Janus nanoparticles were used as collectors, see micrographs in Figure 17. The size of the footprints is homogenous throughout the image and average diameter is similar to the hydrodynamic diameter of the Janus nanoparticle. Hardly any smaller or larger patches can be observed. The SEM micrographs in Figure 18, depicting PS/PB Janus nanoparticles deposited on a glass bead surface provides an explanation for this. Based on the shape of the adsorbed nanoparticles, with the distinctly flattened contact zone between the particle and the bead, it can be concluded that the rigid PS lobe is facing outward, indicating that only PB lobes are present in the collision zone between two colliding PS/PB Janus nanoparticle coated beads. The rigid PS lobe is too hard to stamp a footprint and therefore footprints only form in the scenario when the collision force is sufficiently high to knock off a soft and highly deformed PB lobe of an adsorbed Janus nanoparticle from the bead surface, leaving a footprint size close to the particle diameter.

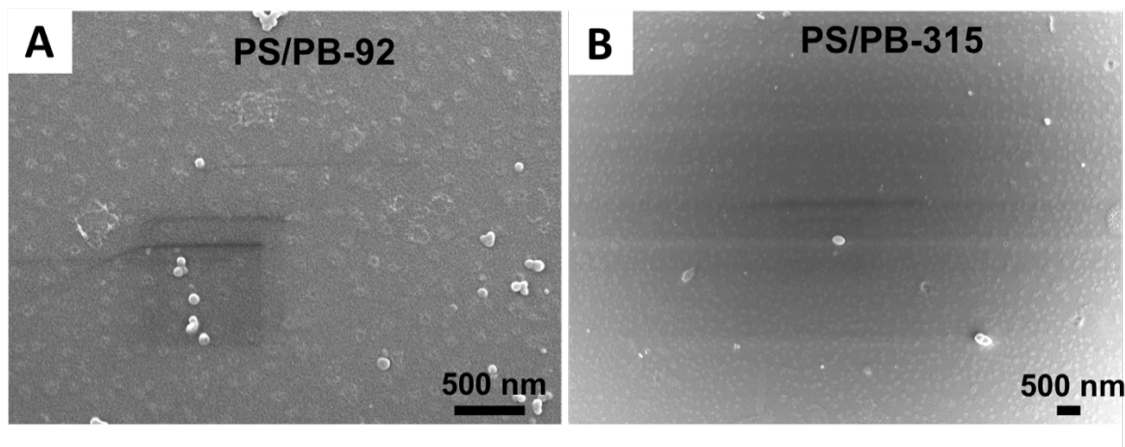


Figure 17 SEM images of glass beads remaining in the flotation cell after 240 minutes of conditioning using (A) PS/PB-92 and (B) PS/PB-315 Janus nanoparticle as collector.

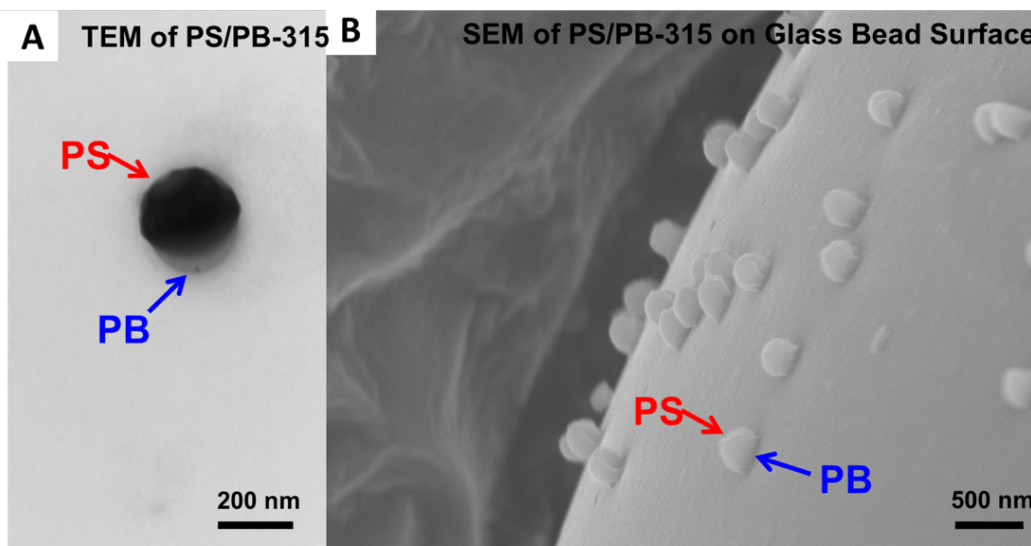


Figure 18 (A) TEM image of PS/PB-315 Janus nanoparticle and (B) SEM image of a PS/PB-315 decorated glass bead.

If the footprints produced by the soft-shelled nanoparticles indeed promote flotation, it suggests a novel approach to collector application - “nanoparticle stamping”, where one nanoparticle can generate many footprints on mineral particle surfaces instead of just adsorbing onto one surface. The captive air bubble pick-up experiments showed that footprints are sufficiently hydrophobic to stick to an air bubble, however in the dynamic model experiment, simulating turbulent flow, the footprint coated beads could not stick to air bubble surface. These model experiments do not however provide enough information to grant the general conclusion that hydrophobic footprint coated solids do not float, since smooth spherical glass beads are harder to float than real mineral particles²⁴. It is possible that rough mineral particles decorated with footprints would float.

On the other hand, we have previously shown that in order to achieve good flotation using hydrophobic nanoparticles, at least 10% coverage of the glass bead surface is required¹⁴. The presence of footprints seems to lower this requirement since glass beads covered with both footprints and nanoparticles floats at very low nanoparticle coverage, e.g. beads shown in Figure 12A and Figure 15C have 5% nanoparticle coverage. We suggest that the hydrophobic footprints promote an expansion of the three-phase contact line (TPCL), facilitating the attachment of the air bubble. As predicted in the foam lamella drainage literature²⁵, the time required to drain out a water film scales with the inverse of the square of the film thickness. The probability of contact nucleus formation increases with nanoparticle diameter¹³. Contact nuclei are more likely to form at the site of neighbouring nanoparticles. At low nanoparticle coverage, the distance between particles is too far for the segments of the TPCL to jump from one hydrophobic particle, over the

hydrophilic patch, to the next hydrophobic particle. Hydrophobic footprints between nanoparticles promote the advancing of the segments of TPCL. With expanded TPCL, nanoparticles and footprints firmly attach to the air bubble surface. The introduction of footprints may compensate for the loss of hydrophobic nanoparticles.

Conclusions

1. Soft nanoparticles provide direct evidence for the removal of adsorbed nanoparticles during conditioning. All evidence suggests that bead-bead collisions (nano-scale ball milling) cause the nanoparticle removal.
2. Dislodged soft-shelled core/shell nanoparticles, and Janus nanoparticles with a soft lobe, leave behind circular patches of soft polymer (footprints), giving contact patch roughly predictable from the thickness of the soft shell.
3. The footprints, based on hydrophobic poly(n-butyl methacrylate), promote bubble/bead adhesion, however, poor bubble/particle attachment values and poor flotation performance suggests that the footprints are inferior to the parent nanoparticles in terms of the efficiency of contact nucleus formation.
4. Combinations of adsorbed nanoparticles and footprints were effective, suggesting a possible route to lower nanoparticle dosage in commercial flotation operations.

Reference

- (1) Wills B., F. J., *Wills' Mineral Processing Technology-An Introduction to the Practical Aspects of Ore Treatment and Mineral Recovery*. Eighth ed. 2016, USA: Elsevier.
- (2) Fuerstenau, M. C.; Jameson, G. J. and Yoon, R.-H., *Froth flotation: a century of innovation*. 2007: SME.
- (3) Rao, S. R., *Surface Chemistry of Froth Flotation*. Second ed. 2004, US: Springer
- (4) Uddin, S.; Rao, S. R.; Mirnezami, M. and Finch, J. A., Processing an ultramafic ore using fiber disintegration by acid attack. *International Journal of Mineral Processing* **2012**, 102–103, 38-44.
- (5) Dai, Z.; Bos, J.; Quinn, P.; Lee, A. and Xu, M. *Flowsheet development for Thompson ultramafic low-grade nickel ores*. in *Advances in Mineral Processing Science and Technology, 48th Annual Conference of Metallurgists of CIM*. 2009. Canadian Institute of Mining, Metallurgy and Petroleum Westmount, Quebec, Canada.
- (6) Xu, M.; Dai, Z.; DONG, J.; Ford, F. and Lee, A., Fibrous minerals in ultramafic nickel sulphide ores. *CIM Journal* **2012**, 3, 223-235.
- (7) Yada, K., Study of microstructure of chrysotile asbestos by high-resolution electron microscopy. *Acta Crystallographica Section A* **1971**, 27, 659-664.
- (8) Mani, H.; Xu, M.; Quinn, P. and Stratton-Crawley, R., The effect of ultramafic mineralogy on pentlandite flotation. *Processing of complex ores* **1997**, 1101, 63-76.
- (9) Pietrobon, M. C.; Grano, S. R.; Sobieraj, S. and Ralston, J., Recovery mechanisms for pentlandite and MgO-bearing gangue minerals in nickel ores from Western Australia. *Minerals Engineering* **1997**, 10, 775-786.
- (10) Dong, J. and Xu, M., Evaluation of environmentally friendly collectors for xanthate replacement. *Proceedings of the 43rd Annual Meeting of the Canadian Mineral Processors Conference, CIM, Ottawa, ON, Canada* **2011**, 289-302.
- (11) Nagaraj, D. R. and Farinato, R. S., Evolution of flotation chemistry and chemicals: A century of innovations and the lingering challenges. *Minerals Engineering* **2016**, 96–97, 2-14.
- (12) Yang, S. and Pelton, R., Nanoparticle Flotation Collectors II: The Role of Nanoparticle Hydrophobicity. *Langmuir* **2011**, 27, 11409-11415.
- (13) Yang, S.; Pelton, R.; Montgomery, M. and Cui, Y., Nanoparticle Flotation Collectors III: The Role of Nanoparticle Diameter. *ACS Applied Materials & Interfaces* **2012**, 4, 4882-4890.

- (14) Yang, S.; Pelton, R.; Raegen, A.; Montgomery, M. and Dalnoki-Veress, K., Nanoparticle Flotation Collectors: Mechanisms Behind a New Technology. *Langmuir* **2011**, *27*, 10438-10446.
- (15) Yang, S.; Razavizadeh, B. B. M.; Pelton, R. and Bruin, G., Nanoparticle Flotation Collectors—The Influence of Particle Softness. *ACS Applied Materials & Interfaces* **2013**, *5*, 4836-4842.
- (16) Yang, S.; Pelton, R.; Abarca, C.; Dai, Z.; Montgomery, M.; Xu, M. and Bos, J.-A., Towards nanoparticle flotation collectors for pentlandite separation. *International Journal of Mineral Processing* **2013**, *123*, 137-144.
- (17) Dong, X.; Marway, H. S.; Cranston, E. D. and Pelton, R. H., Relating Nanoparticle Shape and Adhesiveness to Performance as Flotation Collectors. *Industrial & Engineering Chemistry Research* **2016**, *55*, 9633-9638.
- (18) Dong, X.; Price, M.; Dai, Z.; Xu, M. and Pelton, R., Mineral-Mineral Particle Collisions During Flotation Remove Adsorbed Nanoparticle Flotation Collectors. *International Journal of Mineral Processing* **2016**, Submitted.
- (19) Butt, H.-J. and Kappl, M., *Surface and interfacial forces*. 2009: John Wiley & Sons.
- (20) Albijanic, B.; Ozdemir, O.; Nguyen, A. V. and Bradshaw, D., A review of induction and attachment times of wetting thin films between air bubbles and particles and its relevance in the separation of particles by flotation. *Advances in Colloid and Interface Science* **2010**, *159*, 1-21.
- (21) Wang, G.; Nguyen, A. V.; Mitra, S.; Joshi, J. B.; Jameson, G. J. and Evans, G. M., A review of the mechanisms and models of bubble-particle detachment in froth flotation. *Separation and Purification Technology* **2016**, *170*, 155-172.
- (22) Wang, W.; Zhou, Z.; Nandakumar, K.; Xu, Z. and Masliyah, J. H., Attachment of individual particles to a stationary air bubble in model systems. *International Journal of Mineral Processing* **2003**, *68*, 47-69.
- (23) Goldman, A. J.; Cox, R. G. and Brenner, H., Slow viscous motion of a sphere parallel to a plane wall—I Motion through a quiescent fluid. *Chemical Engineering Science* **1967**, *22*, 637-651.
- (24) Vaziri Hassas, B.; Caliskan, H.; Guven, O.; Karakas, F.; Cinar, M. and Celik, M. S., Effect of roughness and shape factor on flotation characteristics of glass beads. *Colloids and Surfaces A: Physicochemical and Engineering Aspects* **2016**, *492*, 88-99.
- (25) Garrett, P., *Defoaming: Theory and Industrial Applications*. 1993, FL: CRC Press: Boca Raton.

Appendix: Supporting Information for Chapter 4

Table S 1 Recipes for preparation of polystyrene-core-poly(*n*-butyl methacrylate)-shell (PS-PB-315 core-shell) and polystyrene/poly(*n*-butyl methacrylate) (PS/PB-92 and PS/PB-315 Janus) nanoparticles, where the final number on the nanoparticle designation is the average particle diameter determined by dynamic light scattering.

Nanoparticle designation	Seed latex (wt%), g	Water, g	<i>n</i>-butyl methacrylate, g	V50, mg
PS-PB-356 Core-shell	PS-317 (3.6%), 20	20	0.36	18
PS/PB-92 Janus	PS-63 (2.7%), 20	20	1.08	40
PS/PB-315 Janus	PS-205 (2.2%), 20	20	0.87	40

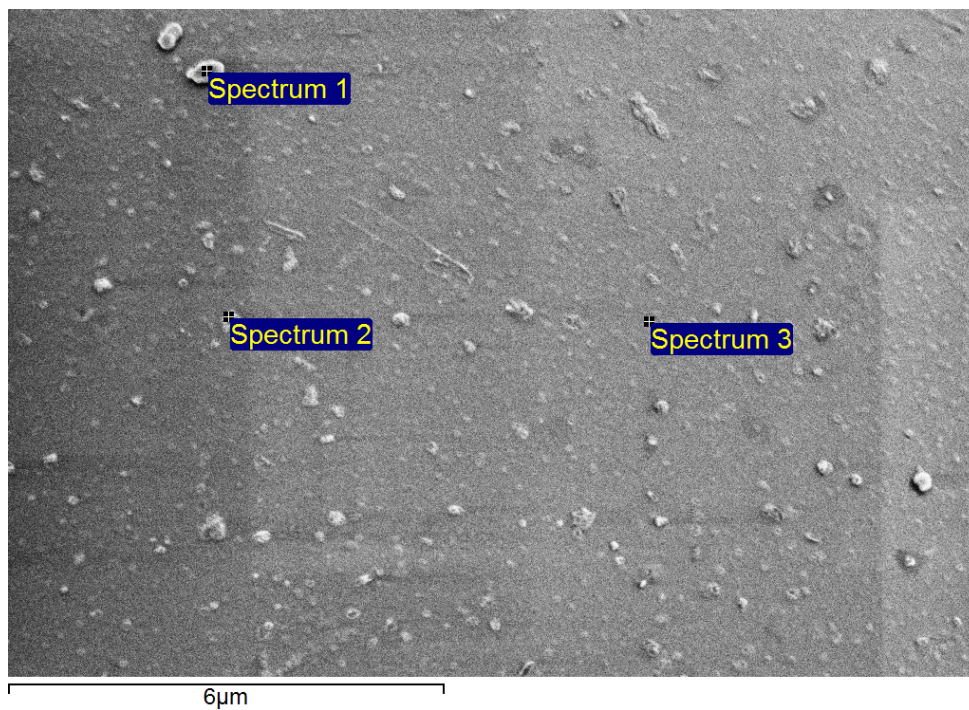


Figure S 1 SEM image of the site of interest for EDS analysis. Three individual footprints were analyzed.

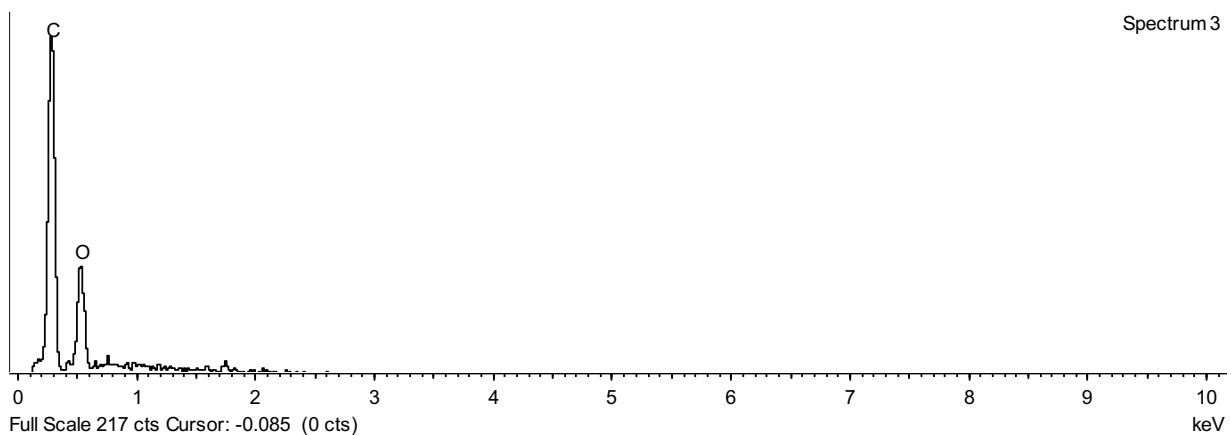
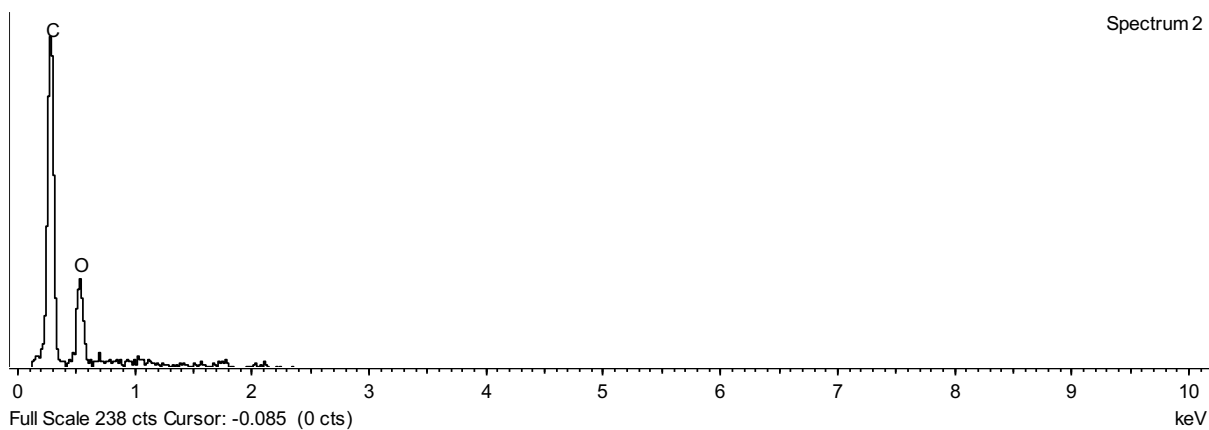
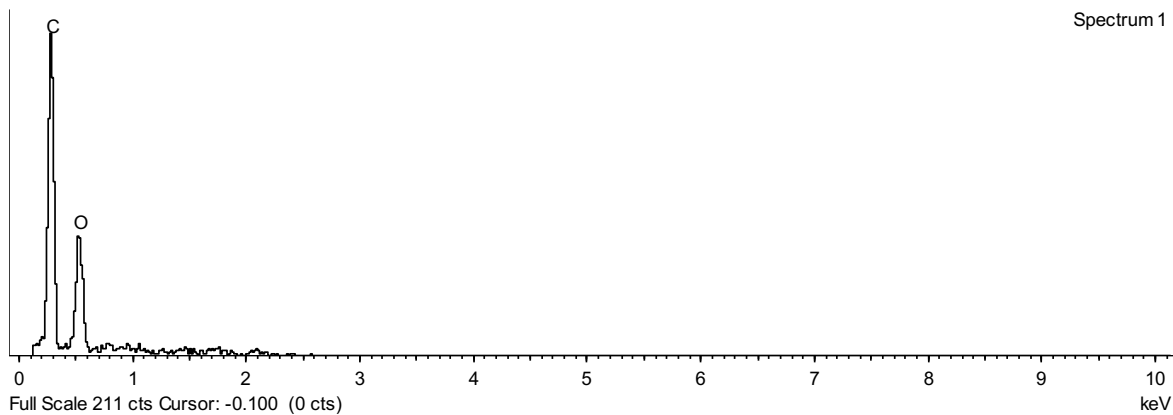


Figure S 2 EDS spectrum of footprints. Note that the corresponding site of the spectrum is indicated in Figure S 1.

Table S 2 Elemental composition of the footprints determined by EDS. Note that the elemental weight ratio of carbon/oxygen of pure shell polymer, poly(n-butyl methacrylate), is 75% / 25%. The measured values in Table S 2 agree with the calculated elemental weight ratio of shell polymer, PB.

	Carbon wt %	Oxygen wt %
Spectrum 1	68.46	31.54
Spectrum 2	75.29	24.71
Spectrum 3	72.59	27.41
Mean	72.11	27.89
Standard Deviation	3.44	3.44

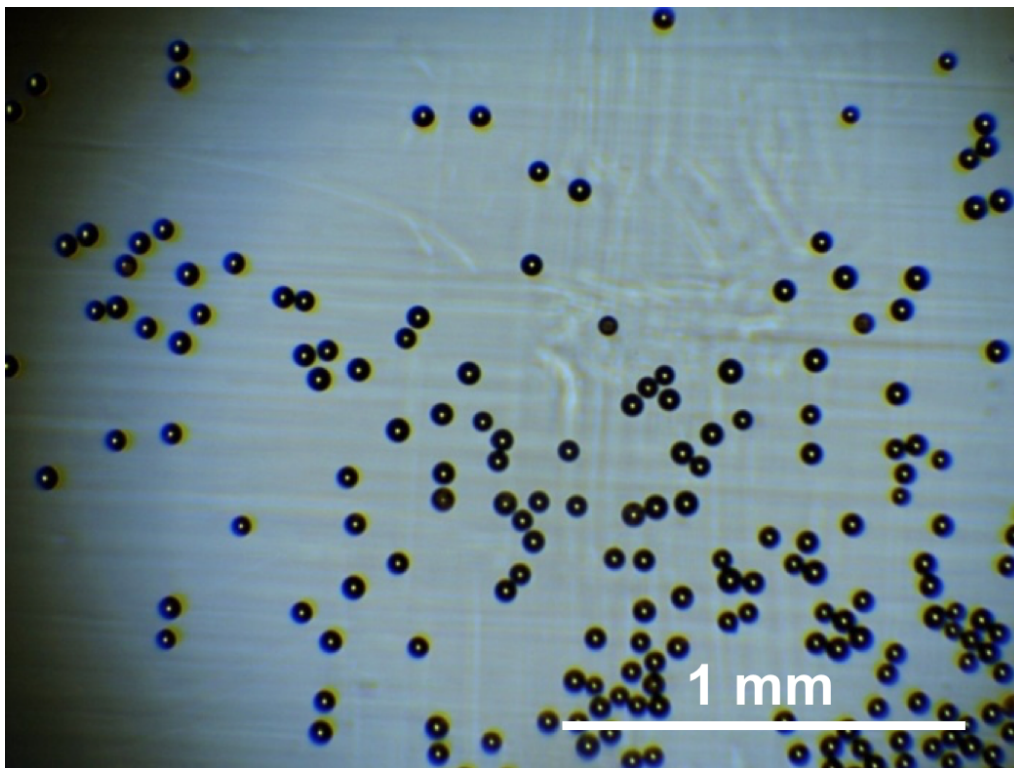


Figure S 3 An example optical micrograph of glass beads collected for counting in captive air bubble pick-up test.

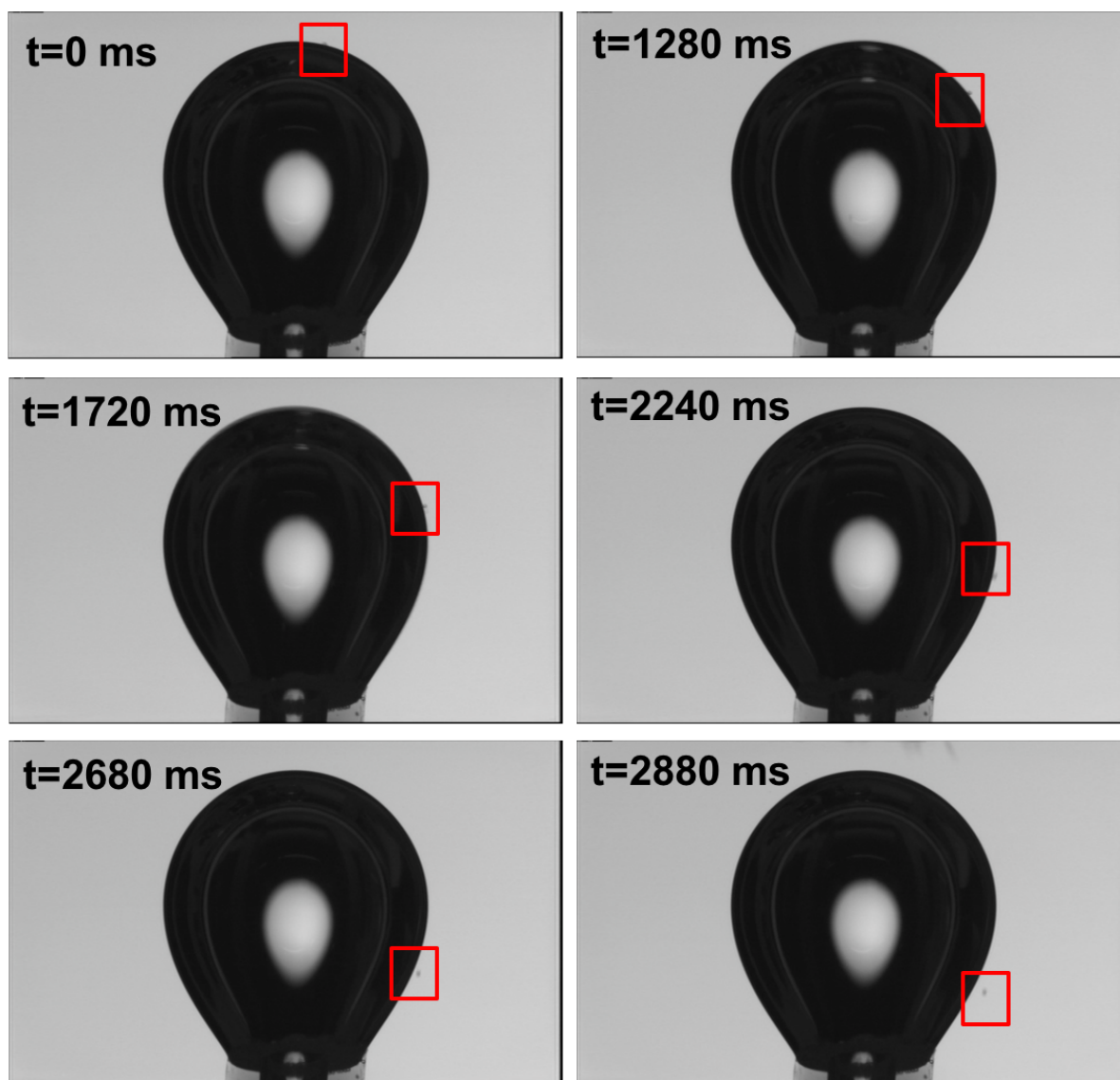


Figure S 4 Typical frames for the plain glass bead-bubble attachment process. Note that time 0 ms was denoted as the reference time.

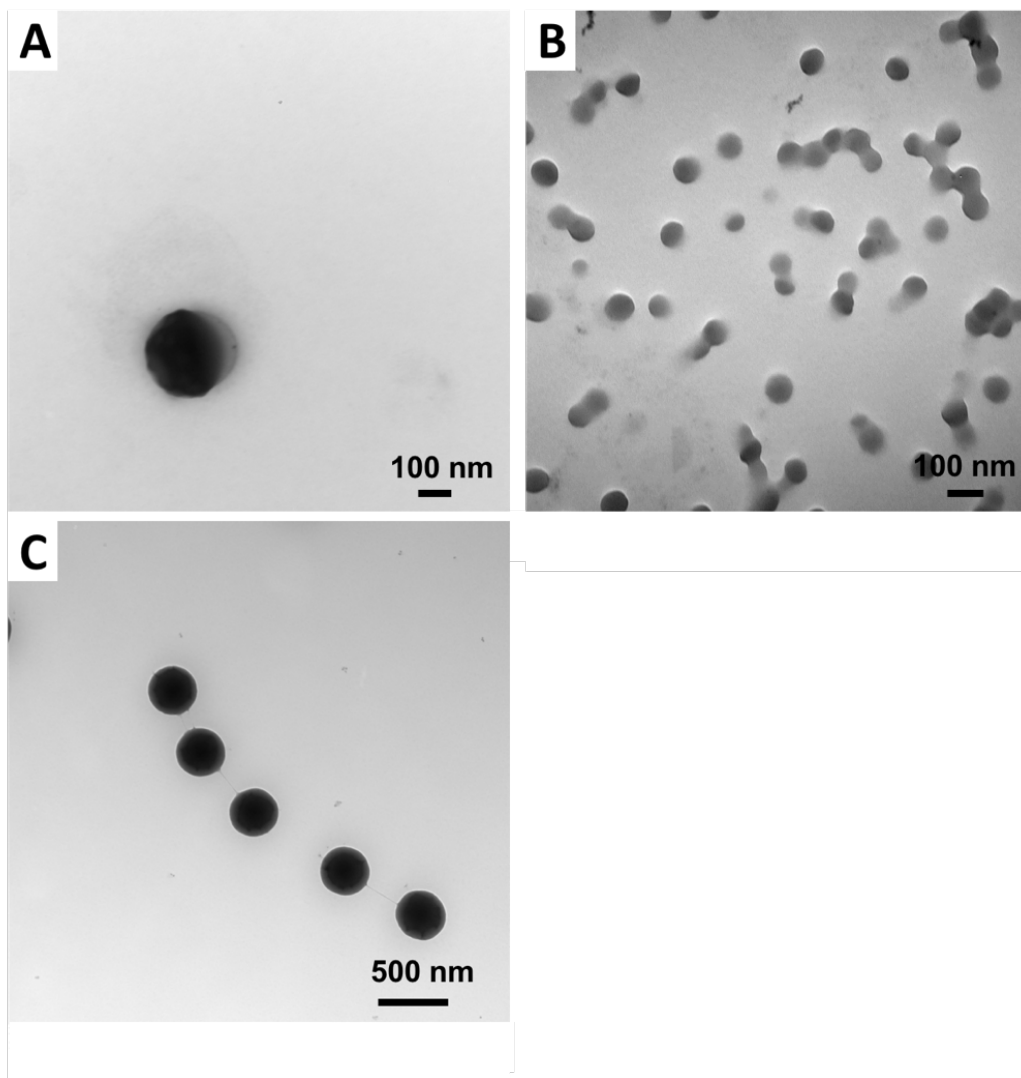


Figure S 5 TEM micrographs of: (A) PS/PB-315 Janus nanoparticle; (B) PS/PB-92 Janus nanoparticle; and (C) PS-PB-356 core-shell nanoparticle.

PS-PB Core-shell

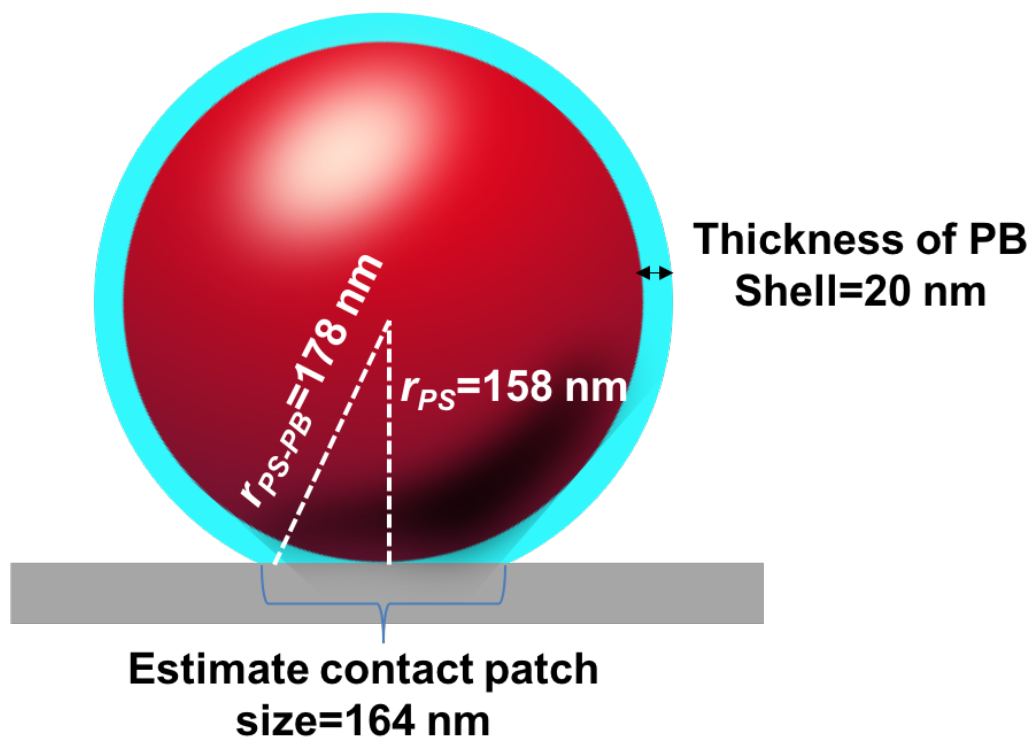


Figure S 6 An illustration of a PS-PB-356 soft shell nanoparticle sitting on surface.

Video S 1 An Example video* shows the attachment process of nanoparticle and footprint decorated glass beads with the air bubble.

**This video is provided in an individual file.*

Video S 2 An Example video* shows the attachment process of footprint decorated glass beads with the air bubble.

**This video is provided in an individual file.*

Chapter 5 Concluding Remarks

This thesis assesses the potential for using soft nanoparticles as flotation collectors. The adhesion between nanoparticles and a model mineral particle was measured quantitatively, and properties required for strong nanoparticle/mineral adhesion have been identified. Nanoparticle adhesiveness and size were correlated to its performance as flotation collector. The research objectives proposed in Chapter 1 were fulfilled and the major contributions of my work in this thesis are listed below:

1. For the first time, it was revealed that adsorbed nanoparticle collectors can be removed from particle surfaces during the flotation process, and that dislodged nanoparticles form large aggregates that do not promote flotation. Removal of hydrophobic nanoparticle collectors from hydrophilic glass bead surfaces leads to a dramatic reduction of the flotation recovery with conditioning time. The extent to which the nanoparticle removal affects the flotation performance depends upon nanoparticle adhesive properties and size.
2. A series of rigid polystyrene nanoparticles with a hydrodynamic diameter ranging from 63 nm to 317 nm were synthesized via monomer-starve semi-bath emulsion polymerization and surfactant emulsion polymerization methods. Soft shelled polystyrene-poly (n-butyl methacrylate) nanoparticles with variable shell thickness and soft lobed polystyrene/poly (n-butyl methacrylate) nanoparticles with variable size were fabricated via seeded emulsion polymerization. The nanoparticle library offered the possibility of exploring two critical parameters, nanoparticle adhesion and particle size, independently in this work.
3. Colloidal probe atomic force microscopy measurements were used to correlate nanoparticle adhesion to the ability to promote hydrophobicity of glass beads, the model of mineral particles. The work of adhesion between 356 nm PS-PB nanoparticles with a 20 nm soft PB shell and glass is one order of magnitude higher than that between 317 nm rigid PS nanoparticles and glass. The glass bead recovery using PS-PB nanoparticles as collector was 90%, whereas only 17% of the beads could be recovered using the equivalent dosage of rigid PS nanoparticles. Additionally, 92 nm soft lobed PS/PB Janus nanoparticles gave better glass bead recovery than a 63 nm rigid PS nanoparticle collector did. The stronger adhesion of soft particles to glass causes the improved flotation performance.
4. The estimated shear rates required for removal of both rigid and soft nanoparticles are very high, over 10000 s^{-1} . Therefore, it was concluded that the requirement for high adhesion between nanoparticle and glass is not a result of hydrodynamic forces that are removing adsorbed nanoparticles from particle surfaces. Instead, it is proposed that bead-

bead collisions remove adsorbed nanoparticles present in the collision zone, by a mechanism named nano-scale ball milling induced erosion. Larger nanoparticles are more susceptible to removal by nano-scale ball milling, as the interaction zone on a bead surface increase linearly with nanoparticle diameter.

5. The coverage of adsorbed rigid nanoparticles on a bead surface as function of conditioning time can be predicted by combing the nanoparticle deposition rate and the nanoparticle removal rate induced by nano-scale ball milling. Simulations revealed that the surface coverage of rigid PS nanoparticle increases during the first few minutes, after which it decreases exponentially. For a given dosage, estimated maximum flotation time, presumably the highest recovery, decrease almost linearly with nanoparticle radius.
6. Flotation results, SEM imaging of the nanoparticle coverage on bead surfaces and nano-scale ball milling simulation all show that smaller and softer nanoparticles are removed more slowly during the flotation process.
7. Although 10% nanoparticle coverage is sufficient to give high bead recovery, high nanoparticle collector dosage is required to compensate for the loss of particles if the removal rate is rapid.
8. The conditioning time of nanoparticle collectors prior to initiation of the flotation should be kept short in order to minimize unfavourable collector detachment.
9. Dislodged soft shelled core/shell nanoparticles and soft lobed Janus nanoparticles leave behind circular patches of soft polymer, footprints. A combination of adsorbed nanoparticles and hydrophobic footprints can effectively promote flotation, suggesting a possible route to lower nanoparticle dosage in commercial flotation operations.